2007-03-14

The Origins of Four Paterae of Malea Planum, Mars

Susan K. Larson
Brigham Young University - Provo

THE ORIGINS OF FOUR PATERAE OF MALEA PLANUM, MARS

by

Susan K. Larson

A thesis submitted to the faculty of

Brigham Young University

in partial fulfillment of the requirements for the degree of

Master of Science

Department of Geological Sciences

Brigham Young University

April 2007

BRIGHAM YOUNG UNIVERSITY

GRADUATE COMMITTEE APPROVAL

of a dissertation submitted by

Susan K. Larson

This dissertation has been read by each member of the following graduate committee and by majority vote has been found to be satisfactory.

_____	_____
Date	Eric H. Christiansen, Chair
_____	_____
Date	Bart J. Kowallis
_____	_____
Date	Jani Radebaugh

BRIGHAM YOUNG UNIVERSITY

As chair of the candidate's graduate committee, I have read the dissertation of Susan K. Larson in its final form and have found that (1) its format, citations, and bibliographical style are consistent and acceptable and fulfill university and department style requirements; (2) its illustrative materials including figures, tables, and charts are in place; and (3) the final manuscript is satisfactory to the graduate committee and is ready for submission to the university library.

_____ _____

Date

Eric H. Christiansen
Chair, Graduate Committee

Accepted for the Department

_____

Michael J. Dorais
Graduate Coordinator

Accepted for the College

_____

Thomas W. Sederberg, Associate Dean
College of Physical and Mathematical Sciences

ABSTRACT

THE ORIGINS OF FOUR PATERAE

OF MALEA PLANUM, MARS

Susan K. Larson

Department of Geological Sciences

Master of Science

Malea Planum is a volcanic plain on the southern rim of Hellas Planitia, the largest impact basin on Mars. Four large circular structures on Malea Planum have traditionally been identified as paterae, or low relief, central vent volcanoes (Plescia and Saunders, 1979). A geologic map was constructed and new crater counts made to explore the ages and origins of the paterae. Amphitrites and Peneus Paterae have radial patterns of wrinkle ridges on their flanks and distinct summit calderas (95 km and 130 km across) with arcuate bounding scarps. In contrast, Malea and Pityusa Paterae are broad depressions with diameters greater than 400 km. In some ways Pityusa and Malea Paterae resemble old, filled impact craters (Plescia, 2003) but they also have characteristics of volcanic subsidence features (Roche et al., 2000). A very strong positive gravity anomaly is centered over Amphitrites and smaller positive anomalies are

associated with Peneus and Malea Paterae. A slight annular positive anomaly is associated with Pityusa.

The geology of the Malea Planum Region has been influenced by impact cratering, volcanic, tectonic, fluvial, and most recently, eolian processes. The Noachian was dominated by impact cratering, the formation of Hellas Basin, and the eruption of flood lavas. Malea Planum formed during the mid- to late-Noachian, likely the result of sills liquefying the volatile-rich crust. Malea and Pityusa Paterae formed during the late Noachian. The Hesperian was marked by the formation of Peneus and Amphitrites and complex valley networks. During the mid-Hesperian, southern Malea Planum may have been covered by a very thick polar mantle deposit that melted and sublimated during the late Hesperian. Smaller episodes of polar mantle deposition continued through the Amazonian to the present. The Amazonian is also characterized by eolian activity creating dune fields, etched surfaces, and dust devil tracks.

Based on the topographic and geophysical evidence, Amphitrites and Peneus are typical highland paterae. We conclude that a mid-crustal sill complex similar to that thought to exist beneath the eastern Snake River Plain in Idaho may be the best explanation for the formation of Malea and Pityusa Paterae. A lack of associated flow features on the surface suggests that the loads are the result of an accumulation of dense intrusions. A surficial load (e.g., lava flows) is insufficient to cause the amount of subsidence observed. A mid-crustal mafic or ultra-mafic sill or a dense network of sills and dikes may have contributed to the subsidence.

ACKNOWLEDGEMENTS

I am indebted to many people in the BYU geology department, my family, and friends for the completion of this work. I am sincerely grateful to Eric Christiansen for investing so much time and energy in this project. Thanks for suggesting a topic that allowed me to expand my appreciation and knowledge of the Earth and the universe.

I would like to express appreciation to my committee, Bart Kowallis and Jani Radebaugh, for their insights and suggestions that helped to improved the project so much. Many thanks to the faculty of the geology department for the mentoring and instruction I have received from them during my time at BYU.

I would like to thank Dave Tingey, Marge Morgan, Kris Mortensen, and Kim Sullivan for their continual support, patience, and friendship. Thanks also to the other graduate students for their friendship and their ArcMap and Illustrator tips.

Finally, I am very grateful to my parents, Paul and Mirriam Larson, and my grandmother, Lila Wilson, for their endless support, love, advice and encouragement, especially when it seemed like this project had no end. Thanks also to my brothers and sisters for their love and encouragement and very much for diverting me from the work when I needed it.

TABLE OF CONTENTS

INDEX OF TABLES

INDEX OF FIGURES

1 INTRODUCTION

Malea Planum is a volcanic plain on the southern rim of Hellas Planitia, the largest impact basin on Mars (Figure 1). Amphitrites and Peneus are two paterae with central depressions 120 km in diameter that mark the center of the plain. A patera, from the Latin word for saucer (Greeley and Crown, 1990) is a shallow, irregular crater or complex crater with scalloped edges (Planetary Geomatics Group, 2005) thought to have a volcanic origin (King, 1978). Amphitrites Patera (58.7° S, 60.9° E), and Peneus Patera (57.8° S, 52.5° E) have been accepted to be low relief, central vent volcanoes (Plescia and Saunders, 1979) with distinct summit calderas (Figures 1, 2, and 3). These paterae are surrounded by smooth plains, also likely volcanic, modified by wrinkle ridges. South of Amphitrites and Peneus are two circular depressions with diameters of 300 km. Malea Patera (63.4° S, 51.9° E) and Pityusa Patera (66.8° S, 36.9° E) were recognized as albedo features on Mars by Antoniadi (1930).

The origins of these depressions are uncertain and are the focus of this study. Tanaka and Scott (1987) mapped Amphitrites, Peneus, and Pityusa Paterae as volcanic centers. Leonard and Tanaka (2001) described Amphitrites Patera as a caldera surrounded by a channeled and ridged shield member and Peneus Patera as a caldera lacking a significant raised edifice. Malea Patera was not recognized in either of these studies, which were based on images from the Viking Orbiters, and was included as older ridged plains. Head and Pratt (2001a) described the geomorphology of Malea and Pityusa Paterae; however, they did not propose a method of formation and accepted the volcanic origin for Pityusa proposed by Tanaka and Scott (1987). In contrast, Plescia (2003) suggests that Pityusa and Malea Paterae are simple sags in the crust, possibly old

impact craters that filled with volcanic plains material and sagged due to loading. In order to resolve this debate, I undertook a detailed study of the Malea Planum region using visible, topographic, and thermal image datasets.

Malea Planum lies between 51° and 70° S latitude. These latitudes are equivalent to the northernmost regions of Antarctica on Earth. The proximity of the plain to the southern polar ice cap of Mars complicated the study. Thick, smooth deposits likely related to the polar ice cap terrain often obscure much of the topography (Head et al., 2003).

2 DATASETS

To explore the origins of the paterae, a geologic map and geologic history of Malea Planum were prepared. The geologic map was created using ESRI's ArcMap software and a Lambert conformal conic projection (Figure 4).

2.1 Viking Data

A digital mosaic (MDIM 2.0) of images acquired during the Viking missions was used as a basemap for the geologic map. The mosaic was created by NASA and the USGS from processed raw images and was downloaded as a georeferenced file from the USGS Map-A-Planet website (Garcia, 2005). The mosaic has a nominal resolution of 256 pixels/degree, equivalent to 112 meters/pixel at 60° S (Kirk and Lee, 2005) (Figure 5).

2.2 Mars Global Surveyor (MOC, MOLA, and gravity data)

In 1999, the Mars Orbiter Laser Altimeter (MOLA) on board the Mars Global Surveyor spacecraft began returning topographic data for the surface of Mars to Earth. The data has been released as a digital elevation model with a resolution of 128 pixels/degree (Slavney, 2005). For this project, the MOLA data were manually georeferenced to the MDIM and a shaded relief map was created in ArcMap from this data (Figure 1). Elevation contour maps were also created from the MOLA data. Selected MOC (Mars Orbiter Camera) images from the Mars Global Surveyor, with resolutions up to 1.5 m/pixel, were also used (Figure 5).

In addition to image and topographic data, the Mars Global Surveyor Radio Science Subsystem measured the Doppler shift of radio waves transmitted from the Surveyor to Earth (Tyler, 2001) to create global high-resolution gravitational field models (Smith and Sjogren, 1999). Here, we have used a free-air gravity anomaly map based on gravity model MGM1025 (Lemoine and Smith, 2001) (Figure 6). The uncertainty in the model is 10-13 mGal, a small fraction of the observed peak amplitudes in Malea Planum (Keifer, 2003).

2.3 THEMIS

Thermal images from the Thermal Emission Imaging System (THEMIS) on the Mars Odyssey Spacecraft (available as visible, daytime infrared, and nighttime infrared) were used as a reference dataset for mapping and interpretations. The visible wavelength images (bands centered at 0.425, 0.540, 0.654, 0.749, and 0.860 microns) (Christensen et al., 2005) have resolutions of 19 m/pixel and the infrared images (bands centered at 6.78,

7.93, 8.56, 9.35, 10.21, 11.04, 11.79, 12.57 and microns) (Christensen et al., 2005) have resolutions of 100 m/pixel. Fine-grained materials appear bright in daytime infrared images whereas coarse-grained material or bedrock appears black. This is reversed for nighttime infrared images because of the high thermal inertia of bedrock. The coverage of daytime infrared images for the area is incomplete. Mosaics of selected images were constructed for the study. The nighttime infrared images covering Malea Planum were of limited use. Noise in the images obscured most of the detail (Figure 5).

2.4 Crater Frequencies

Crater diameters and locations were measured in ArcMap within each map unit and plotted on cumulative frequency vs. diameter graphs (Appendix D). Only craters with rim diameters greater than 5 km were included because of inconsistencies between the resolutions of the datasets. Each point on the graphs represents the addition of a new crater to the cumulative curve. The resulting curves were used to find absolute ages of the surface by comparing the results with published crater densities for the three Martian epochs: Noachian, Hesperian, and Amazonian (Tanaka, 1986). According to Tanaka (1986), the oldest epoch, the Noachian, lasted from 4.6 to 3.8 or 3.5 Ga; the Hesperian from 3.8 or 3.5 Ga to 3.55 or 1.8 Ga.; and the Amazonian from the end of the Hesperian to the present.

Relative ages of the geologic units have also been determined using crater counts, superposition and crosscutting relations, and previous investigations of Malea Planum and other volcanic provinces surrounding Hellas Basin. Appendix C is a correlation chart for map units and Figure 7 lists the sequence of major events in the history of the plain.

3 GEOLOGY OF MALEA PLANUM

The geologic units of the Malea Planum region were grouped into four assemblages as well as impact crater materials and miscellaneous materials. Listed by approximate stratigraphic order, youngest to oldest, the assemblages are the Polar, Malea Planum, Hellas, and Highland Plateau assemblages. The units and their abbreviations are shown in Figure 4, the detailed geologic map (Appendix A), the unit descriptions (Appendix B), and the correlation of units (Appendix C).

The Dorsa Argentia Formation (Nda) and rough plateau materials (Nplr), pedestal crater materials (AHpc) and other units likely related to the south polar layered ice cap deposits make up the Polar Assemblage. The Malea Planum assemblage includes the ridged and dissected plains units as well as the units composing the four paterae. The Hellas Basin assemblage includes units related to the Hellas impact basin. The Highland Plateau Assemblage is composed of the cratered highlands and a plains unit (HNp) on the western margin of the map area. The units composing these assemblages will be described in detail below.

Crater frequencies gave a Noachian age for the cratered unit (Np1), the subdued cratered unit (Np2), the Hellas rim unit (Nhr), the dissected plains units (Nd1, Nd2, and Nd3), ridged plains 1 unit (Nr1), the Malea rim unit (Nmr), the Malea floor unit (Nmf), the Pityusa floor unit (Npif), the shield of Peneus (Nps), the rim of Peneus (Npr), the floor of Peneus (Npf), the hummocky unit (Nhu), the pitted unit (Npi), Dorsa Argentia formation (Nda), the rough plateau material (Nplr), and the scarped unit (Ns). Noachian-Hesperian ages were found for the floor of Hellas basin (HNhf), the ridged plains 2 unit (HNr2), and the rim of Pityusa (HNpi). Hesperian ages were found for the shield of

Amphitrites (Has) and the hilly unit (Hhi). The vallis floor unit (AHv), the rim of Amphitrites (Har), the floor of Amphitrites (Haf), the rim massifs (Nhm), pedestal crater material (AHpc), and the highland massifs (Nm) had an insufficient number of craters to determine ages using this method. Superposition, crosscutting relationships, and previously published ages were used for these units. Leonard and Tanaka (2001) gave a Noachian age to Nhm, a Noachian-Hesperian age to Har, and Haf, and an Amazonian-Hesperian age to AHv. Because of their relationship to Has, Har and Haf were given an age of Hesperian for this study. Nm is embayed by Np2 and so was given a Noachian age. On most crater frequency charts a drop off on the curve for craters of small diameters was observed. This can be attributed to burial of smaller features in the map area.

3.1 Tectonic Features

Ridges on Malea Planum's plains are similar in size and morphology to wrinkle ridges found on lava plains elsewhere on Mars and on the lunar maria. The ridges are asymmetrical in cross-section, similar to thrust fault-related folds on Earth (Figure 8b). The forelimb of the ridge is sharply defined while the backlimb is a broad rise (linear to convex). The crest of the ridge is marked by crenulations. It is thought that the wrinkle ridges may be surface expressions of blind thrust faults in stratified sediments or lava flows (Mueller and Golombek, 2004). Tanaka and Leonard (1995) believe the ridges formed as the weight of the unit compressed relatively strong lava flows overlying weaker units. In this study, scarps refer to extensional ridges and compressional ridges that lack wrinkle ridge morphology.

3.2 Geologic Map Units

3.2.1 Polar Assemblage

South of 57° some low plains and depressions are filled by the Dorsa Argentia formation (Nda) (Head and Pratt, 2001b) (Figures 4 and 9). The unit forms plateaus bounded by scarps with heights of a few hundred meters. The plateaus are sparsely cratered, layered, and have a surface slope of 0° or a slope that follows the underlying topography. The Dorsa Argentia Formation (Nda) embays older highland rocks and ridged plains material (Head and Pratt, 2001b). Small, sinuous valleys are locally present on the plateau surfaces. Irregular, shallow pits with steep northern walls and gentler southern walls are randomly scattered across the plateaus (Figure 5d). The floors of the pits are irregular. The surface is locally etched with shallow parallel grooves (Figure 9), and the margins are often steep with scalloped outlines. Small, isolated remnants of a similar deposit are found locally between 30° and 60° S but are not extensive enough to be mapped. These remnants are only a few meters thick and unlike the smooth plateaus of the Dorsa Argentia Formation, they are not restricted to low-lying areas (Figure 5).

Pedestal materials (AHpc) surround small impact craters with rims less than one kilometer to tens of kilometers in diameter throughout Malea Planum. Pedestals form very flat to rough plateaus surrounded by scarps a few meters to 300 m high (Figure 10 and 11a).

The hilly unit (Hhi), mapped as Noachian-Hesperian undivided by Head and Pratt (2001b), forms a series of closely spaced, rounded hills a few kilometers across rising 1 km above the floor of Pityusa Patera (see Figure 11b). The hills are steep-sided; many

have flat tops and are locally embayed by the Dorsa Argentia formation (Nda). Outside the map area the hilly unit is also found associated with the Dorsa Argentia formation.

The rough plateau unit (Nplr) occurs on the northern rim of Malea Patera and an isolated mound on the west slope of Amphitrites (see Figure 11c). The southern edge of the occurrence associated with Malea Patera terminates in a steep, scalloped scarp 200 m high. The smaller plateau is bounded by a rounded scarp in the east and grades into rougher plains material (Nr_1) in the west.

The hummocky material (Nhu) forms an area of rough, low hills and knobs in the southern portion of the map area (Figures 1 and 4). Few cliffs, valleys or ridges are found within the unit.

Pitted material (Npi) forms an area of irregular smooth and rough plains adjacent to the scarp that marks the southern boundary of Pityusa Patera (Figures 1 and 4). The plains are punctuated by hills and scarps.

3.2.2 Malea Planum Assemblage

3.2.2.1 Amphitrites Patera Formation

The Amphitrites Patera Formation is composed of the flanks of Amphitrites Patera (Has), the rim of Amphitrites (Har), and the caldera floor unit (Haf) (Figures 4 and 12). The Amphitrites shield unit (Has) forms the flanks of the patera with slopes ranging from 0.5° in the west and east to 1.2° on the north, where the topography of the Hellas Basin rim may affect it. It is obscured on the south by ejecta from the Barnard impact crater. The unit is defined by terrain radially dissected by numerous, closely spaced valleys extending approximately 70 km away from the topographic crest of the caldera in

the west and 120 km in the east (Figure 13). A narrow valley emerges from a 200 m deep pit with an amphitheater head on the western flank (Figure 2b). The valleys on Amphitrites have a maximum depth of 100 m and width of 5 km. Concentric scarps and radial wrinkle ridges have modified the flanks. No lobate lava flow fronts can be identified.

The Amphitrites rim unit (Har) forms the summit of the patera (Figure 4) and is defined by a lack of the distinct valleys found on the flanks (Figure 2). The unit ranges from a width of 3 km in the west to 40 km in the northeast. The summit of Amphitrites is highest in the southeast where a linear ridge marks the crest with an elevation of 2 km above the surrounding plains. The highest point on the southwest rim decreases to 1600 m above the surrounding plains. Ejecta from Barnard partially covers the southern caldera rim and forms lobate ridges within the caldera that can be seen in high resolution images (Figure 2b). Radial wrinkle ridges and arcuate scarps extend into the rim unit from the flanks. The rim unit includes the caldera wall and terminates at the caldera floor with an abrupt change in slope. The caldera wall has an average slope of 0.7°.

The caldera of Amphitrites has traditionally been defined by an arcuate ridge on the flanks of the patera, northeast of the caldera depression (Crumpler et al., 1996). If this scarp is included, the caldera is about 120 km across. The caldera depression is 95 km in diameter from crest to crest and an average of 470 m deep. The floor has an average elevation of 1300 m above the plains to the east and west. In profile the rim is domed and the caldera walls slope inward in a funnel shape (Figure 2c). The Amphitrites caldera floor unit (Haf) forms the smooth floor of the central depression and is cut by arcuate scarps and small wrinkle ridges. One set of scarps defines a circular depression

68 km in diameter. Within this depression is a smaller set of circular scarps 38 km in diameter. These circular depressions may represent discrete subsidence events.

3.2.2.2 Peneus Patera Formation

The Peneus Patera formation consists of the Peneus shield unit (Nps), the rim unit (Npr) and the caldera floor unit (Npf) (Figure 4). Unlike Amphitrites, Peneus Patera does not have a large edifice (Figure 3). The shield has a diameter of 160 km, an average slope of 0.5°, and is not dissected by valleys other than a small area on the north. Wrinkle ridges extend radially from both central depressions but both lack the concentric wrinkle ridges found around Malea and Pityusa Paterae. The crest of Peneus is an average of 500 m above the surrounding plains (Figure 3b). The caldera depression is nearly circular and has a diameter that ranges from 129 to 138 km (crest to crest, Figure 3a), slightly larger than Amphitrites. The caldera floor is an average of 300 m below the plains. The rim of Peneus is highest in the southwest at 1300 m where a wrinkle ridge intersects the rim, and descends to an elevation of 300 m in the north, only 100 m higher than the average elevation of the caldera floor (Figure 3d). Ejecta from an unnamed crater partially covers the southeast rim. The Peneus rim unit (Npr) is a region of closely spaced arcuate scarps interpreted to be a horst and graben terrain on the summit of Peneus Patera (Figures 4 and 3b). Segments extend up to 100 km in length and 500 m in height. Horsts are a maximum of 200 m deep. One section of the scarps on the southeast rim appears offset toward the center of the caldera. The northwest rim contains a higher concentration of fractures, forming numerous sharp ridges instead of flat-topped horsts.

The Peneus caldera floor unit (Npf) forms the flat, smooth interior of Peneus caldera, which is 250 m above the surrounding plain (Figure 4). No arcuate scarps are found outside the crest of the central depression. The caldera floor is very subtly bowl-shaped and is deepest in the south where the rim is highest. The floor is smoother than Amphitrite's but not as smooth as Malea Patera's (Figure 3b). It is dotted with several of the small pedestal craters that are common across Malea Planum. A sinuous wrinkle ridge up to 100 m in height and 6 km in width extends northeast across the unit and may trace a circular subsidence feature 30 km in diameter on the west side of the patera and a second 45 km in diameter on the east (Figure 3b). In high resolution images, much of the terrain is covered by a discontinuous, thin mantle material (Figure 5a-g).

3.2.2.3 Malea and Pityusa Patera Formation

The Malea and Pityusa Patera formation includes the Malea rim unit (Nmr), the Malea floor unit (Nmf), the Pityusa rim unit (HNpi), and the Pityusa floor unit (Npif) (Figure 4).

Malea Patera. Malea is a large, complex patera south of Peneus Patera (Figure 14). The Malea rim unit (Nmr) includes the crest and central depression walls of Malea Patera. The extent of the unit was determined by the positions of wrinkle ridges associated with the patera. The patera does not rest on a significant edifice. There is no evidence for lava flows and no radial valleys are found on the flanks. In total, the depression is approximately 400 km in diameter measured from rim crest to crest. The rim crest is highest (absolute elevation of 1800 m) in the southwest where it is shared with the rim crest of Pityusa Patera and lowest (500 m) in the east where the rim crest is

poorly defined. The northwest rim of the depression is marked by a series of arcuate, flat-topped ridges resembling horsts approximately 100 m high with lengths up to 70 km (Figure 14a). The ridges once may have extended along the northern rim of the depression, but the rim has since been buried by younger rough plateau material (Nplr) (Figure 14a). Linear wrinkle ridges with heights of 200 m and lengths up to 150 km extend radially away from Malea (Figure 8). Arcuate wrinkle ridges up to 100 m high and 100 km in length are concentric to the depression, particularly in the south and west. Arcuate, flat-topped ridges ring the northwest corner of the patera. The walls of the interior depression slope gently (0.4°) into a flat floor and are deformed by the wrinkle ridges.

Unlike Peneus and Amphitrites, the floor of Malea Patera sits an average of 950 m below the surrounding plains. It is the smoothest of the four paterae. The Malea Patera floor unit (Nmf) forms featureless plains with small (meters high) scarps and few impact craters. It is similar in appearance to the Dorsa Argentia Formation (Nda) found by Tanaka and Scott (1987) but is not bounded by a steep scarp. A smooth plateau of Nda covers the northeast area of the depression (Figures 4 and 14b). A series of small ridges trending northwest covers the southern half of the depression. A higher wrinkle ridge extends northeast across the floor. The unit terminates at the depression walls, usually with an abrupt change in slope. An embayment in the southern wall (Figure 14a) may indicate that the depression is a complex of at least two smaller depressions, approximately 200 and 100 km in diameter. A sinuous ridge extends NE and smaller linear ridges extend E-W through the unit.

Pityusa Patera. Pityusa Patera is a circular depression 440 km in diameter (Figure 15) much like Malea Patera but larger in diameter and deeper from crest to floor. Unlike Malea, Pityusa rests on an edifice 500 km in diameter. The Pityusa rim unit (HNpi) includes the crest and central depression walls of Pityusa Patera. The extent of the unit was determined by the positions of wrinkle ridges associated with the patera. The crest of Pityusa reaches a maximum elevation of 2500 m in the south where it terminates in a scalloped scarp 1.5 km high that is concentric to the depression. The average elevation of the crest is 1900 m (700 m above the surrounding plain). A strong, radial pattern of wrinkle ridges extends outward from Pityusa. These ridges reach heights up to 300 m and lengths of 100 km and are most pronounced on the rim common to the two depressions. Arcuate wrinkle ridges (100 m high and up to 80 km in length) concentric to the depression are more numerous than around Malea patera and are most prominent in the west. The walls of the depression are steepest in the west and gentlest in the east. A small valley on the eastern rim continues onto the depression floor.

The Pityusa Patera floor unit (Npif) is rougher terrain than the floor of Malea Patera. The patera floor is an average of 1000 m below the surrounding plains. The Dorsa Argentia formation (Nda) of Tanaka and Scott (1987) and the hilly unit (Hhi) are superimposed on it. Dunes are present in the northwest, in isolated patches adjacent to Nda and in some craters. A few small ridges and valleys extend across the unit.

3.2.2.4 Valleys

Malea Planum has been modified by channeling, primarily in the north and west, which has formed the dissected plains units. Dissected unit 1 (Nd_1) is a region of rough

plains cut by many linear to sinuous valleys (collectively known as Axius Valles) on the slope of Hellas impact basin (Figures 1 and 4). The unit includes the highest concentration of valleys on Malea Planum (Figure 13). The deepest valleys are 200-300 meters deep and many are overlain by smaller valleys a few meters deep that utilized the pathways of the pre-existing, larger valleys (Figure 13B). The valleys cross-cut the few ridges found in this terrain and some are deflected by craters. While some valleys divert around preexisting impact craters, others cut crater rims, indicating fluid flow into the crater bowls. Some Malea Planum valleys are continuous with the valleys found on the flanks of Amphitrites Patera.

Dissected unit 2 (Nd_2) forms channeled plains south of dissected unit 1 (Nd_1) and west of Peneus Patera. The valleys are sinuous, only a few meters deep, and are comparable to the smaller set of valleys found within dissected unit 1 (Nd_1) (Figure 13C). Large linear and arcuate wrinkle ridges 200 m high trend roughly NNE. Smaller ridges up to 50 m high are randomly oriented.

Dissected unit 3 (Nd_3) is a region of smooth plains on the western margin of Malea Planum, south of dissected unit 2 (Nd_2). The plains are similar to dissected unit 2 but with fewer valleys and many small, sinuous, wrinkle ridges less than 100m high with no consistent orientation. No larger wrinkle ridges are present.

3.2.2.5 Ridged Plains

Ridged plains make up the southern half of Malea Planum. Their topography is similar to the dissected plains except that they have fewer valleys and more east-west ridges. Ignoring the ridges radial and concentric to the paterae, the ridges on Malea

Planum generally trend ENE (Figure 8b). Ridged plains A (Nr_1) forms a smooth plain deformed by numerous linear to arcuate wrinkle ridges as much as 200 m high and several hundred km long. The wrinkle ridges increase in length and height toward the center of the unit. Few smaller ridges are present but they increase in number toward the edges of Malea Planum. The smooth plains between the ridges are locally dissected by narrow valleys and dotted with small pedestal craters, indicating a partially stripped mantle covers the plains. The shallow valleys are also more common toward the edge of the plain. The unit slopes gently toward Hellas Basin.

The Ridged plains B unit (HNr_2) is a flat plain deformed by small ridges reaching 50 m in height. It is similar to dissected unit 3 (Nd_3) but valleys are present only along the eastern contact with the cratered unit (Np_1). The contact between this unit and the scarped unit (Ns) is marked by an abrupt change in slope. In Mitchel crater, Nr_2 terminates in a lobate scarp 100 m high, resembling a lava flow front (Figure 16).

Wrinkle ridges are sparse within the central depressions of the four paterae and in Axius Valles (Nd_1). Assuming wrinkle ridges once extended through these areas, this suggests these areas have been reworked or buried since their formation. Many of the ridges in Axius Valles are discontinuous and appear to be cut by the valleys.

Ridges on Malea Planum's ridged plains are similar in size and morphology to wrinkle ridges found on lava plains elsewhere on Mars and on the lunar maria, however they are more obscure here because they have been covered by younger mantle deposits. Consequently, we conclude that the plains are volcanic in origin and were fed by sources in the center of the plain. Most of the ridges on Malea Planum are linear but some form arcs surrounding subtle central depressions. These have been called ghost craters

(Tanaka et al. 2003) or quasi-circular depressions (QCD's, Figure 17) (Buczkowski et al., 2004). Arcuate wrinkle ridges found throughout Malea are assumed to form through deformation above buried impact craters (Buczkowski et al., 2004). The distribution of wrinkle ridges and ghost craters may reveal the extent of the lavas that form the plains units in Malea Planum. The number of ghost craters with smaller diameters increases towards the edge of the plain suggesting that the lavas thin towards the edges of the plain.

3.2.2.6 Vallis Units

The Vallis floor unit (AHv) includes the smooth flat deposits forming the floors of Mad Vallis -- a series of wide, sinuous, flat bottomed valleys along the eastern contact of Malea Planum and the Hellas Rim unit (Nhr). The valley walls are steep and locally scalloped. In places smooth deposits completely fill the valleys. The unit is sparsely cratered and deflation pits are common. Lineations in the deposits run parallel to the valley walls.

3.2.3 Hellas Planitia Assemblage

Massifs (Nhm) form rough mountains on the rim of Hellas basin and are mapped as Hellas massifs (Nhm). They are concentrated within the northern Hellas rim unit (Nhr) with a few isolated features in dissected unit 1 (Nd1). The lengths of the massifs range from a few meters to 100 km and they have heights up to 4 km. The massifs are interpreted to be remnant blocks of ejecta emplaced during the formation of the Hellas impact basin.

The Hellas rim unit (Nhr) forms the rim of the Hellas impact basin on the eastern and western sides of Malea Planum. It resembles the intercrater plains in the cratered highland units (Np_1); however, the Hellas rim unit (Nhr) contains numerous isolated massifs (Nhm). The Hellas rim unit has an average elevation 1 km lower than the cratered unit (Np_1). Small valleys and ridges are rare within the unit.

The Hellas basin floor unit (HNhf) forms smooth plains on the floor of Hellas basin with large, north trending ridges (250 m high) and a set of smaller ridges (100 m high) trending east (Figures 4 and 8). Shallow valleys (1 to 50 m deep) and a few deeper valleys (100 m deep) run parallel to the ridges (Figure 13).

3.2.4 Highland Plateau Assemblage

The Highland Plateau Assemblage consists of the units forming the cratered highlands surrounding Malea Planum. The cratered unit (Np_1) consists of heavily cratered plains that are roughly 1 kilometer higher than Malea Planum. Most of the craters lack ejecta and have flat floors. Some are buried by smooth intercrater plains or mantle material. Ghost craters (Figure 17) and eroded or buried rims are common. Some small ridges and sinuous valleys are found within the unit (Figure 4).

The subdued cratered unit (Np_2) (Leonard and Tanaka, 2001) forms highland plains similar to the cratered unit (Np_1) but contains fewer impact craters, more ridges, and more ghost craters (Figure 4). The contact between the cratered unit (Np_1) and the subdued cratered unit (Np_2) is defined by a break in slope. The flatter surface of the subdued cratered unit (Np_2) drops down a steep scarp 1 km to the Hellas rim unit (Nhr) which slopes down into Hellas basin.

3.2.5 Miscellaneous and Crater Materials

The highland massif unit (Nm) within the subdued cratered unit (Np_2) west of Malea Planum consists of isolated, roughly conical hills rising 900 m above the surrounding plains of the subdued cratered unit (Np_2) and two smaller hills to the south. The massifs are similar to several other features outside the mapped area to the west (Figure 18). These features are generally conical or elongated cones. Some have flat tops and some are arranged in a roughly linear pattern. Tanaka and Kolb (2001) observe that these mounds are oriented roughly concentric to Hellas basin and may be controlled by structures related to the impact. Head and Wilson (2002) identify several similar features in the north circumpolar region that may be volcanic in nature and possibly erupted sub-glacially.

The scarped unit (Ns) is a region of fractured terrain that forms the southern boundary of Malea Planum. It includes the scarps forming Dorsa Brevia and Pityusa Rupes (Figure 1). The scarps are linear and roughly concentric to the Hellas Impact basin. Individual scarp segments have heights up to 1 km and extend up to 200 km in length. No horizontal displacement is apparent.

In addition to the pedestal craters discussed above, craters on Malea Planum also display rampart and rayed morphologies (Figure 10). Rampart craters form when an object strikes a surface containing a significant amount of frozen water or other volatiles. The impact fluidizes the volatiles and forms a lobate ejecta pattern (Barlow et al., 2000). Rayed (or radial) craters form when the surface does not contain enough volatiles to liquefy. Craters with ejecta patterns that are still visible (pedestal, rampart, or rayed)

have been classified as younger crater materials (AHc). These craters are also distinguished by sharp rims that are intact to moderately degraded. The ejecta has often been mantled or mantled and exhumed. The crater floors are bowl shaped or filled with apron material lineated parallel to the crater walls. Some young craters contain central peaks.

The older crater material (Nc) consists of highly degraded crater rims and ejecta. No central peaks remain. The craters are usually filled with flat, smooth deposits.

3.3 Volcanic Features of Malea Planum

The highland paterae are a class of Martian volcanoes found only in the highlands (Greeley et al. 2000). They are interpreted to be low-relief, areally extensive, central-vent volcanoes and are thought to be the oldest central vent volcanoes on Mars based on crater counts conducted by Plescia and Saunders (1979). The paterae are characterized by low-shield morphologies, central caldera complexes, and radial valleys and ridges (Greeley et al. 2000) (Figure 12). The extremely low flank slopes (<2°) and easily eroded nature of their shield materials, suggests that their origin is pyroclastic rather than effusive (Gregg and Farley, 2006). The four paterae in the Malea Planum region -- Amphitrites, Peneus, Malea, and Pityusa paterae -- have unique characteristics that assist in interpreting the origins of the paterae. Table 1 compares major morphological features of the four paterae.

Amphitrites easily fits the description of a highland patera. It has a low shield with a slope of 0.5° – 1.2°, radial wrinkle ridges, and highly dissected flanks. The central caldera complex can be defined as a nested caldera because the geometric center of later

collapse calderas lies within the circumference of an earlier caldera (Crumpler et al., 1996). Evidence of at least two subsidence events can be seen. According to Greeley and Crown (1990), Amphitrites and Peneus sit on a structural ring of Hellas Basin along with Hadriaca Patera on the northeast rim of Hellas. Tyrrhena Patera, also on the northeast rim of the basin, sits on a second interpreted structural ring of Hellas (Greeley and Crown, 1990). Peneus Patera has a typical basaltic shield caldera morphology with a highly fractured rim with arcuate scarps and possible nested calderas that were buried following subsidence. However, Peneus lacks an areally extensive shield and dissected flanks. A few ridges may be radial to the caldera complex. Peneus has the shallowest central depression of the four paterae on Malea Planum.

Malea and Pityusa paterae have very similar morphologies. Both have similar diameters with radial and concentric wrinkle ridges. In contrast to Peneus and Amphitrites, the floors of Malea and Pityusa are below the regional topography. Neither is significantly dissected. Malea has a more complex shape than Pityusa that may result from overlapping subsidence events (the geometric center of the latest depression lies outside the circumference of the earlier depressions (Crumpler et al., 1996)). Arcuate scarps form a region of ridges comparable to horst and graben terrain on the northwest rim of Malea. A distinctive feature of Pityusa Patera is its southern rim which terminates in a steep scarp 1.5 km in height. Pityusa has the deepest central depression of the four paterae.

3.4 Comparison of Malea Planum Paterae with Volcanoes on Earth and Venus

The paterae on Mars appear to be unique features in the inner solar system. The term "patera" has been used to describe features on Mars, Venus, and the Jovian moon Io (Head et al., 1992). In its simplest definition a patera is a shallow depression with complex scalloped edges and little or no associated edifice. On Mars the term has evolved to describe broad, low, shield-like volcanoes with irregular summit craters. Using this definition, only a few features on Venus can be described as paterae (Head et al., 1992).

Volcanoes on Mars reach sizes that exceed anything found on Earth. The largest caldera found on Earth is the 77 km diameter Huckleberry Ridge ash-flow caldera in Yellowstone, which erupted high silica rhyolite ignimbrites. On the other hand, eruption products from Martian highland paterae are likely basaltic to andesitic, based on lava flow morphologies and thermal emission spectroscopy from the Mars Global Surveyor (Bandfield et al., 2000). The largest basaltic shield caldera on Earth has a diameter of 18.5 km (Radebaugh, 1999). Larger calderas on Earth may exist but they are difficult to recognize due to erosion (Crumpler et al., 1996). The depressions of Malea and Pityusa Paterae have topography comparable to some volcanic basins surrounding volcanoes on Earth. One example is the circular valley which surrounds Mt. Shasta in California (Heiken, 1976). The valley is about 90 km in diameter and a corresponding negative gravity anomaly suggests a mass of anomalously low density rock exists beneath the depression. The depression may have been formed by collapse when material was removed from a large magma chamber or series of chambers within a batholith (Heiken, 1976).

Pityusa and Malea Paterae resemble volcano-tectonic features known as coronae and arachnoids on Venus. A corona is a large, generally circular feature typically dominated by concentric tectonic features with a raised rim, a featureless central region, and a moat (e.g., Squyres et al., 1992). Twenty-five percent of coronae are a depression surrounded by a raised rim and another seven percent are a depression with no discernable rim (Grindrod and Hoogenboom, 2006). Most coronae have diameters less than 200 km. Watters and Janes (1995) have compared Alba patera and other circular fracture systems on Mars with Venusian coronae. They measured the annulus of fractures surrounding the features to be about 250 km in diameter, comparable to the diameters of Malea and Pityusa paterae. Figure 19 compares generalized profiles of coronae containing central depressions with the four paterae on Malea Planum. The profiles of Malea and Pityusa are most comparable to the coronae.

Arachnoids are circular patterns of fractures (Hamilton and Stofan, 1996) and ridges surrounding a topographic depression with extensional ridges extending radially away from the center (Aittola and Kostama, 2000). The ridges merge with regional ridge and fracture patterns (Head et al. 1992). Most arachnoids are 50-175 km in diameter with some greater than 200 km (Head et al., 1992). Malea and Pityusa paterae resemble arachnoids in that they also have radial ridge patterns that merge with regional ridge patterns.

3.5 Gravity Data

Figure 6 shows a free-air gravity anomaly map of Malea Planum (185 mGal at spherical harmonic degree 50) (Keifer, 2003). Positive anomalies are found spotted

throughout the cratered highlands, 1,000 km above the plain (units NP_1 and Np_2), and at Amphitrites Patera. The lowest gravity signature in the area is associated with the floor of the Hellas impact basin (unit HNhf). The positive anomaly centered over Amphitrites is one of the largest known anomalies in the southern hemisphere of Mars. The diameter of the anomaly is 500 to 600 km, elongated east-west (Walter S. Keifer, personal communication) and may include a slight positive anomaly associated with Peneus. Similar positive gravity anomalies exist over Tyrrhena, Hadriaca and Nili paterae on Mars, as well as mafic terrestrial volcanoes, such as Hawaii (Walker, 1988). Although Malea Patera is topographically low, it also appears to be the site of a small, circular, positive anomaly, and lies on a broad gravity ridge connecting Pityusa and Amphitrites. There is no significant gravity anomaly centered on Pityusa but a moderately high gravity annulus circles the topographic depression. In addition, unit HNr_2 is associated with a low gravity signature even though it is topographically one of the highest regions in Malea Planum.

4 GEOLOGIC HISTORY OF MALEA PLANUM

4.1 Noachian

The earliest geologic event in the region was the creation of the cratered highland terrain (Np_1) beginning ~4.0 Ga (Kring and Cohen, 2002). Heavy bombardment during the Noachian created a 2-3 km thick megaregolith of poorly consolidated breccia and ejecta (Mueller and Golombek, 2004). High obliquities of the Martian pole allowed ground ice to be stable globally (Mellon and Jakosky, 1995), causing the regolith to be ice-rich. The formation of outflow valleys in and adjacent to the cratered terrain is

evidence of volatiles in the regolith (Tanaka et al., 2002). Other evidence for high volatile content of the Noachian crust includes the abundance of young craters with fluidized ejecta (Tanaka et al., 2003). The cratered terrain is higher in elevation than most of Malea Planum with the exceptions of the rims of Amphitrites and Pityusa (Figure 1). The highlands were sparsely modified by ancient wrinkle ridges, such as the one at 29° 20'E, 54° S, which are thought have formed as the planet cooled and contracted (Mueller and Golombek, 2004).

Based on crater counts, the subdued crater unit (Np_2) was initially formed during the Noachian, however the sparsity of large impact craters compared to unit (Np_1) and the lower topographic elevation suggest the unit was modified after its creation, possibly through erosion. It is inferred that the highland massifs (Nm) formed by ice-volcano interaction during the early Noachian. These may be the oldest volcanic features in the region.

The formation of the Hellas impact basin later, during the mid- to late-Noachian, modified or buried the cratered highlands in the northeast map area. The rim of Hellas Basin (Nhr) is characterized by clusters of massifs (Nhm) surrounded by smooth plains. The massifs and associated terrain are missing in a section of the rim 1800 km wide north of Amphitrites and Peneus Paterae. It is likely that the rim of Hellas originally extended across Malea Planum at an elevation similar to the Hellas rim unit (Nhr) to the west and east. During the mid- to late- Noachian the material was destroyed or obliterated. The exact process is unclear. Simple burial by younger units is unlikely because the elevation of the Hellas rim in Malea Planum is approximately 1 km lower than the rim to the west and east. Tanaka et al. (2002) proposed that the dikes that eventually fed Amphitrites and

Peneus during the Hesperian caused the erosion of the rim. Heat from the dikes and sills intruding the friable, volatile-rich megabreccias and ejecta of the basin rim melted interstitial ices of H_2O, CO_2, and CO_2 clathrate. The debris was fluidized and flowed into the adjacent impact basin, contributing to the formation of the Hellas basin floor unit (HNhf). Subsequent eruptions of lava plains that were later eroded to form Nd1, lavas from Amphitrites and possibly Peneus covered the eroded surface (Tanaka et al. 2002) (Figure 20). Catastrophic erosion may account for the scarps that separate Malea Planum (units Nd_1, Nd_2, Nd_3, Nr_1, and HNr_2) from the Hellas rim (Nhr) cratered highlands (Np_1, and Np_2). If so, approximately 1 vertical km of material may have been removed from an area of 1.3 million km^2.

Buried ghost craters on Malea Planum indicate that if the erosional process proposed by Tanaka et al. (2002) occurred, a significant amount of time passed between the removal of the rim materials and the deposition of the lavas, or removal of the rim did not completely obliterate large craters. For example, a few craters straddle the border scarp between the plain and cratered highlands. Only arcuate wrinkle ridges or subdued rims mark the locations of these craters in the younger plains, but the portion of the crater rim remaining in the highlands resembles other highland craters (Figure 16). The interiors of these craters form depressions similar to ghost craters.

4.2 Late Noachian-Early Hesperian

Based on crater counts (Appendix D) and past research (Leonard and Tanaka, 2001) volcanic activity in Malea Planum was very active at the end of the Noachian and beginning of the Hesperian. Much of the depression created by the removal of the Hellas

rim was likely covered by flood lavas, which formed the ridged plains units (Nr_1 and Nr_2) and the initial surfaces of the dissected plains units (Nd_1, Nd_2, and Nd_3) that were later modified by channeling, however, vents and flow fronts were not detected. The lack of evidence for embayment of Amphitrites and Peneus by the ridged plains suggests that the flood lavas were emplaced prior to the development of the paterae or concurrent with them. Mangold et al. (2000) suggest that most wrinkle ridge formation on Mars was limited to the Hesperian based on cross cutting relationships. It is likely that the ridges deforming Malea Planum developed during this time as the weight of the lavas compressed weaker layers beneath (Tanaka and Leonard, 1995). Mangold et al. (2000) proposed that the timing of most wrinkle ridges on the planet is similar and the ridges may be the result of one planet-wide event such as thermal cooling of the martian interior.

Greeley and Spudis (1981) proposed that magma on Mars has to travel through water-charged megaregolith, resulting in phreatomagmatic eruptions of ash. Greeley et al. (2000) suggested that martian explosive volcanism, including the highland paterae, should produce widely dispersed, poorly consolidated deposits of fine material, forming broad, low-relief edifices. The fine-grained ash deposits would be easily eroded by dewatering of the lavas, and would form the valleys on the slopes of highland paterae (Crown and Greeley, 1993). A major pyroclastic stage appears to have been followed by effusive volcanism on other highland paterae. For example, a small amount of effusive lavas caps Tyrrhena Patera (Greeley and Crown, 1990).

Subsequent mantling on Peneus and Amphitrites has obscured any stratigraphic evidence that may have indicated which of the two paterae formed first. It is possible

that Amphitrites and the erosion of Amphitrites' flanks occurred first during a pyroclastic stage, and the much lower, undissected Peneus formed shortly after, during an effusive stage. Alternatively, the two formed concurrently, with flows from one interfingering with flows from the other. Crater frequency counts do not distinguish the ages of the two paterae (Appendix D) and no ridges or other features associated with one patera obviously superposes the features of the other.

If the crater frequency ages of the Dorsa Argentia formation (Nda) and the hilly unit (Hhi) are correct, their presence on the floor of Pityusa and Malea paterae implies that the depressions were in place earlier than the other two paterae by the late Noachian. The radial pattern of wrinkle ridges on the rims and flanks of the paterae suggests the ridges formed concurrent with the depressions in thin deposits or thinly bedded lavas or sediments (Mueller and Golombek, 2004). The wrinkle ridges appear to crosscut the flat-topped ridges on the northwest rim of Malea Patera and a profile of one ridge shows it has been deformed by the wrinkle ridges (Figure 14). The flat-topped ridges appear to be extentional features related to the subsidence of the Malea depression. A scalloped scarp forming the southern contact of the depression rims unit (HNdr) is concentric to the depression and may be related to the subsidence of the patera (Figure 15). The morphology of this scarp is different from the scarps forming Dorsa Brevia and Pityusa Rupes. The scarp south of Pityusa appears to be eroded, however Pityusa Patera is superposed over the apparently more intact ridges of Dorsa Brevia and Pityusa Rupes. A possible explanation is that the Pityusa scarp exposed a water ice rich layer beneath the capping layer of the Pityusa rim. Exposure to the atmosphere causes the ice to sublimate and the scarp to degrade. This layer may not be exposed in Dorsa Brevia or Pityusa

Rupes. There is no evidence for extrusive lava flows originating from Malea and Pityusa Paterae. Magmatism associated with the paterae may have been intrusive.

Crater frequencies place the formation of the dissected plains units (Nd_1, Nd_2, and Nd_3) at the end of the Noachian and possibly into the Hesperian (particularly Nd1). This also places the formation of Axius Valles in that time frame (Figure 13). Axius Valles may have formed as the Malea Planum lavas covering the rim of Hellas Basin were partially removed, exposing the volatile rich material beneath. This material then released the volatiles in liquid form, carving the valleys of Axius Valles. The concentration of valleys in the northern half of Malea Planum is possibly a result of increased slope as the plain tilts towards Hellas Basin. The number of valleys increases as the slope increases. Another possibility is that latitudes higher than 60 degrees are subjected to greater climate variability, melting (or sublimating) and freezing in repeated cycles. Water may collect at the base of the icy deposits in a process similar to basal melting of snow on Earth (Head and Wilson, 2002).

4.3 Hesperian

As the Hesperian continued, radial ridges formed on the slopes of Amphitrites and to a much lesser extent, radial to Peneus, deforming the units formed during the early Hesperian based on crater frequencies. These ridges cross-cut regional ridge systems trending N and E (Figure 8).

Radial valleys formed on the flanks of Amphitrites, defining the extent of the shield. Rare valleys also formed in the cratered highlands. Amphitrites' flanks were apparently more friable (Greeley et al., 2000) and more susceptible to erosion (or had a

higher moisture content) than the surrounding units. Similar valleys are found radial to Tyrrhena and Hadriaca Paterae (Greeley and Crown, 1990; Crown and Greeley, 1993). Three theories have been proposed for the origin of these valleys: 1) Primary structures formed during the deposition of the flank material (Gulick and Baker, 1990); 2) Secondary channeling occurred from dewatering of the volcanic material through sapping (Crown and Greeley, 1993); 3) Secondary valleys were carved by rain or snowfall (Crown and Greeley, 1993) as heat from the volcano caused basal melting of the ice (Figure 21). Groundwater sapping is more likely than rain or snowfall because of the amphitheater morphologies of the valley heads (Head and Wilson, 2002).

The oldest volatile-rich mantle deposits on Malea Planum may also be of Hesperian age but are possibly older (Leonard and Tanaka, 2001). Arvidson et al. (1976) believed these layers were mostly eolian dust mixed with some CO_2 and H_2O ice. However, recent comparisons of Martian landforms to ice-rich terrains on Earth (Head et al., 2003), and results from the gamma ray spectrometer on the Mars Odyssey spacecraft suggest a higher water content (up to 35%) (Day, 2002). The gamma ray spectrometer on board the Mars Odyssey spacecraft has measured backscattered neutrons from cosmic rays striking the planet's surface to find concentrations of hydrogen in near surface soils (Day, 2002). Gamma ray data implied soil water content greater than 10% for most of Malea Planum. Craters with fluidized ejecta patterns (Figure 10a), are found at all latitudes on Mars (Barlow et al., 2000), suggesting ground ice is a planet-wide phenomenon. Head and Wilson (2002) suggest that this cryosphere has existed since the late Noachian and any ice-rich deposits, such as the smooth plateaus, may have begun to form then.

Like Earth, the obliquity of Mars' axis changes over time, but the variations are much more extreme (from 14° to 48°) than for Earth, which causes episodic ice ages accompanied by an equator-ward migration of surface volatile deposits (Head et al. 2003). The mantle deposits are likely thin, blanketing layers of eolian dust and ice that form during Martian ice ages and sublimate or melt during inter-glacial periods (Head et al., 2003). The proximity of Malea Planum to the southern pole of Mars has apparently resulted in multiple mantling events during Martian ice ages. Evidence for multiple mantling events includes separate layers with varying thicknesses and extents, and layers superimposed on existing mantle erosional scarps, as can be seen on the floor of Malea Patera. The thickest mantle deposits are found poleward of 60° latitude and thinner deposits are found up to 30° latitude. Between 30 and 60 degrees the deposits are degraded and discontinuous (Head et al., 2003) (Figure 4). The thickest remnants in Malea Planum are found in the lowest elevations such as the Malea and Pityusa paterae depressions. Head and Pratt (2001b) propose that Hhi may represent the remnants of a massive polar deposit emplaced in the early to mid-Hesperian (~3.5 – 3.3 Ga). This episode created deposits up to one kilometer in thickness within a few 100 My. During the late Hesperian, changing climate conditions caused a large scale meltback and sublimation of Nda and Hhi. Mad Vallis possibly formed as water migrated to the base of these deposits and flowed into Hellas Planitia. Conditions later stabilized and meltback of the deposits slowed dramatically or ceased completely, leaving scattered remains north of 60° S and more continuous sheets to the south. Based on topographic relationships, Head and Pratt (2001b) believe that Hhi and Nda are topographically

continuous. However, in Pityusa patera, Nda appears to embay Hhi and is likely a younger deposit of mantle material.

Pedestal craters are found in every unit of the map area and are related to the mantle deposits (Figure 10). The ejecta of these craters is raised up to 100 m above the surrounding terrain while the base of the crater depression is below the level of the plains (Figure 10b and c). The rims of these craters can appear poorly preserved (Bleacher et al., 2000) or fresh (Mutch and Woronow, 1979). They probably form when a meteorite impacts a ground surface covered by loose or weakly cemented deposits. The crater ejecta forms a resistant cap on top of the weak layer. As the weak layer is regionally removed by eolian processes or sublimation, the portion of the layer beneath the crater ejecta is preserved producing a mesa with a scalloped margin (Figure 10) (Arvidson et al., 1976). The ejecta often appears truncated at the edges of a plateau. The volatile-rich, weak layer that is capped by ejecta is likely polar mantle material (Nda). In some cases, pedestal craters are perched on top of other mantle layers, indicating several mantling events. A cluster of craters at (64° S 39° E) and another at (58° S 32.5° E) sit on plateaus similar to pedestals (Figure 11). The ejecta surrounding these craters is very rough when compared to other pedestal craters and the plateaus are 200 to 300 m high. These pedestals, the hilly unit (Hhi) in Pityusa, and the rough plateau material (Nplr) are possibly remnants of the very thick polar deposit formed during the early to mid-Hesperian proposed by Head and Pratt (2001b).

4.4 Late Hesperian-Early Amazonian

Mad Vallis is a series of sinuous, flat bottomed valleys up to 25 km wide with steep walls that follows the eastern contact of Malea Planum and the Hellas rim unit (Nhr) (Figure 22). A lack of large craters in these valleys suggests they formed during the Hesperian to the early Amazonian (Leonard and Tanaka, 2001) following the formation of the volcanic constructs. Head and Pratt (2001b) attribute similar valleys flowing into Argyre basin to the melting of a very large, ancient polar deposit (the Dorsa Argentia formation, Nda). The valleys of Mad Vallis are discontinuous but generally run downhill from an occurrence of Nda in the southern map area. They may be connected to a series of shallow, sinuous valleys such as those found at 73.5° E, 61.5° S and 39° E, 55° S. The small valleys are a few meters to tens of meters wide and hundreds of kilometers long and are found throughout Malea Planum. These smaller valleys are concentrated in the dissected plains (Nd_1, Nd_2, and Nd_3) but are found in nearly every geologic unit on the plain. They follow the preexisting valleys of Axius Valles in dissected plains unit 1 (Nd_1) and are locally dendritic. The patchy distribution of the young, small, dendritic valleys bears resemblance to the basal melting of snow on Earth (Head and Wilson, 2002). They may have formed as water migrated to the base of an ice sheet and flowed laterally (Head and Pratt, 2001b).

The walls of Mad Vallis are locally scalloped and the valley is partially filled (Figure 22). Much of the fill material may be debris from the landslides that formed the scallops in the walls. This was later covered by younger mantle deposits that can be seen as a smooth or pitted surface in high resolution images.

4.5 Amazonian

The Amazonian epoch in Malea Planum is dominated by eolian processes and sparse cratering. Some Malea Planum surfaces, particularly the mantle deposits, have been etched by wind. Windstreaks and dust devil tracks are very common across all surfaces. High resolution MOC images show that isolated dune fields are found in low-lying areas such as craters and the floor of Pityusa Patera (Figure 9).

It is likely that mantling events, interrupted by periods of degradation, continued during the Amazonian. The youngest mantle deposits are the most continuous and can be found covering nearly every surface on Malea Planum with deposits only a few meters thick. Pitting of the Hesperian mantle deposits (Figure 5) possibly continued in the Amazonian.

4.6 Cratering

Impact cratering occurred throughout the history of Malea Planum. Impact rates were greatest during the Noachian and tapered off during the Hesperian and Amazonian (Kring and Cohen, 2002). Noachian craters have degraded rims, flat floors, and lack ejecta. Ejecta of Hesperian and Amazonian craters is visible but has been covered by mantle deposits that often obliterate much of the ejecta texture. Most pedestal craters are also likely Hesperian. The youngest Amazonian craters are rayed or rampart craters that show little or no mantling. Mantling events and lava flows are most likely responsible for the destruction of small craters.

5 DISCUSSION

5.1 Evolution of Amphitrites Patera

Of the volcanic features on Malea Planum, Amphitrites Patera bears the most resemblance to the highland paterae. Our crater data suggests that Amphitrites formed during the Hesperian, when most highland paterae were thought to have formed (Tanaka et al., 1992). Other highland volcanoes have central calderas on top of low shields that have been carved by numerous valleys (Greeley et al., 2000), and are thought to be composed of easily eroded mafic pyroclastic rocks that formed as rising magma interacted with water in the crust (Francis and Wood, 1982). Explosive basaltic volcanism on Earth is typically weak due to the low volatile content, low volatile content and viscosity of basalt (Greeley et al., 2000). However, the lower atmospheric pressure and lower gravity on Mars might enable mafic magmas to be explosive even with relatively low water contents (Mitchell and Wilson, 2001). Francis and Wood (1982) suggested that phreatomagmatic eruptions formed the highland paterae. Such eruptions are driven by explosive interaction of hot magma with volatiles in the subsurface. If Amphitrites is the result of phreatomagmatic explosions, then the flank valleys may be the result of dewatering of the wet tephra. Steam may have recondensed immediately above the still hot deposits and eroded the narrow valleys before it sublimated, sank into the ground or evaporated. The valleys on Amphitrites are more numerous on the eastern flanks (Figure 13). Prevailing winds may have controlled the distribution of valleys on the volcano as snow or rain that formed from the steam collected preferentially on the eastern flanks (Figure 21). If the precipitation fell as snow, the radial valleys may have formed as heat released from the volcanic center caused basal melting of the ice.

Amphitrites' caldera is probably a 'stepped funnel' similar to the calderas of some Hawaiian volcanoes. Walker (1988) identified the calderas of Kilauea and Koolau volcanoes as stepped funnel calderas that formed through a combination of collapse over evacuated magma chambers and loading by dense intrusions along the magma conduits. They are marked by a centripetal dip in lava flows within the caldera and arcuate faults surrounding and within the subsided area. In addition, smaller arcuate faults may be found outside the caldera as on Kilauea (Figure 23a). The positions of arcuate faults resemble those in the stepped funnel model proposed by Walker (1988), including arcuate scarps ringing the caldera depression and several smaller scarps within the caldera and on the flanks of the volcano (Figure 23). The interior walls of Amphitrites' caldera are gentle slopes punctuated by steep scarps.

The arcuate scarps on the flanks of the patera may be expected to step down towards the center of the volcano, in common with other caldera faults. However, a few of these scarps step down away from the center of the volcano (Figure 2). The scarps may have become reverse faults as caldera subsidence was reversed, creating an inversion of the caldera floor. In THEMIS images of the eastern flanks of Amphitrites, shallow channels appear to crosscut an arcuate scarp. Channeling on the flanks may have developed previous to the formation of the scarps and the formation of the caldera.

The high positive gravity anomaly centered over Amphitrites may be attributed to a buried high density mass beneath the volcano. Areas with similar altitudes in the cratered highlands and on the rim of Pityusa Patera have gravity anomalies much smaller than Amphitrites'. Keifer (2003) found anomalies of a magnitude similar to Amphitrites' beneath other highland paterae and attributed them to very large, buried magma chambers

up to many times the diameter of the caldera. It is possible that the gravity anomaly is due in part to a dense system of solidified magma chambers, dikes and sills rather than a single, large, solidified magma chamber (Walker, 1988) (Figure 23 A). The close correspondence of topography and gravity suggests the load is supported by a strong lithosphere.

5.2 Evolution of Peneus Patera

Peneus formed during the late Noachian to early Hesperian (Appendix D). Peneus' caldera is a flat-floored, circular depression ringed by a succession of nearly vertical, arcuate fault scarps (Figure 3). The floor of Peneus appears to be essentially coherent; however, arcuate wrinkle ridges may indicate locations of subsidence faults that were later buried (Figure 3a). The main caldera appears to have formed as a coherent piston collapse caldera, in which a coherent block subsided along a series of well-defined, ring faults (Figure 23 C). Later, two smaller subsidence features formed but were nearly buried by subsequent eruptions. Many silicic calderas with ashflows on Earth appear have formed by piston collapse (Roche et al., 2000). Later subsidence created radial wrinkle ridges over the small interior caldera. Uplift along some ring fault blocks also suggests later compression induced by subsidence of the entire volcano.

Compared with the large gravity anomaly associated with Amphitrites, the anomaly over Peneus Patera is very small. This suggests that if there is a dense system of magma chambers, dikes, and sills beneath Peneus it is much smaller than the system that may exist beneath Amphitrites, or the load has been mostly compensated.

5.3 Evolution of Malea and Pityusa Paterae

Malea and Pityusa Paterae were first discovered in Earth-based telescopic observations (e.g., Antoniadi, 1930). Recent higher resolution images and topographic data have brought the volcanic origin of the paterae into question. While Pityusa's central depression is located on a significant topographic edifice (Figure 1) and Malea's rim is punctuated by arcuate scarps (Figures 8 and 14) similar to caldera subsidence scarps, they have little else in common with other Martian volcanoes. Both lack radial flow-like features that are often associated with volcanic calderas. If they are calderas, they would be the largest on Mars. The floors of Malea and Pityusa are below the surrounding plain, unlike Peneus and Amphitrites Paterae and most terrestrial calderas (Table 1). The diameters of the depressions are more similar to large impact craters than volcanic calderas; however, the morphology of their rims does not resemble those of buried impact craters. Malea Patera formed during the late Noachian and Pityusa Paterae formed during the late Noachian to late Hesperian (Appendix D). They may have formed at a time when the lithosphere was thin and easily deformed. Malea Patera is associated with an elongated, moderately high gravity anomaly, but Pityusa has, at most, only a weak, annular, positive anomaly. Both are significantly lower than the anomaly over Amphitrites (Figure 6). This suggests that either significant high density intrusive complexes do not exist beneath Malea and Pityusa Paterae, or that the loads have been compensated by subsidence. Several possibilities are outlined below that may explain the origins of the Malea and Pityusa depressions (Figure 24). Each is then discussed in detail.

A. *Surface Load:* The depressions may simply be impact craters that filled with high density material (basaltic lava) and sagged into the crust, as has occurred in some lunar (Freed et al., 2001) and martian (Mauldin and Grimm, 1995) impact craters (Figure 24 A-B).

They may be locations of sagduction (Chardon et al., 1998), where, dense lavas were pulled gravitationally back through the less dense lower crust (Figure 24c).

B. *Subsurface Load:* The crust under these features has sagged due to the intrusion, solidification, and subsidence of high density sills (Walker et al., 1988), similar to sills proposed beneath the eastern Snake River Plain in Idaho (McQuarrie and Rodgers, 1998).

C. *Caldera Collapse:* They may be collapse calderas formed as a result of the draining of large magma chambers, accompanied by subsidence of the crust as dense volcanic material accumulated (Figures 23 and 24e).

D. *Mantle Plumes:* Mantle plumes developed beneath the crust, then cooled, contracted, and deformed the crust, similar to the processes that formed coronae and arachnoids on Venus (Squyres et al., 1992).

5.3.1 Loading by dense lavas at the surface

5.3.1.1 Sagged Impact Craters

The depressions of Malea and Pityusa may have evolved from impact basins that formed prior to eruptions of flood lavas of the ridged plains (Nr_1). Filling with dense lavas could have caused them to subside into the thermally weakened crust. Crater frequencies suggest Malea and Pityusa Paterae predate the formation of Peneus and

Amphitrites. Crater counts give a Noachian age for surfaces associated with Malea Paterae, comparable to the surrounding plains (Nr1). The ages of surfaces associated with Pityusa Paterae are late Noachian to early Hesperian, closer to those obtained for the ridged plains surrounding Pityusa ($HNr_{2,}$ Figure 4).

If Malea and Pityusa Paterae are impact craters filled with volcanic material, we can expect them to share traits with lunar impact basins known to be filled with basalts. Like impact basins, both Malea and Pityusa are nearly circular, but Malea appears to be a composite of at least two sub-circular features (Figure 14). Their current maximum depths are comparable to fresh impact craters of similar diameters on Mars. Filled impact craters can be expected to have shallower depths than fresh craters. Many flooded lunar basins have compressional ridges within the flooded basin material and extensional features (linear rilles) on the edges of the floors (Solomon and Head, 1980). Both Hellas and Isidis basins on Mars also show evidence of extension on their rims and compression on their floors (Wichman and Schultz, 1989). The arcuate scarps on the northwest rim of Malea Patera could be interpreted as a region of rim extension (Figure 14). No extensional features are apparent on Pityusa. Some wrinkle ridges are visible through the thin mantle deposits covering the floor of Malea Patera but any ridges on the floor of Pityusa have been covered by thicker mantle deposits. Some ridges on the walls of the depression extend up to the mantle deposits. No rim materials or ring structures appear to protrude through the fill material of lunar impact basins (Plescia, 2003). Neither Pityusa nor Malea Patera has evidence of any ejecta or impact basin structural rings.

Some of the basalt-filled lunar craters are the sites of mascons, positive gravity anomalies flanked by annular gravity lows in topographic depressions (Keifer, 1999). One model attributes the anomalies to the uncompensated, high-density flood basalts filling the basins (Conel and Holstrom, 1968) (Figure 24a). In a second model, the anomaly is a plug of uplifted mantle material formed during impact (Phillips and Dvorak, 1981). A combination of the two models may also be responsible (Keifer, 1999). Most craters on Mars lack positive gravity anomalies however, suggesting this isn't the case (Figure 6). The slight positive anomaly, approximately +65 mGals, centered over Malea Patera (Figure 6) is much smaller than the positive gravity anomalies centered on lunar mascons (>140 mGals for Imbrium basin, 75^{th} degree) (Potts and von Frese, 2003). Moreover, there is no low-gravity annulus surrounding the Malea Patera anomaly. A slight gravity low is centered on Pityusa and is flanked by a high gravity annulus.

Subsidence models indicate that when a surface load (such as a series of lava flows) is placed within a basin, not only will the floor of the impact basin subside, but the topographic elevation of the upper surface of basin fill should increase because of thickening of the buoyant crust (Turcotte and Schubert, 1982; Lillie, 1999) (Figure 24b). If the loading of the basin is confined to the surface, the basin should fill and become a topographic high (McQuarrie and Rodgers, 1998). Pityusa and Malea Paterae are topographic lows. In short, the tectonic features, topography, and gravity anomalies do not support the origin of Malea and Pityusa paterae as subsided impact basins.

5.3.1.2 Sagduction

Structures within Archean greenstone belts on Earth show radial convergence and downward flow with respect to the underlying granite and gneiss basement rocks

according to Chardon et al. (1998). They believe that these structures may have developed when hot spots placed dense, mafic lavas on young, thermally weakened, lower density, granitic basement. The mafic material then sank back partially through the crust, forming a radially furrowed pattern analogous to a tablecloth being pulled down through a hole in a table (Chardon et al., 1998) (Figure 24c). This process has been called sagduction. Thermal emission spectroscopy has indicated that the Martian southern highlands are largely basaltic in composition (Bandfield et al., 2000). Sagduction of basalt may be a possibility if the basement underlying newly emplaced mafic lavas is composed of low density, weak megabreccia. Radial ridges associated with sagduction are sinusoidal in cross section. The wrinkle ridges radial to Malea and Pityusa are asymmetric in cross section, indicating that the wrinkle ridges around Malea and Pityusa are not likely the result of sagduction. A high gravity anomaly may be expected over a column of high density material sinking through lower density crust, unless the subsidence went to completion. The lack of a positive anomaly associated with Pityusa suggests it was not formed through sagduction.

5.3.2 Mid-Crustal Sill

The eastern Snake River Plain in Idaho is a topographic trough partially filled with basaltic and rhyolitic volcanic rocks interbedded with sediments. The plain is the site of a positive gravity anomaly (McQuarrie and Rodgers, 1998). McQuarrie and Rodgers (1998) submitted evidence that the Snake River Plain is subsiding, including elevation, tilted ash-flow sheets, and tilting of fold axes in adjacent mountain ranges. They suggest the subsidence is caused by the emplacement of a 17-25 km thick, dense,

mafic sill in the mid-crust. Another explanation is that a complex of many sills intruded over a prolonged time (Shervais et al., 2006).

Malea Patera is the site of a positive gravity anomaly; however the lack of a positive anomaly associated with Pityusa indicates either that a large sill does not exist beneath the depression, or that the load has been gravitationally compensated. The eastern Snake River Plain is elliptical (Shervais et al., 2006) while Malea and Pityusa are circular. The different shapes could be explained by plate tectonics on Earth. A plate moving over a fixed source on Earth would result in the emplacement of an elliptical sill complex but a lack of moving plates on Mars would allow the sill complex to remain sub-circular. Head and Wilson (2002) suggest that in the highlands a layer of breccia overlies a fractured basement which becomes annealed at depth. The base of the fractured basement is 50km below the surface. This boundary may be a contrast that provides a location for the formation of sills in the martian crust (Figure 24d).

5.3.3 Collapse Calderas

A second possibility is that Malea and Pityusa Paterae are volcanic collapse calderas (Figure 24e). The arcuate horst and graben structures on Malea are comparable to the complex structures of collapse calderas. Malea's basin has a shape similar to a collapse caldera with two overlapping subsidence events. The pattern of radial wrinkle ridges on both Malea and Pityusa resembles the radial ridges on Amphitrites. The proximity of Malea and Pityusa to other volcanic features supports the possibility of a volcano-tectonic origin, however there are no lava flow features that can be directly associated with the paterae. Also, caldera walls and margins are not well defined for the

paterae. They may have been eroded or blanketed, or never did form by traditional caldera collapse mechanisms. Both depressions are greater than 200 km in diameter from rim crest to crest. This is twice as large as the largest accepted caldera on Mars, Arsia Mons (115 km) (Crumpler et al., 1996). There are few examples of calderas of this size anywhere else on Mars or in the solar system. However, volcanic subsidence of this extent has been suggested to explain a circular basin surrounding at least one terrestrial silicic volcano, Mount Shasta, resulting from collapse over a batholith that was partially drained from the emplacement of surface volcanic formations (Heiken, 1976).

5.3.4 Surface Expression of a Mantle Plume

Coronae and arachnoids are large, sub-circular features on Venus that appear to have volcano-tectonic origins (Head et al., 1992). Coronae range in diameter from less than 200 km to at least 1000 km (Squyres et al., 1992). One possible corona, Artemis, has a diameter of 2600 km but most are less than 200 km (Head et al., 1992). A corona is characterized by an elevated wreath of extensional deformation features that surrounds a central, less deformed region that is higher or lower than the surrounding plain (Squyres et al., 1992). Arachnoids are similar to coronae; however, they have a smaller average diameter (115 km) and long radial fractures or compressional ridges (Head et al., 1992) that extend up to several radii beyond the circumferential fractures (Hamilton and Stofan, 1996). The fractures often merge with regional fracture or ridge belts (Head et al., 1992). Hamilton and Stofan (1996) observe that while the topography of arachnoids is variable, most are depressions. Aittola and Kostama (2000) note that volcanic features, such as small interior cones or lobate flows, are commonly associated with coronae but are rare

around arachnoids. In most arachnoids there is little evidence of a central volcanic edifice or of radial flows emanating from a central source, leading Head et al. (1992) to believe that if any magmatism is associated with arachnoids, it is intrusive. The elevated topography, volcanism, circular shape, and extensional tectonism of coronae has led researchers to believe that mantle upwelling is a possible mechanism of coronae formation (Grindrod and Hoogenboom, 2006) (Figure 24f).

Malea and Pityusa Paterae are comparable in size and profile to some coronae but are morphologically similar to arachnoids. Twenty-five percent of Venusian coronae have a rim surrounding a central depression and another 7% are depressions that lack significant rims (Figure 19) (Hoogenboom and Houseman, 2006). A topographic profile of Pityusa resembles the profile of a corona with a rim surrounding a depression. Malea appears to be a depression without a significant rim (Figure 19). Like many arachnoids, the paterae have central depressions with circumferential compressional ridges close to the depression and radial compressional ridges that appear to be continuous with regional ridge patterns (Figure 8). No clearly extrusive central vent volcanic features have been observed associated with the paterae other than the regional ridged plains (Nr_1 and HNr_2). If the paterae are related to an upwelling of mantle material, any magmatism has been intrusive. Volcanic plains, such as those surrounding Malea and Pityusa Paterae, have not been associated with Venusian coronae. A withdrawal of mantle material and the cooling and subsidence of any intrusive magma bodies, or the plume itself, both may have contributed to the formation of a topographic depression ringed by an elevated deformation wreath. Models developed by Hoogenboom and Houseman (2006) show that negative free-air gravity anomalies almost always develop over subsiding mantle

plumes. While Pityusa may have a slight negative signature, Malea's gravity signature is positive.

5.3.5 Summary

The topographic, gravity, and tectonic features of Malea and Pityusa Paterae do not fit any of the above models precisely enough to decisively suggest a method of formation. However, in view of these associations and arguments, we conclude that a mid-crustal sill complex similar to that thought to exist beneath the eastern Snake River Plain in Idaho may be the best explanation for the formation of Malea and Pityusa Paterae. The walls of the paterae slope inward with increasing slope towards the center, similar to the topography bordering the ESRP. The high gravity anomalies over the paterae can be explained by this method of formation, although the weak anomaly associated with Pityusa suggests the load has been gravitationally compensated.

6 CONCLUSIONS

The geology of the Malea Planum Region has been influenced by impact cratering, volcanic, tectonic, and fluvial processes, and most recently, eolian processes. The beginning of the Noachian was dominated by intense impact cratering. During the mid-Noachian, formation of the Hellas impact basin obliterated the cratered terrain in the northeast map area. The basin was ringed by rugged terrain including massifs and concentric expansional scarps. In the mid to late Noachian, the southern rim of Hellas was obliterated. This was likely the result of sills migrating upward through the crust that had been fractured by the formation of Hellas Planitia. The sills melted and vaporized

H_2O and CO_2 in the crust. The liquefied debris flowed into Hellas basin leaving a new surface one kilometer lower than the original rim height (Tanaka et al., 2002). Eruptions of flood lavas covered the eroded surface of the depression left by the removal of the Hellas rim, forming a lobate flow front in Mitchel crater (Figure 16). Subsidence and compression of the lavas formed blind thrust faults expressed as wrinkle ridges oriented roughly ENE on the surface of the plain. Malea and Pityusa paterae formed following the emplacement of the lavas. Radial and concentric wrinkle ridges on the rims of the two paterae formed in the layered flows. The floors of the paterae were later filled and the wrinkle ridges covered, possibly by lavas from Amphitrites and Peneus in Malea and thick mantle material in Pityusa.

The beginning of the Hesperian was marked by an onset of central vent volcanic activity on Malea Planum. Peneus and Amphitrites erupted on an interpreted structural ring of Hellas basin. It is unclear which patera formed first or if the volcanoes were concurrent. Peneus has a collapse caldera on a low edifice while Amphitrites consists of a stepped funnel caldera on a significant shield. Amphitrites is probably an example of mafic pyroclastic volcanism typical of other highland patera. Lavas originating from Peneus were likely more effusive. Erosion of the lavas covering the rim of Hellas basin north of Peneus and Amphitrites may have exposed the underlying, volatile-rich material, allowing it to dewater and form Axius Valles.

During the mid-Hesperian, southern Malea Planum may have been covered by a very thick polar mantle deposit. The deposit melted and sublimated during the late Hesperian, forming Mad Valles and possibly utilizing the existing valleys of Axius Valles. Remnants of this thick polar deposit may include the hilly unit (Hhi) in Pityusa

Patera, the Dorsa Argentia formation (Nda), and impact craters resting on thick, rough pedestals. Smaller episodes of polar mantle deposition continued through the Amazonian to the present. Evidence of these includes meters-high blankets of smooth material and pedestal craters found across most of Malea Planum. Shallow valley networks were possibly formed by basal melting of these smaller mantling deposits. The Amazonian is also characterized by eolian activity creating dune fields, etched surfaces, and dust devil tracks.

Based on the topographic evidence, Malea and Pityusa paterae are most likely regions that sagged due to an imposed load. A lack of associated flow features on the surface suggests that the load is the result of an accumulation of dense intrusions. A surficial load is insufficient to cause the amount of subsidence observed. A mid-crustal mafic or ultra-mafic sill or a dense network of sills and dikes may have contributed to the subsidence.

The increase in the size of positive gravity anomalies from Pityusa to Malea to Amphitrites may suggest an increase in the strength of the lithosphere. The lack of a positive gravity signature over the oldest, Pityusa, suggests the load beneath it has been nearly compensated. Malea is partially compensated and Amphitrites is uncompensated.

Additional crater counting using craters with diameters less than 5 km will further refine the ages of the geologic units of Malea Planum. Future nighttime infrared images and high resolution images from THEMIS and MOC may assist in refining the sequence of geologic events. Data from the European Space Agency's current Mars Express mission, including high resolution stereo images of the surface and a mineral mapping

spectrometer (SciTech Web Team, 2006) will also assist future research in refining the geology of the area.

References Cited

Aittola, M., and V.P. Kostama, 2000, Comparison of Venusian novae and arachnoids: Proceedings of the Lunar and Planetary Science Conference 31st, abstract 1093.

Antoniadi, E.M., 1930, Map of albedo features of Mars, (plates 2-5): In La Planéte Mars, Librairie Scientifique, Hermann et Cie., Paris.

Arvidson, R.E., M. Coradini, A. Carusi, A. Coradini, M. Fulchignoni, C. Federico, R. Funiciello, and M. Salomone, 1976, Latitudinal variation of wind erosion of crater ejecta deposits on Mars: Icarus, v. 27, p. 503-516.

Bandfield, J.L., V.E. Hamilton, and P.R. Christensen, 2000, A global view of Martian surface compositions from MGS-TES: Science, v. 287, p. 1626-1630.

Barlow, N.G., J.M. Boyce, F.M. Costard, R.A. Craddock, J.B. Garvin, S.E.J. Sakimoto, R.O. Kuzmin, D.J. Roddy, L.A. Soderblom, 2000, Standardizing the nomenclature of Martian impact crater morphologies: Journal of Geophysical Research, v. 105, p. 26,733-26,738.

Bleacher, J.E., J.B. Garvin, and S.E.J. Sakimoto, 2000, South polar pedestal craters on Mars: Implications for the south polar erosional regimes from Mars Orbiter Laser Altimeter (MOLA) data: Lunar and Planetary Science Conference XXXI Abstracts, no. 1964.

Buczkowski, D.L., H.V. Frey, J.H. Roark, and G.E. McGill, 2004, Topographic analysis of quasi-circular depressions around the Utopia Basin, Mars: Lunar and Planetary Science Conference Abstracts, No. 1150.

Chardon, D., P. Choukroune, and M. Jayananda, 1998, Sinking of the Dharwar Basin (South India): implications for Archean tectonics: Precambrian Research, v. 91, p. 15-39.

Christensen, P.R., N.S., Gorelick, G.L., Mehall, and K.C., Murray, 2005, *THEMIS Public Data Releases*, Accessed 12 November 2005 from the Planetary Data System Node, Arizona State University: http://themis.asu.edu/.

Conel, J.E., and G.B. Holstrom, 1968, Lunar mascons—A near-surface interpretation: Science, v. 162, p. 1403-1405.

Crown, D.A., and R.Greeley, 1993, Volcanic Geology of Hadriaca Patera and the Eastern Hellas Region of Mars: Journal of Geophysical Research, v. 98, p. 3431-3451.

Crumpler, L.S., J.W. Head, and J.C. Aubele, 1996, Calderas on Mars: characteristics, structure, and associated flank deformation: In Volcano Instability on Earth and Other Planets (eds. McGuire, W.J., A.P. Jones, and J. Neuberg), Geological Society of London Special Publication, no. 110, p. 307-348.

Day, C, 2002, Remotely sensed neutrons and gamma rays reveal ice beneath the Martian surface: Physics Today, v. 55, p. 16-17.

Francis, P.W., and C.A. Wood, 1982, Absence of silicic volcanism on Mars: Implications for crustal composition and volatile abundance: Journal of Geophysical Research, v. 87, p. 9881-9889.

Freed, A.M., H.J. Melosh, and S.C. Solomon, 2001, Tectonics of mascon loading: Resolution of the strike-slip faulting paradox: Journal of Geophysical Research, v. 106, p. 20,603-20,620.

Garcia, P., 2005, *PDS Map-a-Planet Mars Levels Page*, Accessed 12 November 2005 from the U. S. Geological Survey and National Aeronautics and Space Administration Astrogeology Research Program website: http://pdsmaps.wr.usgs.gov/maps.html.

Greeley, R., and D.A. Crown, 1990, Volcanic Geology of Tyrrhena Patera, Mars: Journal of Geophysical Research, v. 95, p. 7133-7149.

Greeley, R., and P.D. Spudis, 1981, Volcanism on Mars: Reviews of Geophysics and Space Physics, v. 18, p. 13-41.

Greeley, R., N.T. Bridges, D.A. Crown, L. Crumpler, S.A. Fagents, P.J. Mouginis-Mark, and J.R. Zimbelman, 2000, Volcanism on the Red Planet: Mars in environmental effects on volcanic eruptions: From deep oceans to deep space, J.R. Zimbelman and Gregg, eds., New York, Kluwer Academic/Plenum Publishers, p. 75-112.

Gregg, T.K.P., and M.A. Farley, 2006, Mafic pyroclastic flows at Tyrrhena Patera, Mars: Constraints from observations and models: Journal of Volcanology and Geothermal Research, v. 155, p. 81-89.

Grindrod, P.M., and T. Hoogenboom, 2006, The corona conundrum: Astronomy and Geophysics, v. 47, p. 3.16-3.21.

Gulick, V.C., and V.R. Baker, 1990, Origin and evolution of valleys on Martian volcanoes: Journal of Geophysical Research, v. 95, p. 14,325-14,344.

Hamilton, V.E., and E.R. Stofan, 1996, Global characteristics of "Arachnoids" on Venus: Proceedings of the Lunar and Planetary Science Conference 27th, p. 483-484.

Head, J.W., L.S. Crumpler, J.C. Aubele, J.E. Guest, and R.S. Saunders, 1992, Venus volcanism: Classification of volcanic features and structures, associations, and global distribution from Magellan data: Journal of Geophysical Research, v. 97, p. 13,153-13,197.

Head, J.W., J.F. Mustard, M.A. Kreslavsky, R.E. Milliken, and D.R. Marchant, 2003, Recent Ice Ages on Mars: Nature, v. 426, p. 797-802.

Head, J. W. III, and S. Pratt, 2001a, Malea Planum Hesperian volcanic province: Characterization using MOLA data: Proceedings of the Lunar and Planetary Science Conference XXXII Abstracts, no. 1627.

Head, J. W. III, and S. Pratt, 2001b, Extensive Hesperian-aged south polar ice sheet on Mars: Evidence for massive melting and retreat, and lateral flow and ponding of meltwater: Journal of Geophysical Research, v. 106, p. 12,275-12,299.

Head, J.W. III, and L. Wilson, 2002, Mars: a review and synthesis of general environments and geological settings of magma-H_2O interactions, in J. L. Smellie and M. G. Chapman, eds., Volcano-Ice Interaction on Earth and Mars, Geological Society of London, Special Publications no. 202, p. 27-57.

Heiken, G., 1976, Depressions surrounding volcanic fields: A reflection of underlying batholiths?: Geology, v. 4, p. 568-572.

Hoogenboom, T, and G.A. Houseman, 2006, Rayleigh-Taylor instability as a mechanism for corona formation on Venus; Icarus, v. 180, p. 292-307.

Ivanov, M.A., J. Korteniemi, V.P., Kostama, M. Aittola, J. Raitala, M. Glamoclija, L. Marinangeli, and G. Neukum, 2005, Major episodes of the hydrologic history in the region of Hesperia Planum, Mars: Journal of Geophysical Research, v. 110, no. E12S21.

Keifer, W.S., 1999, Lunar gravity models: Large, near side impact basins: Lunar and Planetary Science Conference XXX Abstracts, no. 1995.

Keifer, W.S., 2003, Gravity evidence for extinct magma chamber systems on Mars, Proceedings of the Sixth International Conference on Mars, no. 3252.

Keifer, W. S., 2005, personal communication from kiefer@lpis53.usra.edu, 2/11/2005.

King, E.A., 1978, Geologic Map of the Mare Tyrrhena quadrangle of Mars, U.S. Geological Survey Miscellaneous Investigation Series Map I- 1073.

Kirk, R., and E.M. Lee, 2005, *MDIM 2.1: Mars Global Digital Image Mosaic*, Accessed 11 November 2005 from the USGS Astrogeology Research Program website: http://astrogeology.usgs.gov/Projects/MDIM21 .

Kring, D.A., and B.A. Cohen, 2002, Cataclysmic bombardment throughout the inner solar system 3.9-4.0 Ga: Journal of Geophysical Research, v. 107, p. 4-1 – 4-6.

Lemoine, F.G., and D.E. Smith, 2001, Reduced data from Mars Global Surveyor Radio Science Investigations: File GGM1025A, http://www.igpp.ucla.edu/cgi-bin/ditdos?volume=MORS_1015&folder=SHA&style=full

Leonard, G. J., and K.L. Tanaka, 2001, Geologic Map of the Hellas Region of Mars: U.S. Geological Survey Miscellaneous Investigation Series Map I- 2694, scale 1:5,000,000.

Lillie, R.J., 1999, Whole Earth Geophysics: An Introductory Textbook for Geologists and Geophysicists, Upper Saddle River, New Jersey, Prentice-Hall, 361 p.

Mangold, N., P. Allemand, P.G. Thomas, and G. Vidal, 2000, Chronology of compressional deformation on Mars: Evidence for a single and global origin: Planetary and Space Science, v. 48, p. 1201-1211.

Mauldin, L.C., and R.E., Grimm, 1995, Crustal and Lithospheric Structure of Martian Impact Basins, Abstracts of Papers Submitted to the Lunar and Planetary Science Conference, v. 26, p. 911-912.

McQuarrie, N., and D.W. Rodgers, 1998, Subsidence of a volcanic basin by flexure and lower crustal flow: The eastern Snake River Plain, Idaho: Tectonics, v. 17, no. 2, p. 203-220.

Mellon, M.T., and B.M. Jakosky, 1995, The distribution and behavior of Martian ground ice during past and present epochs: Journal of Geophysical Research, v. 100, p. 11,781-11,799.

Mitchell, K.L., and L. Wilson, 2001, Explosive volcanic eruptions on Mars: Misconceptions and new insights: Lunar and Planetary Science Conference XXXII Abstracts, no. 1190.

Mueller, K., and M. Golombek, 2004, Compressional structures on Mars: Annual Review of Earth and Planetary Sciences, v. 32, p. 435-464.

Mutch, P., and A. Woronow, 1979, Martian rampart and pedestal craters' ejecta-emplacement: Coprates Quadrangle: Icarus, v. 41, p., 259-268.

Phillips, R.J., and J. Dvorak, 1981, The origin of lunar mascons: Analysis of the Bouguer gravity associated with Grimaldi, in Schultz, P.H., and Merrill, R.B., eds., Proceedings of the Conference on Multi-ring Basins, formation and evolution, New York, Pergamon Press, p. 91-104.

Planetary Geomatics Group, 2005, *Gazetteer of Planetary Nomenclature*, Accessed 12 November 2005 from the U. S. Geological Survey and National Aeronautics and Space Administration Astrogeology Research Program website: http://planetarynames.wr.usgs.gov.

Plescia, J. B., 2003, Amphitrites-Peneus Paterae / Malea Planum geology: Lunar and Planetary Science Conference XXXIV Abstracts, no. 1478.

Plescia, J. B., and R.S. Saunders, 1979, The chronology of Martian volcanoes: Proceedings of the 10th Lunar and Planetary Science Conference, p. 2841-2859.

Potts, L.V., and R.R.B. von Frese, 2003, Comprehensive mass modeling of the Moon from spectrally correlated free-air and terrain gravity data: Journal of Geophysical Research, v. 108, p. 5-1 - 5-27.

Radebaugh, J., 1999, Terrestrial pluton and planetary caldera sizes: Implications for the origins of calderas: M.S. Thesis, Brigham Young University, 180 p.

Roche, O., T.H. Druitt, and O. Merle, 2000, Experimental study of caldera formation: Journal of Geophysical Research, v. 105, p. 395-416.

SciTech Web Team, 2006, *Mars Express*, Accessed 17 August, 2006 from the European Space Agency Science and Technology website: http://sci.esa.int/science-e/www/object/index.cfm?fobjectid=31022.

Shervais, J.W., S.K. Vetter, and B.B. Hanan, 2006, Layered mafic sill complex beneath the eastern Snake River Plain: Evidence from cyclic geochemical variations in basalt: Geology, v. 34, p. 365-368.

Slavney, S., 2005, *Mars Global Surveyor: MOLA Mission Experiment Gridded Data Records (MEGDR's)*, Accessed 11 November 2005 from the National Aeronautics and Space Administration PDS Geosciences Node website: http://pds-geosciences.wustl.edu/missions/mgs/megdr.html.

Smith, D.E., and W.L. Sjogren, 1999, The gravity field of Mars: Results from Mars Global Surveyor: Science, v. 286, p. 94-97.

Solomon, S.C., and J.W. Head, 1980, Lunar mascon basins: Lava filling, tectonics, and evolution of the lithosphere: Reviews of Geophysics and Space Physics, v. 18, p. 107-141.

Squyres, S.W., D.M. Janes, G. Baer, D.L. Bindschadler, G. Schubert, V.L. Sharpton, and E.R. Stofan, 1992, The Morphology and Evolution of Coronae on Venus: Journal of Geophysical Research, v. 97, p. 13,611-13,634.

Tanaka, K. L., 1986, The stratigraphy of Mars: Journal of Geophysical Research, v. 91, p. E139-E158.

Tanaka, K.L., J.S. Kargel, D.J. MacKinnon, T.M. Hare, and N. Hoffman, 2002, Catastrophic erosion of Hellas basin rim on Mars induced by magmatic intrusion into volatile-rich rocks: Geophysical Research Letters, v. 29, p. 37-1 – 37-4.

Tanaka, K.L., and E.J. Kolb, 2001, Geologic history of the polar regions of Mars based on Mars Global Surveyor data: Icarus, v. 154, p. 3-21.

Tanaka, K.L., and G. Leonard, 1995, Geology and landscape evolution of the Hellas region of Mars: Journal of Geophysical Research, v. 100, p. 5407-5432.

Tanaka, K. L., and D.H. Scott, 1987, Geologic Map of the Polar Regions of Mars: U.S. Geological Survey Miscellaneous Investigation Series Map I-1802-C, scale 1:15,000,000.

Tanaka, K.L., D.H., Scott, and R. Greeley, 1992, Global stratigraphy: In Mars (Eds. H.H. Kieffer, B.M. Jakosky, C.W. Synder, and M.S. Matthews), Univ. Arizona Press, Tucson, p. 354-382.

Tanaka, K.L., J.A. Skinner, T.M. Hare, T. Joyal, and A. Wenker, 2003, Resurfacing history of the northern plains of Mars based on geologic mapping of Mars Global Surveyor data: Journal of Geophysical Research, v. 108, p. 24-1--24-32.

Turcotte, D.L., and G. Schubert, 1982, Geodynamics: Applications of continuum physics to geological problems, New York, John Wiley, 450 p..

Tyler, G.L., 2001, Radio Science Investigations (RS): NSSDC Master Catalog: Experiment, http://nssdc.gsfc.nasa.gov/database/MasterCatalog?sc=1996-062A&ex=4

Walker, G.P.L., 1988, Three Hawaiian Calderas: An origin through loading by shallow intrusions?: Journal of Geophysical Research, v. 93, p. 14,773-14,784.

Watters, T.R., and D.M. Janes, 1995, Coronae on Venus and Mars: Implications for similar structures on Earth: Geology, v. 23, p. 200-204.

Watts, A.B., 2001, Isostasy and Flexure of the Lithosphere: United Kingdom, Cambridge University Press, 458 p..

Wichman, R.W., and P.H. Schultz, 1989, Sequence and mechanisms of deformation around the Hellas and Isidis impact basins on Mars: Journal of Geophysical Research, v. 94, p. 17,333-17,357.

Table 1

PATERA	Location	Diameter of Central Depression[1]	Average Rim Height	Average Caldera Depth[2]	Elevation of floor with respect to surrounding plain	Shape of Central Depression
Amphitrites	58.7° S, 60.9° E	95 km (68 km) (38 km)	1770 m	470 m	+ 1300 m	Circular (Two or more Nested[3])
Peneus	57.8° S, 52.5° E	129-138 km (30)(45)	550 m	200 m	+300 m	Circular (Two smaller Nested?)
Malea	63.4° S, 51.9° E	400 km (100 km) (200 km)	650 m	600 m	- 950 m	Circular (Two overlapping[4])
Pityusa	66.8° S, 36.9° E	400-480 km	1900 m	1700 m	- 1000 m	Circular

PATERA	Shield Diameter	Flank Slope	Arcuate Fractures	Radial Wrinkle Ridges	Concentric Wrinkle Ridges	Other Features
Amphitrites	190 km	0.5-1.2°	✓	✓		Smooth, arching rim; funnel shaped caldera; dissected flanks; outer rim scarps.
Peneus	160 km	0.5°	✓	✓		Multiple fractures on rim; some dissected terrain on north.
Malea	NA	NA	✓	✓	✓	"Horst and graben" terrain on northwest rim.
Pityusa	500 km	0.2-0.4°		✓	✓	Rim terminates in 1.5 km high scarp on south.

[1]Diameter measured from crest to crest. Parentheses indicate diameters of smaller subsidence events.
[2]Depth is the difference between the average elevation of the rim and the average elevation of the floor.
[3]Nested calderas: The geometric center of the latest caldera lies within the circumference of earlier calderas (Crumpler et al., 1996).
[4]Overlapping calderas: The geometric center of the latest caldera lies outside the circumference of the earlier calderas (Crumpler et al., 1996).

Figure 1. Mars Orbiter Laser Altimeter (MOLA) shaded relief map of Malea Planum showing major features, including Amphitrites, Peneus, Malea, and Pityusa paterae. Numbers and boxes show locations of figures. (Lambert Conformal Conic projection.)

FIGURE 1: Shaded Relief Map of Malea Planum

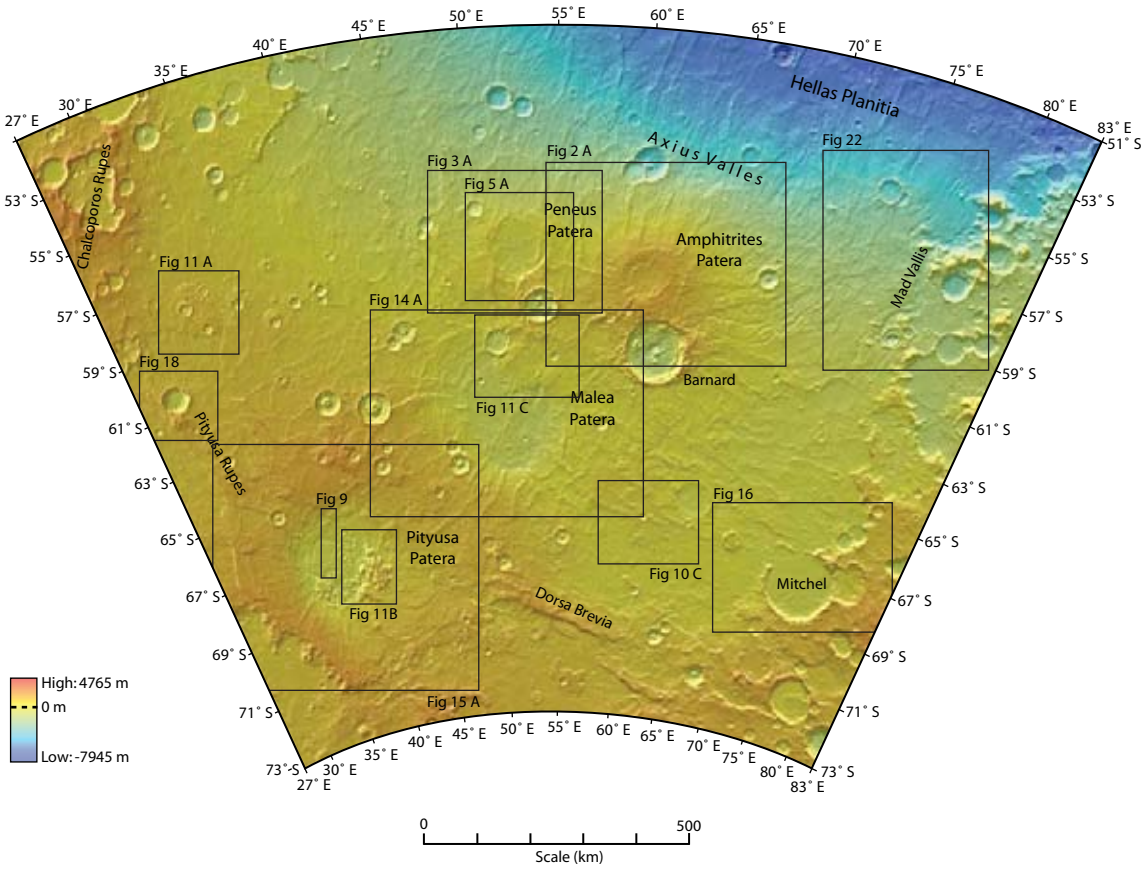

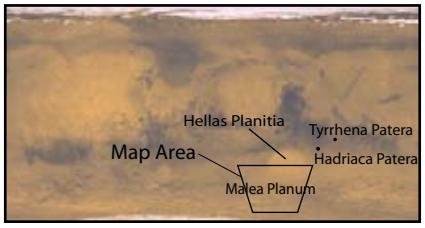

Figure 2. (A) MOLA shaded relief map of Amphitrites Patera with 200 m topographic contours. Dashed green circles represent scarps of discrete subsidence events within the caldera and red dashed line represents the topographic crest of the caldera rim. (B) THEMIS daytime infrared mosaic of Amphitrites Patera. No images are available for the dark grey areas. Black lines indicate unit contacts and red dashed line represents the topographic crest of the caldera rim. Unit symbols correspond to units mapped in Figure 4.

FIGURE 2: Amphitrites Patera

A.

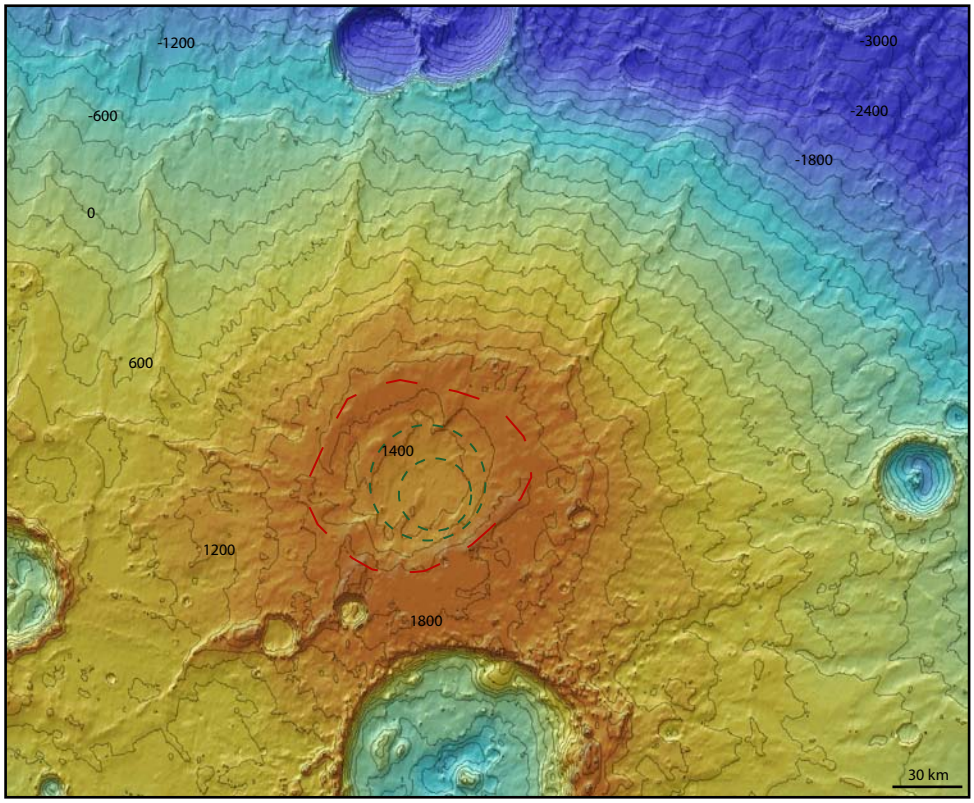

B.

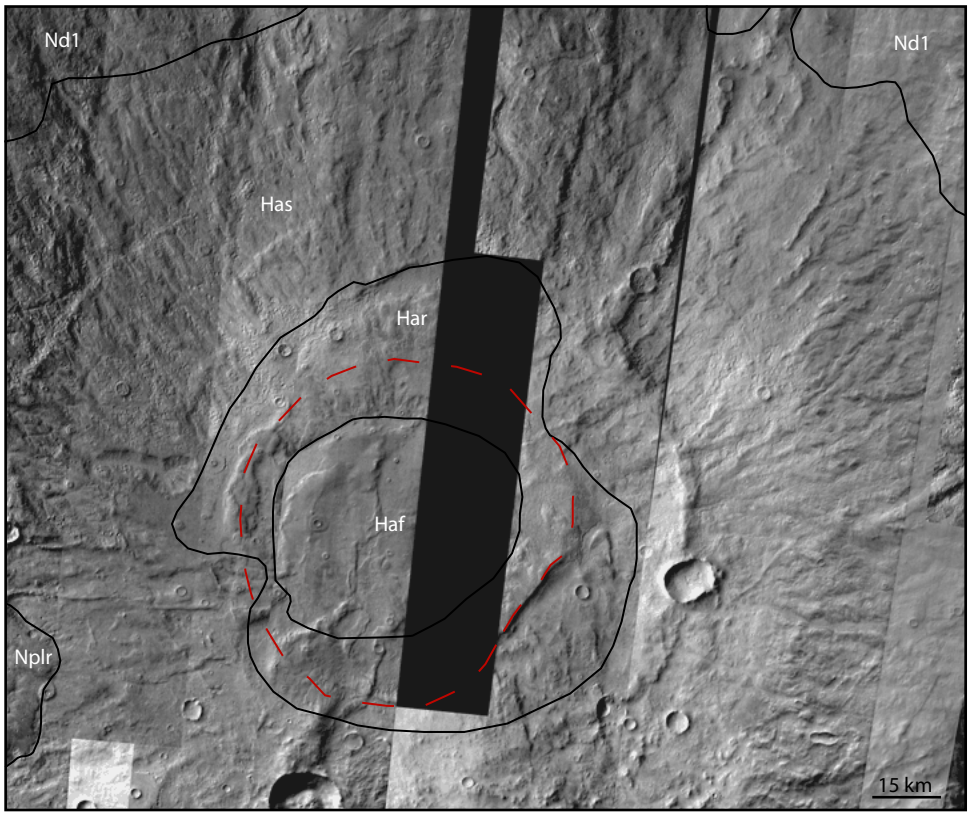

Figure 3. (A) MOLA shaded relief map of Peneus Patera with 200 m topographic contours. (B) THEMIS daytime infrared mosaic of Peneus Patera. Dashed grey circles show interpreted subsidence events within the caldera. Dashed red line indicates the topographic crest of the caldera rim. Solid black lines indicate unit contacts. Unit symbols correspond to units mapped in Figure 4.

FIGURE 3: Peneus Patera

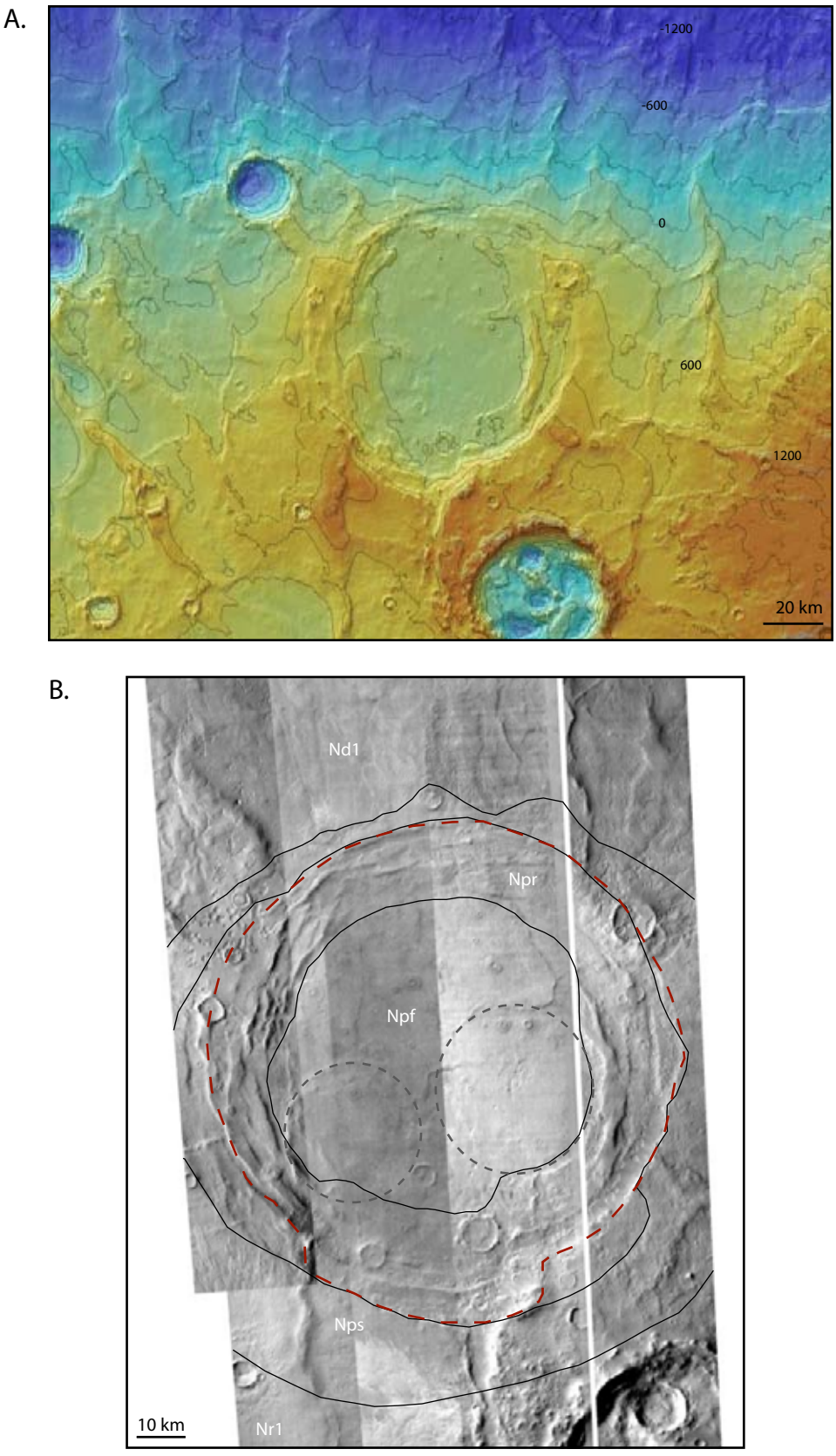

Figure 4. Simplified geologic map of Malea Planum. (See Appendix A, Geologic Map of the Malea Planum Region, Mars, and Appendix B for a description of map units, and Appendix C for a correlation of units. Brown lines show locations of topographic profiles in figure 6.5.

FIGURE 4: Simplified Geologic Map of Malea Planum

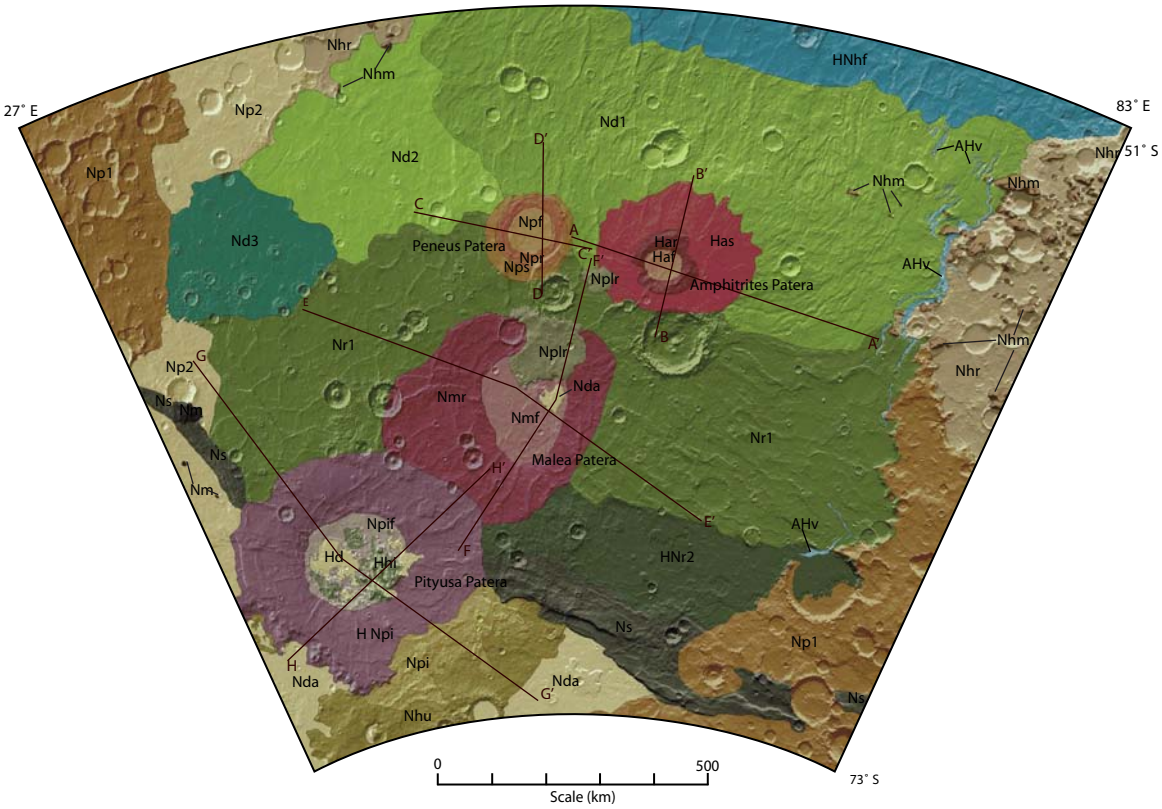

Amazonian/ Hesperian

- AHv Vallis floor unit
- Haf Amphitrites caldera floor
- Har Amphitrites rim
- Has Amphitrites shield
- Hhi Hilly unit

Hesperian/ Noachian

- HNpi Pityusa Patera rim
- HNr2 Ridged plains 2
- HNhf Hellas Basin floor

Noachian

- Npif Pityusa Patera floor
- Nd1 Dissected plains 1
- Nd2 Dissected plains 2
- Nda Dorsa Argentia Formation
- Nr1 Ridged plains 1
- Nd3 Dissected plains 3
- Nhu Hummocky material
- Npi Pitted material
- Nmf Malea Patera floor
- Nmr Malea Patera rim
- Npf Peneus caldera floor
- Npr Peneus rim
- Nps Peneus shield
- Nplr Rough plateau material
- Ns Scarped unit
- Nm Highland massif unit
- Nhr Hellas rim
- Nhm Rim massifs
- Np2 Subdued cratered unit
- Np1 Cratered unit

Figure 5. Images of the Peneus caldera rim in Malea Planum from (A) MOLA shaded relief (128 pixels/degree) (boxes show locations for B-G), (B) the Viking Orbiter (70 m/pixel), (C) Viking Mars Digital Image Mosaic (256 m/pixel), (D) the Mars Orbiter Camera (MOC, 4 m/pixel), (E) THEMIS Daytime visible (17 m/pixel), (F) THEMIS Daytime infrared (100 m/pixel), and (G) THEMIS Nighttime infrared (100 m/pixel). Thin mantle deposits a few meters thick cover the rim of the Peneus caldera and many other areas between 30° and 60° S and are particularly obvious in B, D, E, and F. The mantle is pitted and discontinuous. The pits are steep-walled on their northern sides with gentler slopes on the south.

FIGURE 5

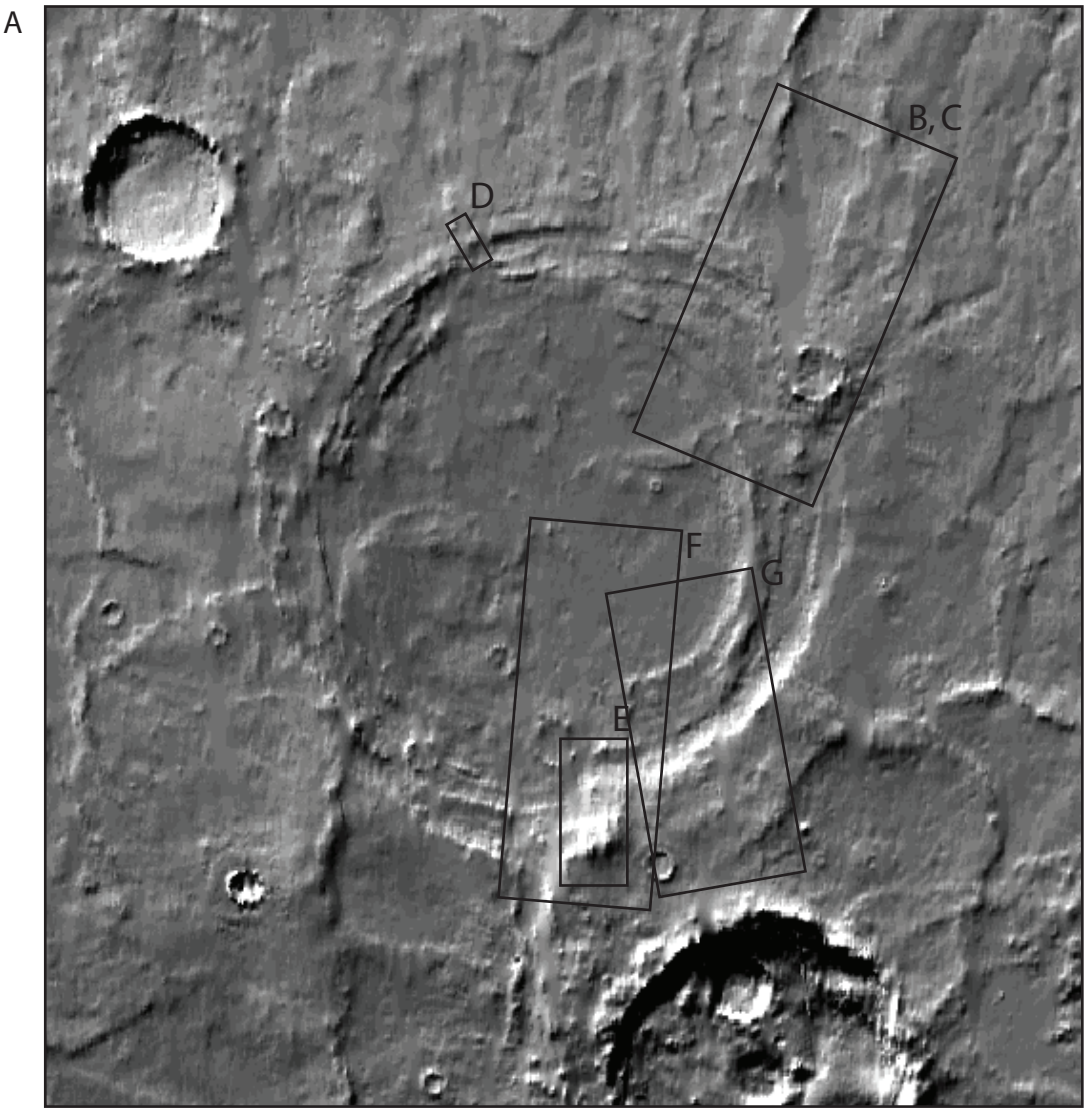

FIGURE 5 (Continued)

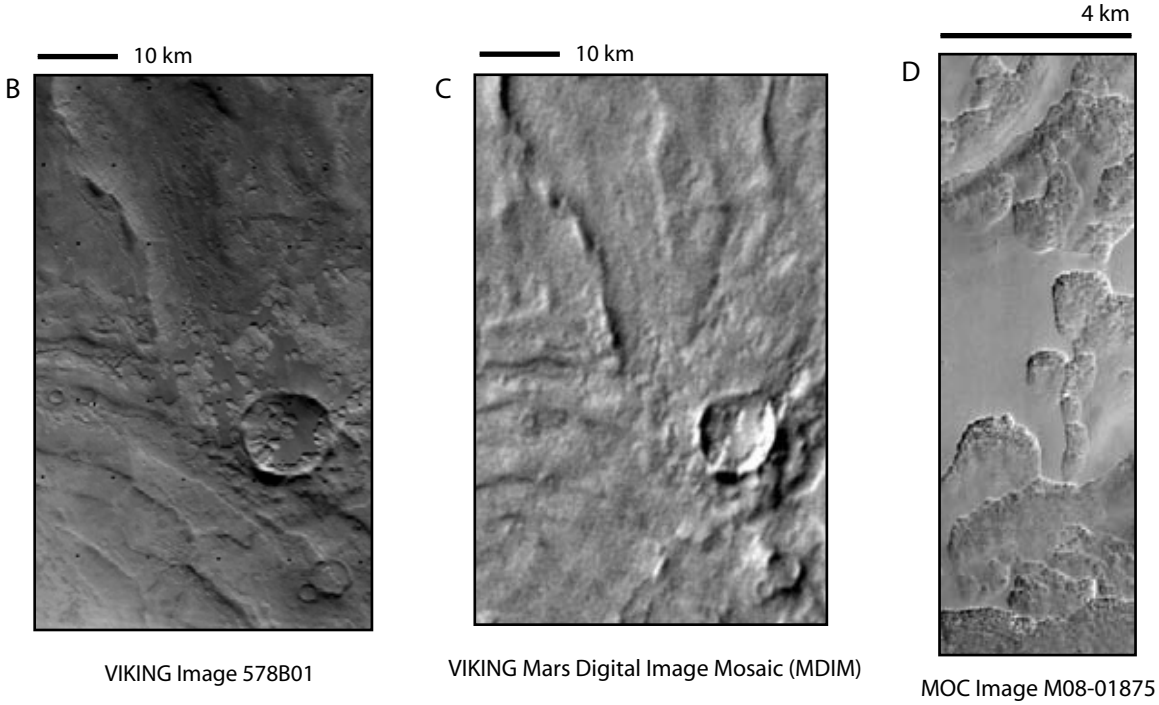

Figure 6. Map of free-air gravity anomalies superposed on a shaded relief map of Malea Planum from Lemoine (2001). Amphitrites sits at the center of a very large positive anomaly (suggesting a solidified magma chamber system exists beneath the patera that is not isostatically compensated). A smaller gravity high marks Malea Patera. Peneus and Pityusa lack strong gravity signatures.

FIGURE 6: Free-Air Gravity Anomalies

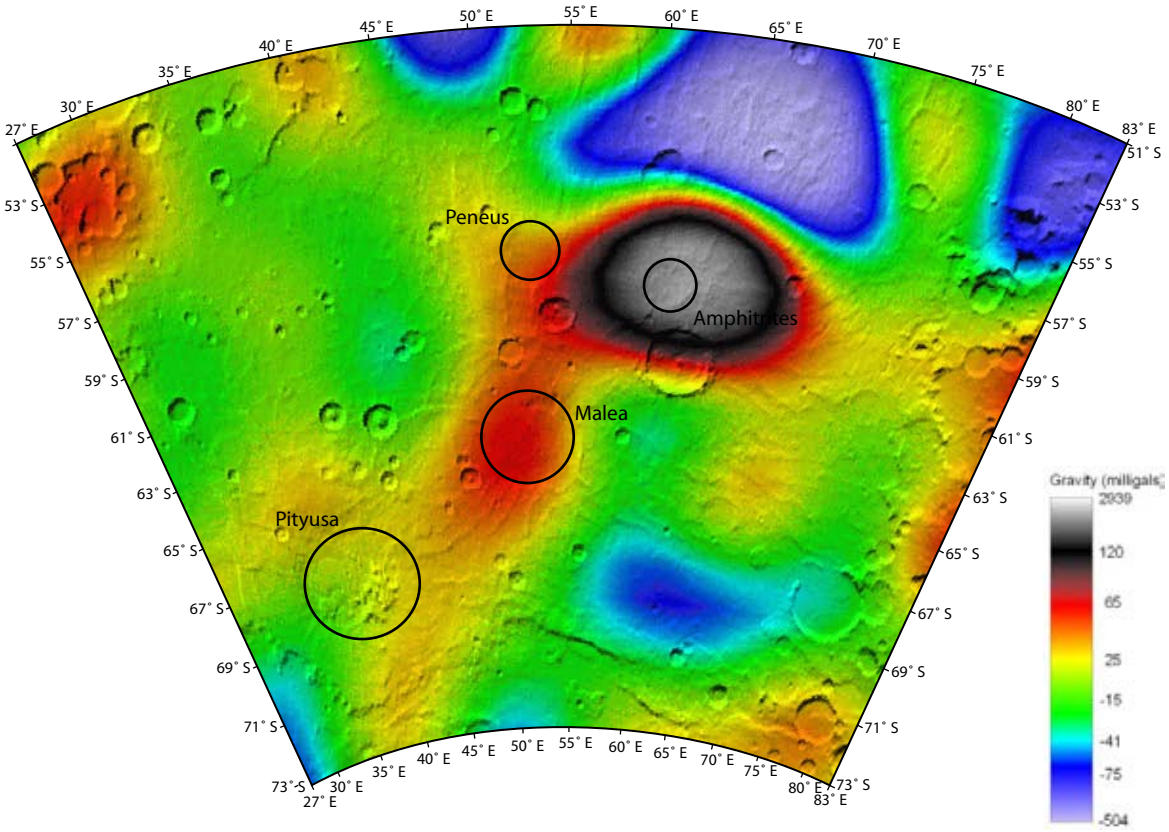

Figure 7. Correlation of major geologic events in Malea Planum adapted from Ivanov et. al. (2005). 1. The earliest event was the formation of the cratered highlands. 2. The formation of the Hellas Impact Basin removed the highlands from the north eastern map area, forming rugged massifs and a series of extensional scarps around the rim. 3. The rim of Hellas eroded and was partially covered by flood lavas originating in Malea Planum. 4. Pityusa and Malea paterae formed on the smooth lava plains. 5. Amphitrites and Peneus formed on the plains. 6. Mantling, Mad Vallis, smaller channeling events, and eolian activity modified the surface of the plain.

FIGURE 7: Correlation of Major Geologic Events

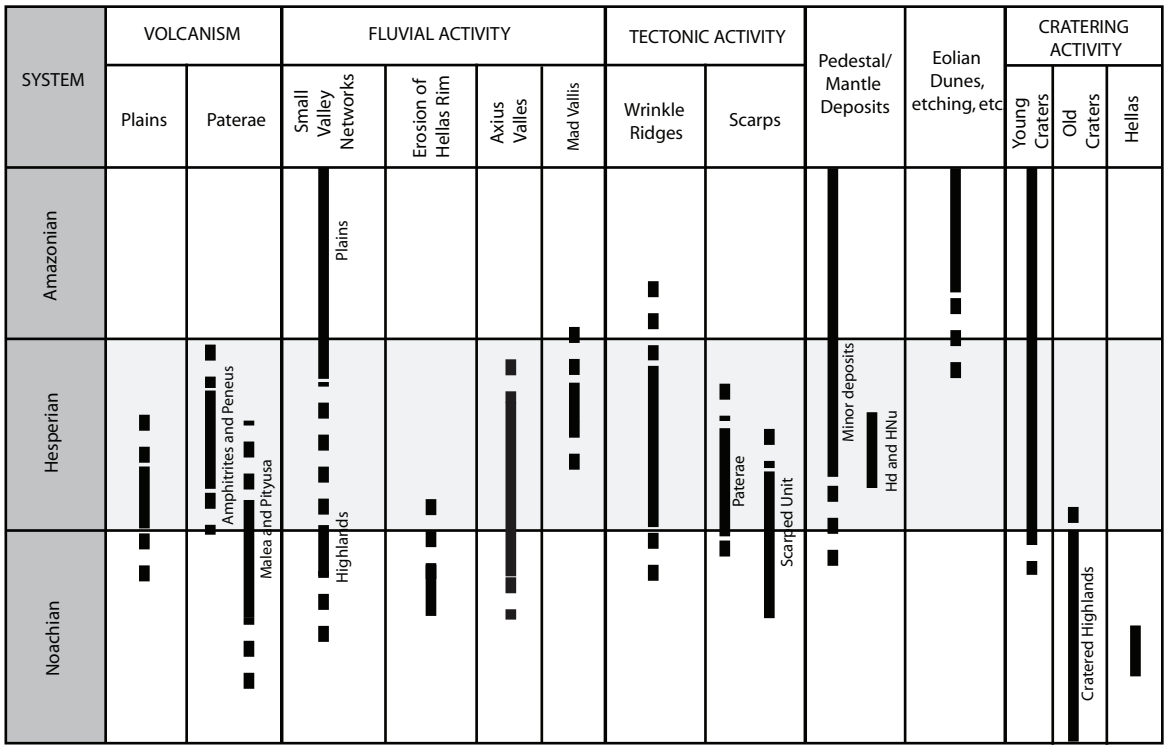

Figure 8. (A) Tectonic Map of Malea Planum showing locations of wrinkle ridges and extensional scarps. The ridges are mostly confined to the smooth lavas covering Malea Planum and become smaller at the edges of the plain. The ridges are radial around Amphitrites, Peneus, Malea, and Pityusa paterae. Ridges are missing or incomplete in Axius Valles where they may have been removed by channeling events. Extensional scarps ring the plain, roughly parallel to the rim of the Hellas impact basin. Additional scarps ring the calderas of Peneus and Amphitrites and the northwest rim of Malea Patera. (B) THEMIS image I08150007 showing detail of a ridge south of Amphitrites Patera. (C) Rose diagram for all ridges in the map area. Ridges trend east to west. (D) Rose diagram for all extensional scarps in the map area. The scarps generally trend northwest.

FIGURE 8: Tectonic Map of Malea Planum

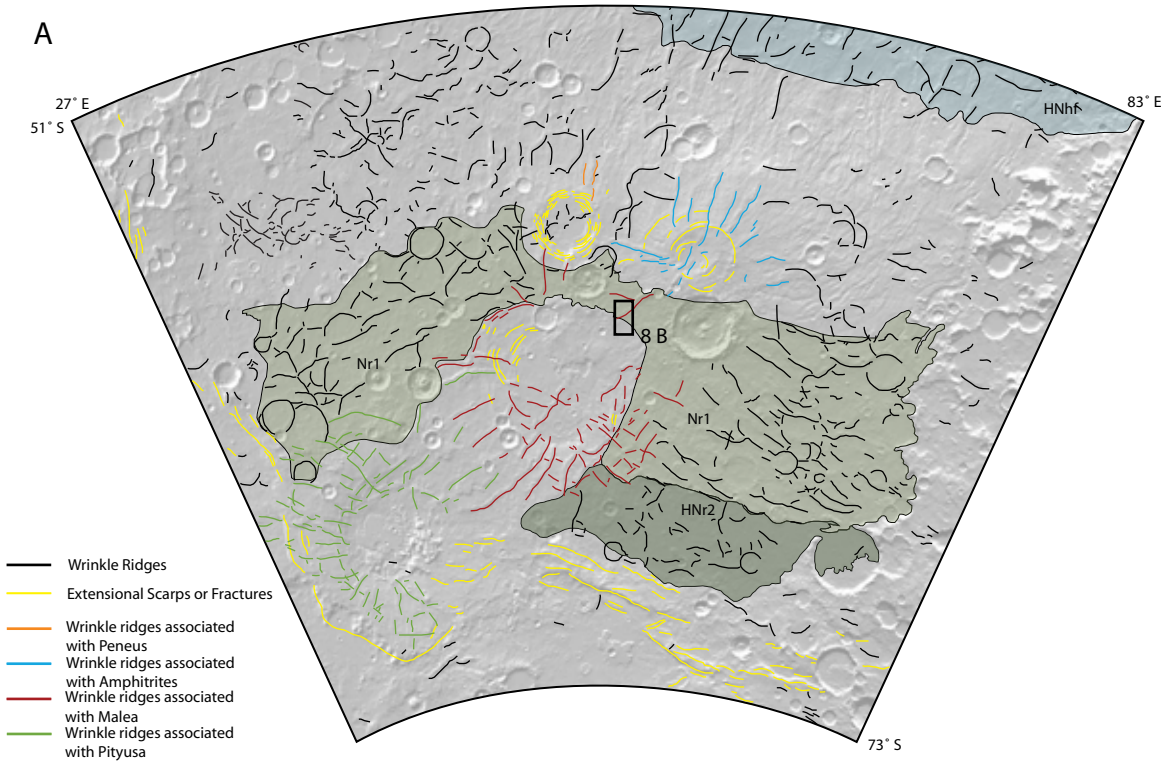

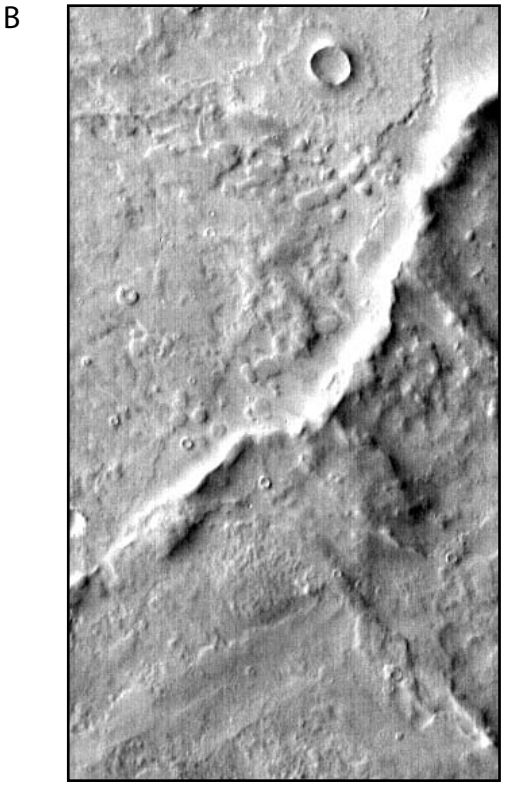

FIGURE 8 (continued)

C. All Ridges

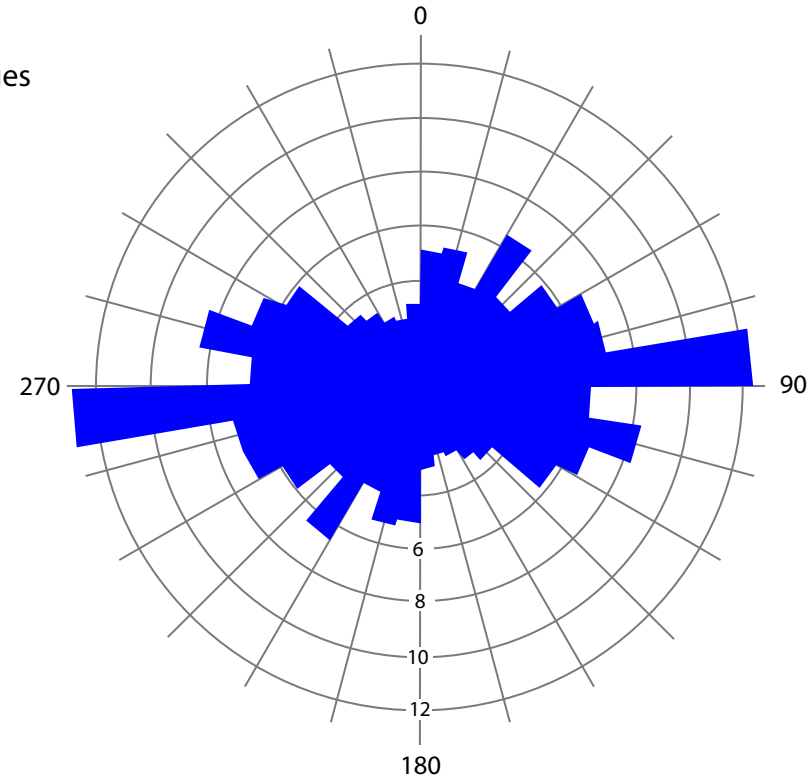

D. All Scarps

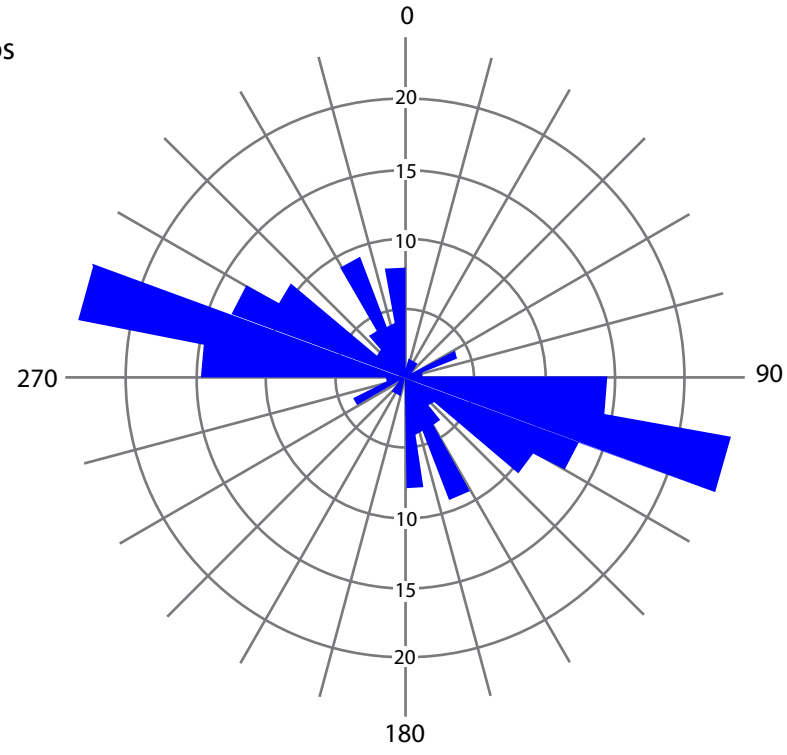

Figure 9. THEMIS daytime infrared image I08263008 showing a smooth plateau of the Dorsa Argentia formation (Nda) in Pityusa Patera. Smooth plateau deposits hundred of meters high are remnants of a mantle deposit that once covered much of southern Malea Planum. The plateaus are thought to be eolian deposits of ice and dust that form during Martian ice ages. Also illustrated in this image are eolian processes currently active on Mars. The plateau surface has been etched by the wind. Light-colored windstreaks trending NNW cross the surface and a field of sand dunes, likely formed from material removed from the mantle deposit, has formed north of the plateau. The plateau scarp is formed as ice exposed in the cliff face sublimes.

FIGURE 9

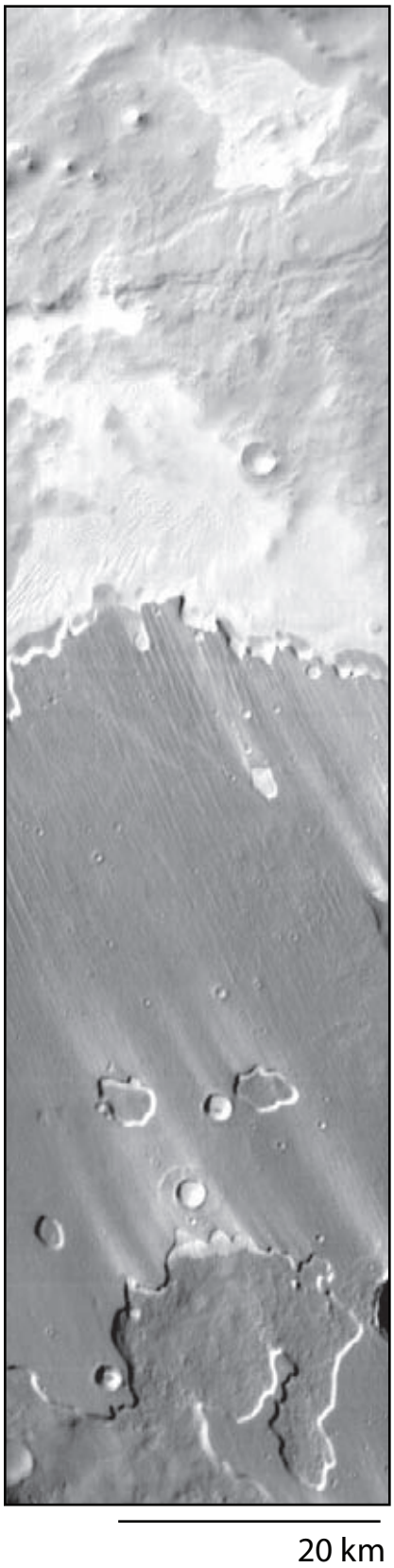

Figure 10. (A) Types of craters found on Malea Planum. 1. Rampart craters are thought to form when the heat from impact melts ground ice and fluidizes the ejecta. 2. Rayed craters form when dry material is excavated from the crater. 3. Pedestal craters. (B) Pedestal craters form when a meteorite strikes a surface of loosely consolidated or volatile rich material (mantle deposits). The ejecta protects the mantle beneath it. As the rest of the layer erodes through deflation or sublimation, the mantle beneath the crater ejecta remains. (C) A pedestal crater at 72° S 56° E.

FIGURE 10: Types of craters on Malea Planum

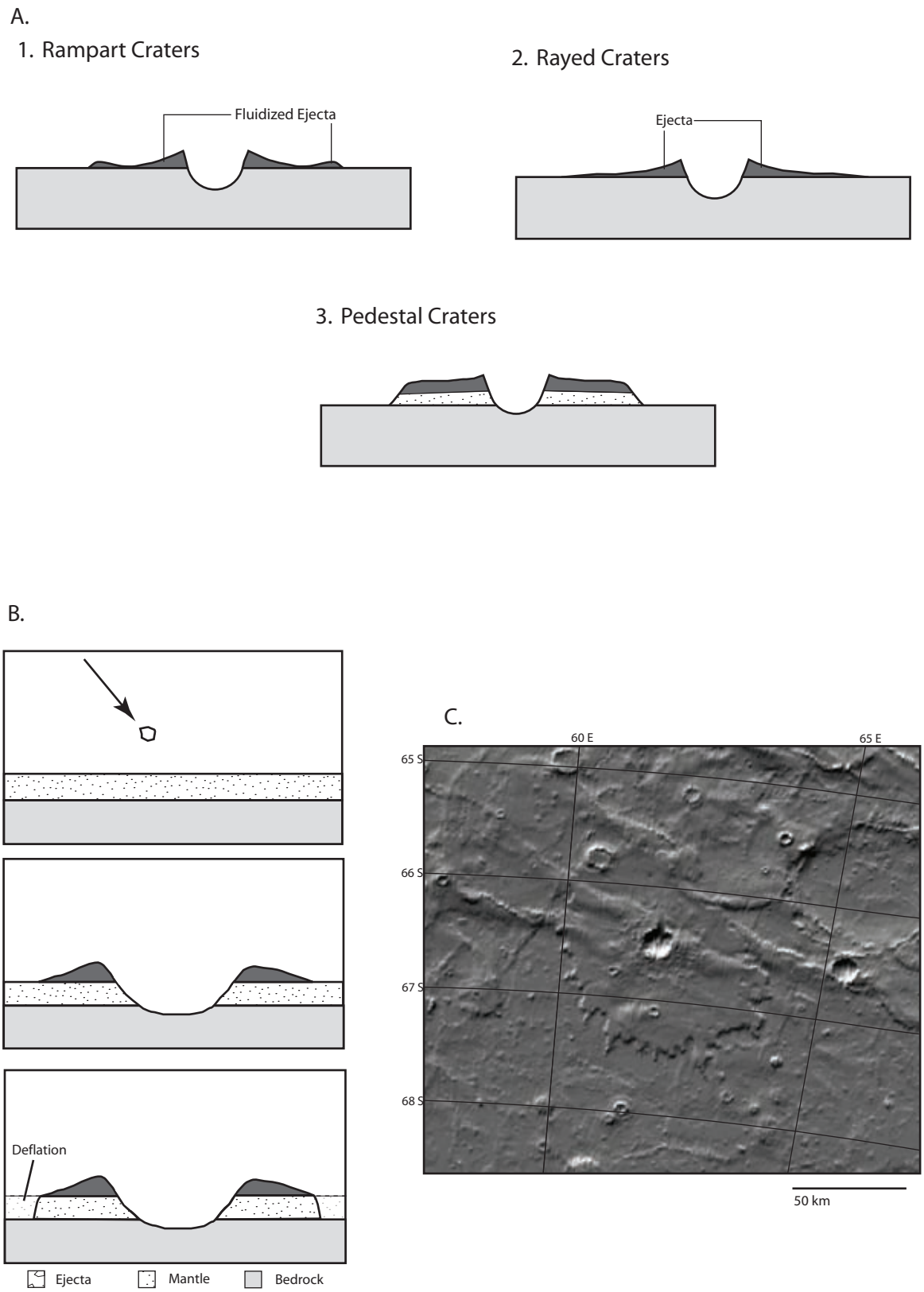

Figure 11. An old, thick mantle deposit (or a series of them) may have once covered much of southern Malea Planum. (A) Thick pedestals around small impact craters, (B) the hilly unit (Hhi) within Pityusa Patera (rough hills in the center of the image; smooth plateaus on the right and left are occurrences of Nda), and (C) the rough plateau unit (Nplr) are possible remnants of this polar mantle deposit.

FIGURE 11

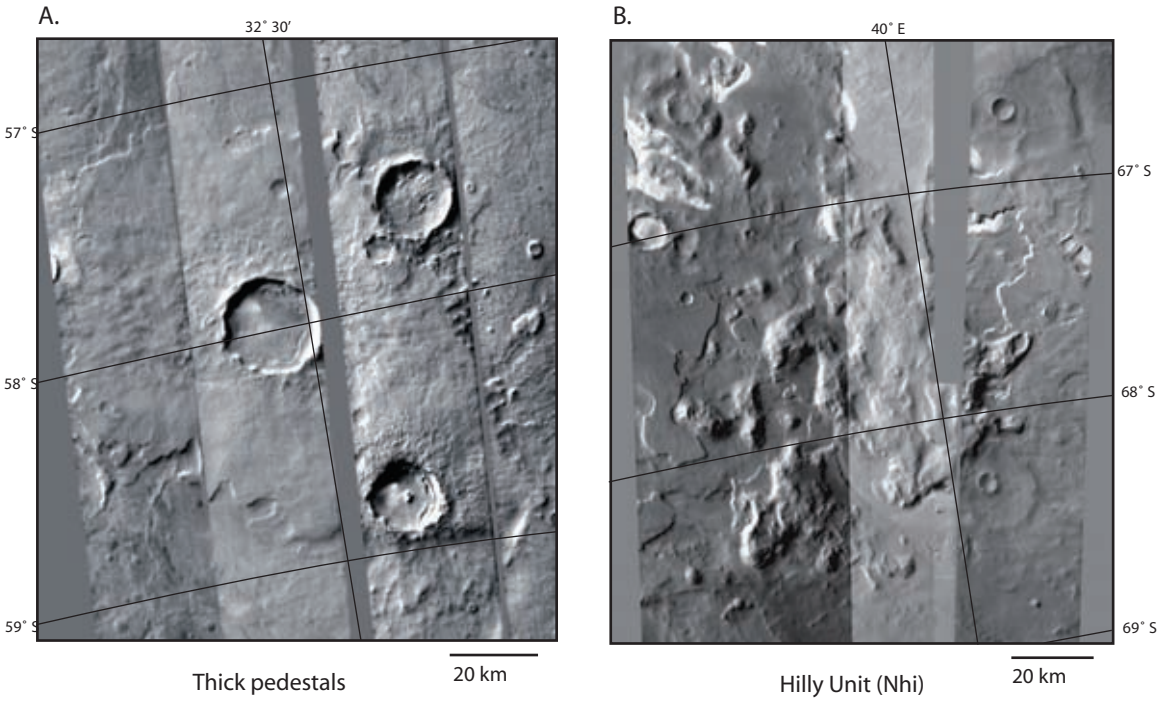
A.
32° 30′
57° S
58° S
59° S
Thick pedestals
20 km
B.
40° E
67° S
68° S
69° S
Hilly Unit (Nhi)
20 km
C.
50° E
55° E
60° S
61° S
62° S
63° S
Rough Plateau (Nplr)
20 km

Figure 12. Parts of a typical patera on Malea Planum shown in map view (A) and cross section (B). Most paterae are characterized by low shields topped by circular depressions. Radial compression ridges mark the flanks and arcuate scarps ring the central caldera.

FIGURE 12: Parts of a Patera

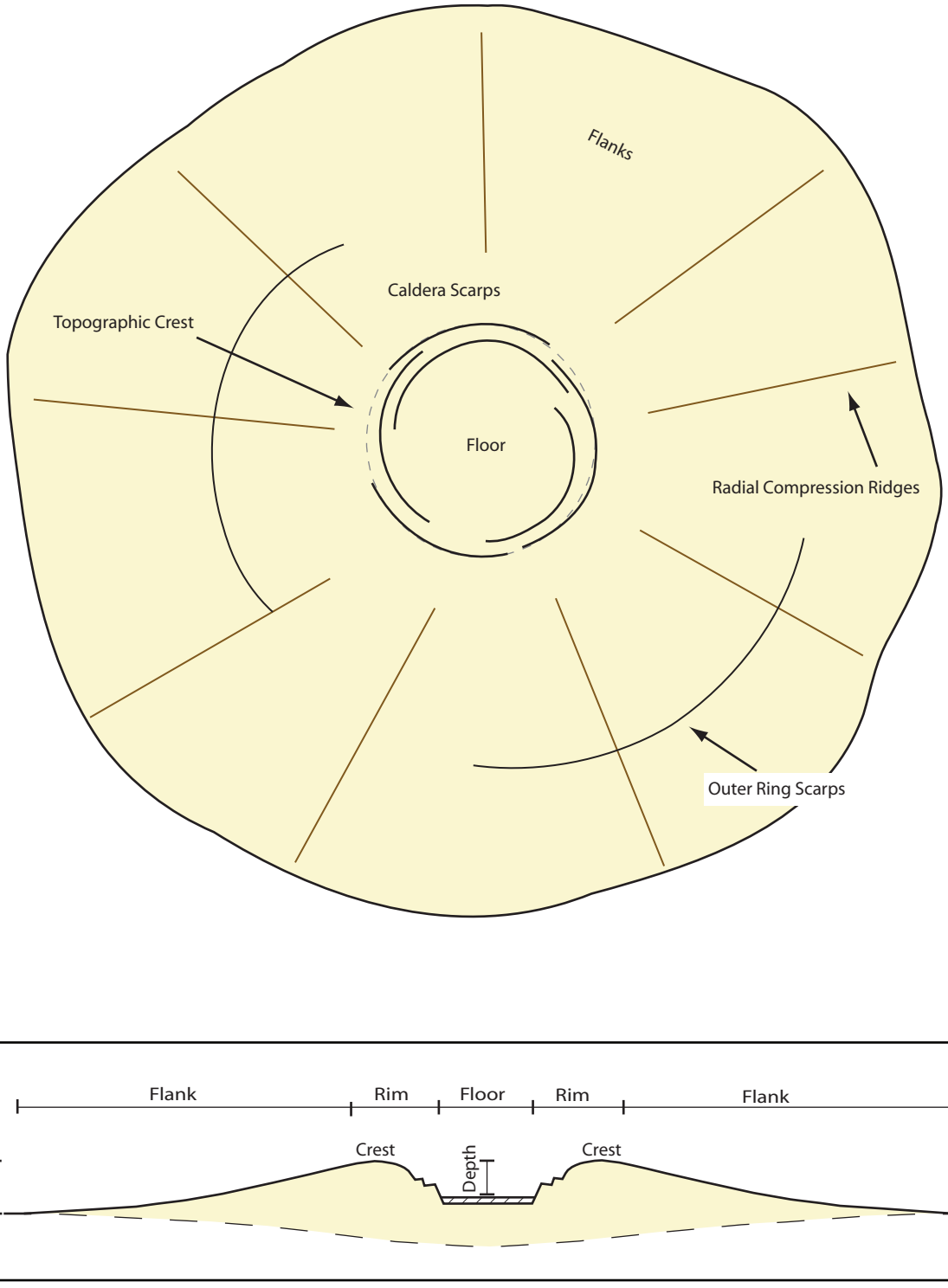

Figure 13. (A) Distribution of channels on Malea Planum. Green shaded areas indicate the main concentration of valleys, including Nd_1, Nd_2, and Nd_3. Red shaded area indicates valleys on the flanks of Amphitrites Patera. Green dotted lines show the approximate topographic crests of the four paterae. The valleys of Axius Valles are straight, parallel to each other, and up to 300 m deep. Smaller valleys tens of meters deep are found across the plain and are often superposed on the larger channels of Axius Valles. Semi-dendritic networks run along the north-west boundary of the plain. (B) THEMIS image I08537003. Small channel juxtaposed on a large valley in Axius Valles (58° 15'E, 55° 30'S). (C) THEMIS image I09873008. Meandering, semi-dendritic channels in western Malea Planum (38° 30'E, 55° 30' S).

FIGURE 13: Channels on Mars

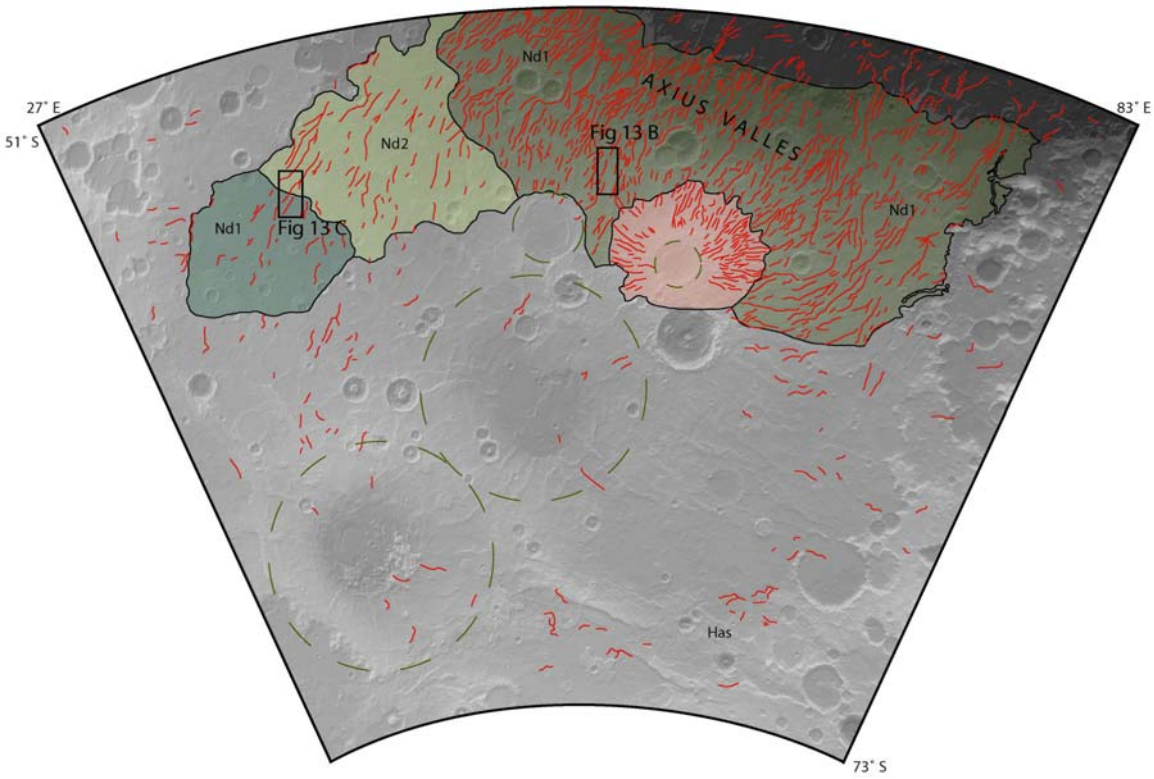

Figure 13 (continued): Channels in Malea Planum

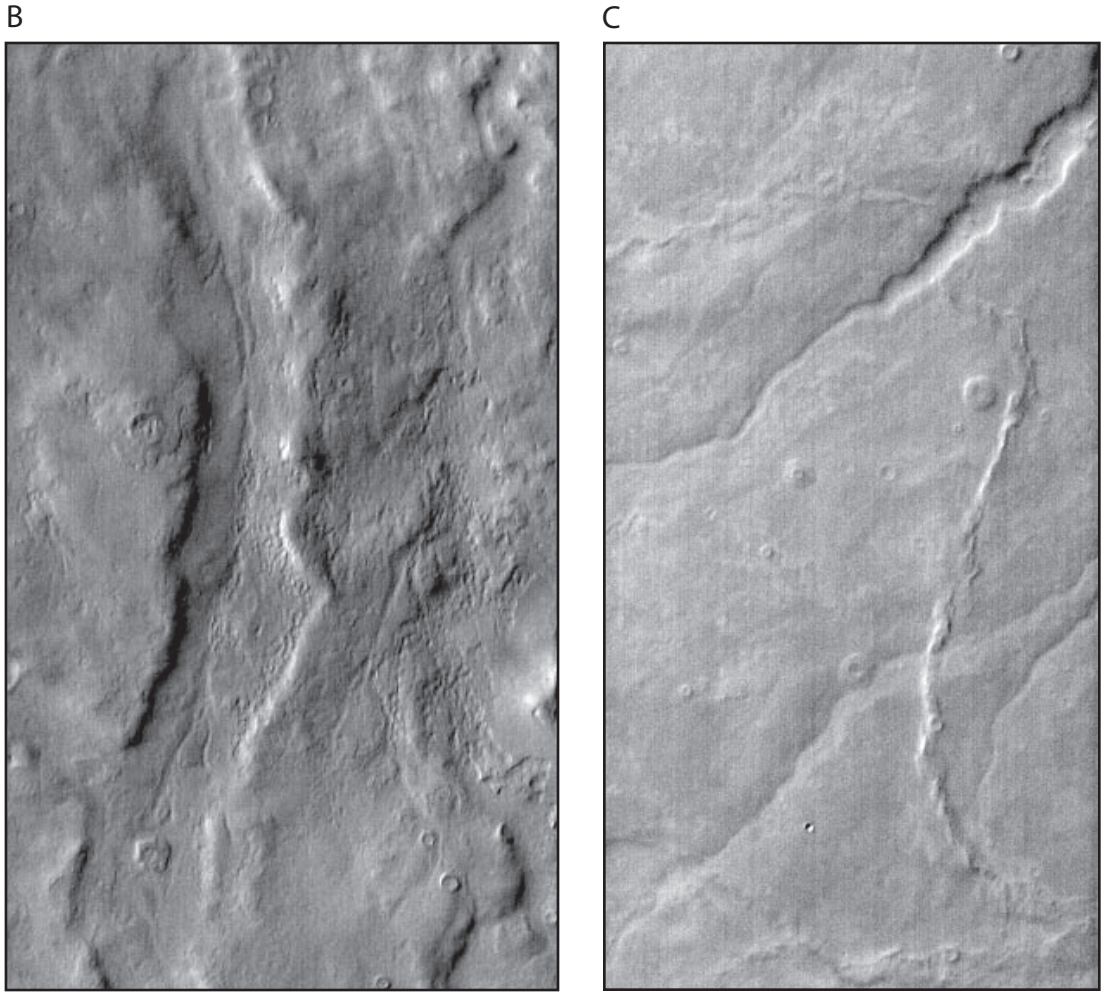

Figure 14. (A) MOLA shaded relief map of Malea Patera with 200 m topographic contours. Dashed grey circles represent possible discrete subsidence events. Dashed black line indicates the topographic crest of the depression rim. (B) THEMIS daytime infrared mosaic of Malea Patera. Solid black lines indicate unit contacts.

FIGURE 14: Malea Patera

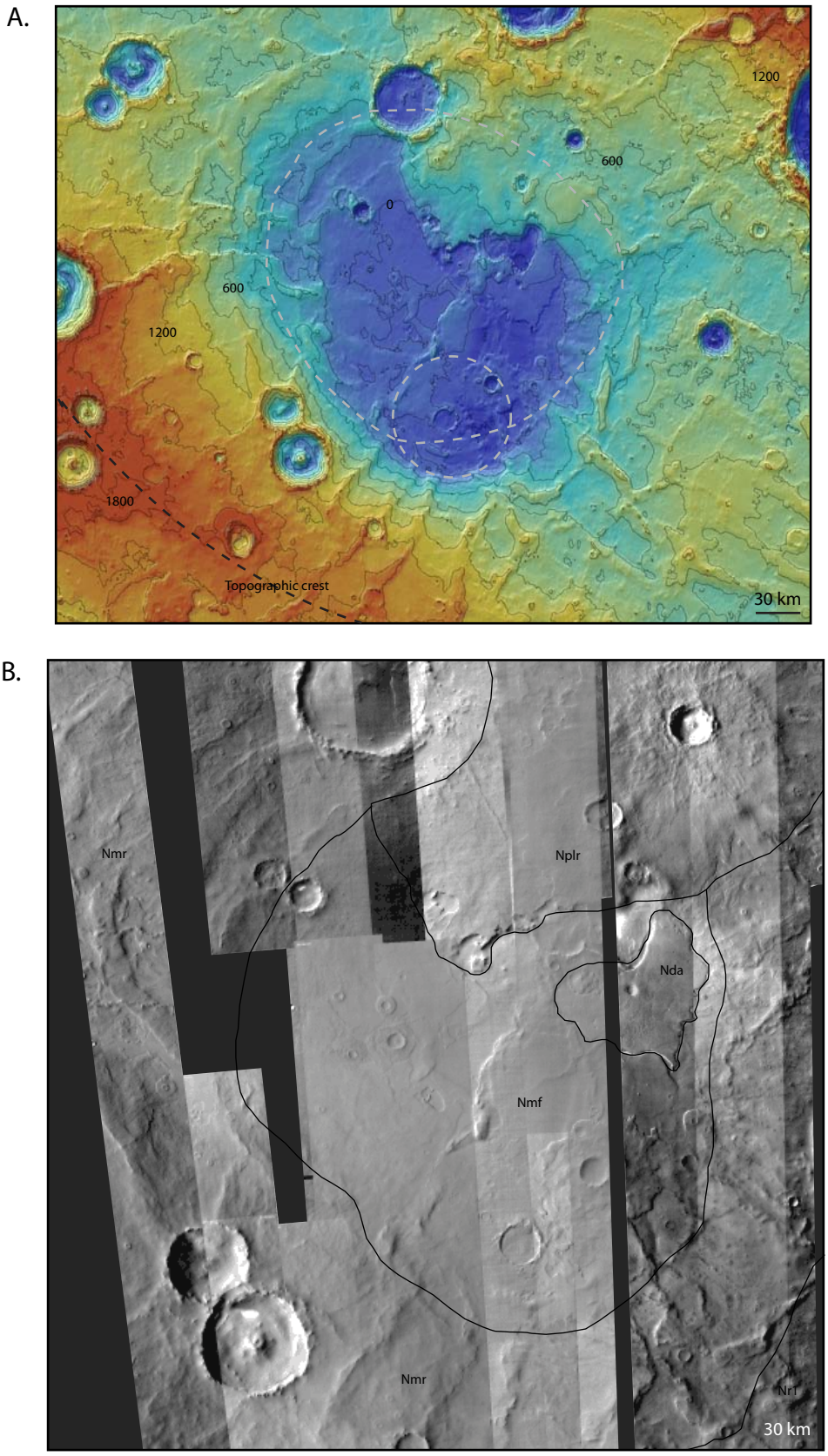

Figure 15. (A) MOLA shaded relief map of Pityusa Patera with 200 m topographic contours. Black dashed line indicates topographic crest of depression rim. (B) THEMIS daytime infrared mosaic of Pityusa Patera. Solid black lines indicate unit contacts.

FIGURE 15: Pityusa Patera

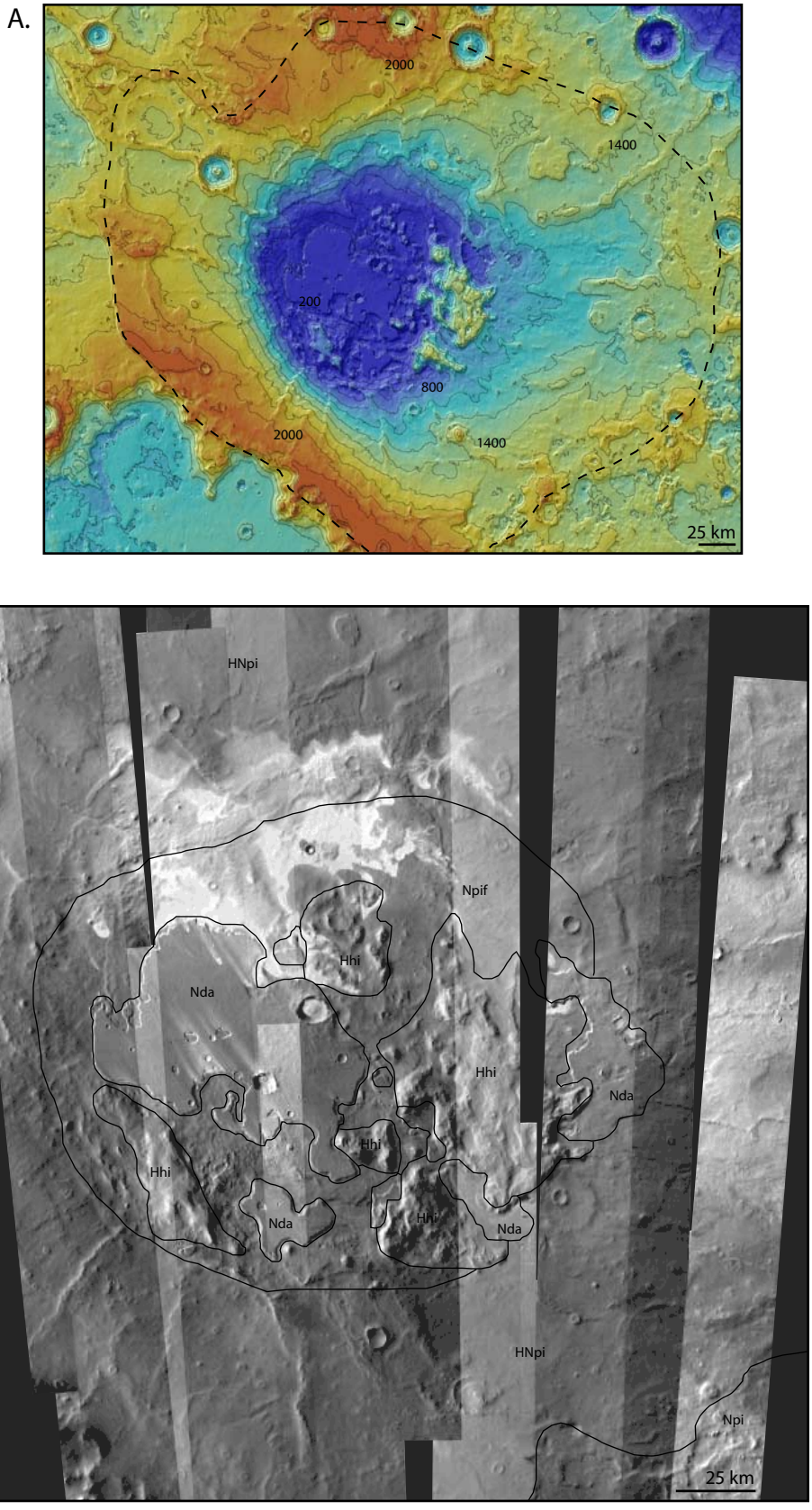

Figure 16. The highland/Malea Planum boundary is scalloped by craters that are half-buried by the plains material. A lobate front in Mitchel crater shows the extent of the plains material and is the strongest evidence of a lava origin for the plains (black arrows). Dotted circles indicate crater rims with diameters greater than 20 km (red arrows). B. MOC image E1001949. C. MOC image M0202512. D. MOC image E0302490.

FIGURE 16

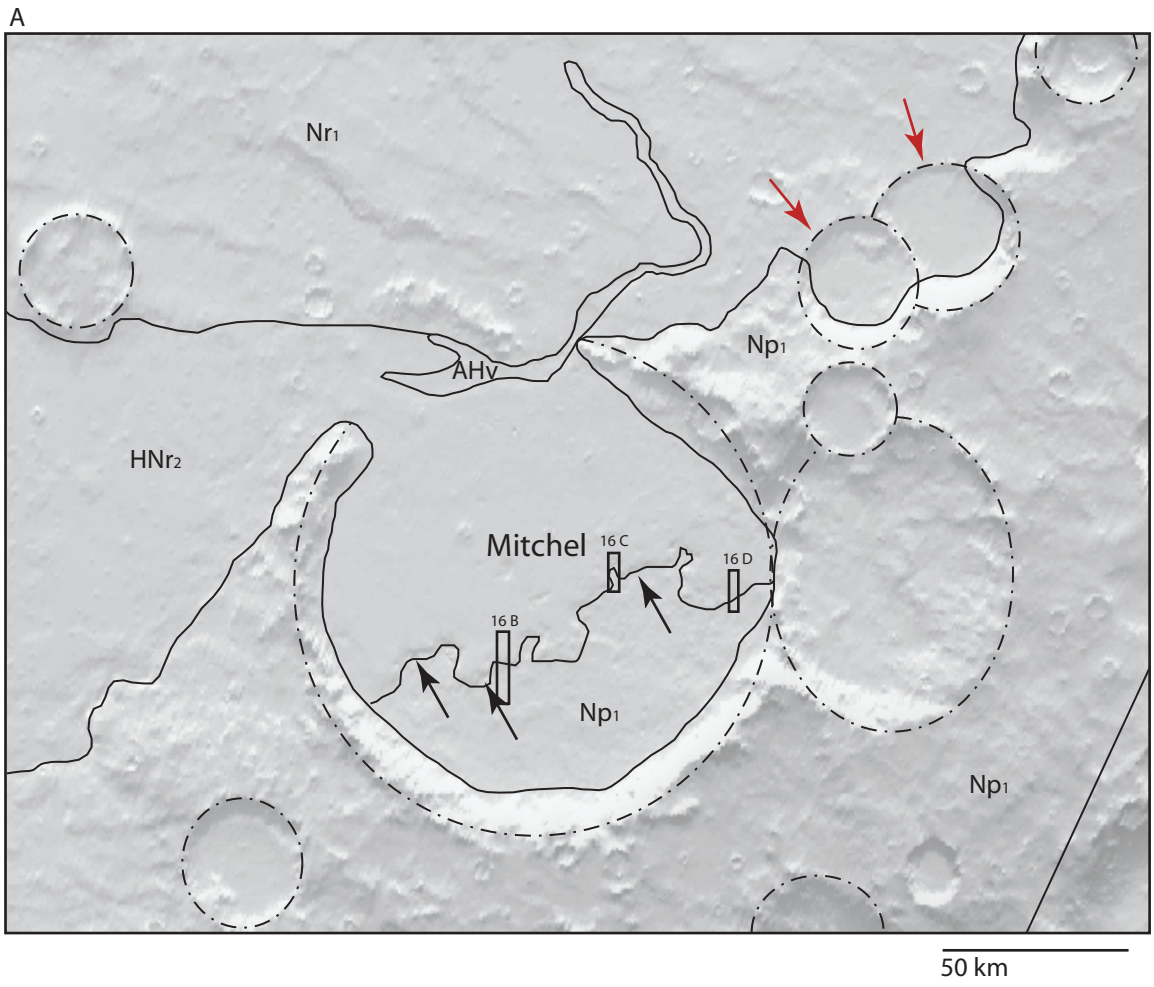

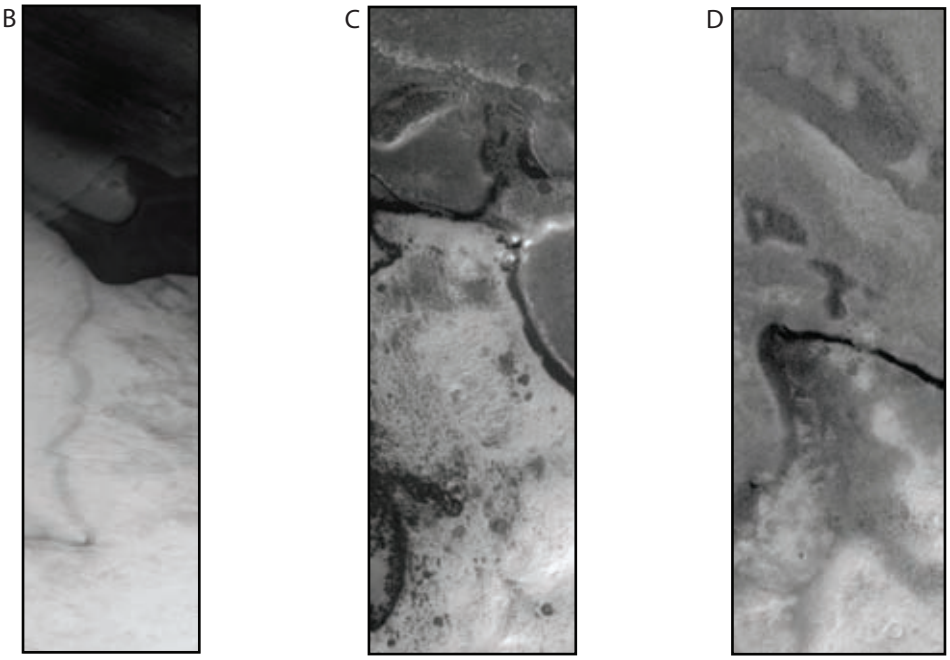

Figure 17. Map showing the distribution of ghost craters or quasi-circular depressions (QCD's) on Malea Planum. The depressions are concentrated within the interpreted lava plains of Malea Planum but are not restricted to this area. They are interpreted to be impact craters buried by shallow layers of lava or sediments.

FIGURE 17: Distribution of Ghost Craters

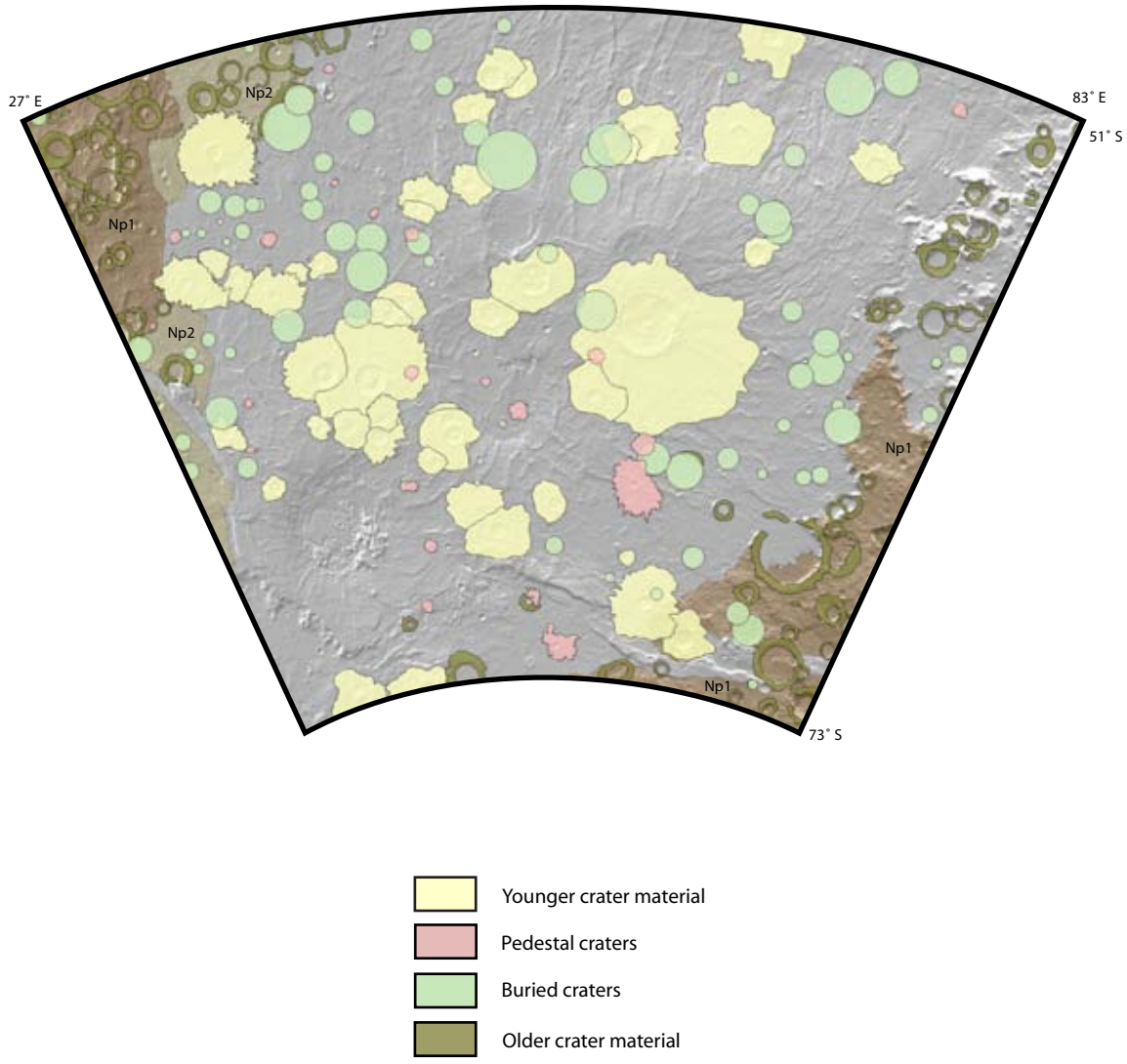

Figure 18. A lone highland massif within the subdued cratered unit (Np_2) is similar to others found outside the map area to the west. The conical, sometimes flat-topped morphology of the massifs suggest they may be subglacial volcanoes.

FIGURE 18

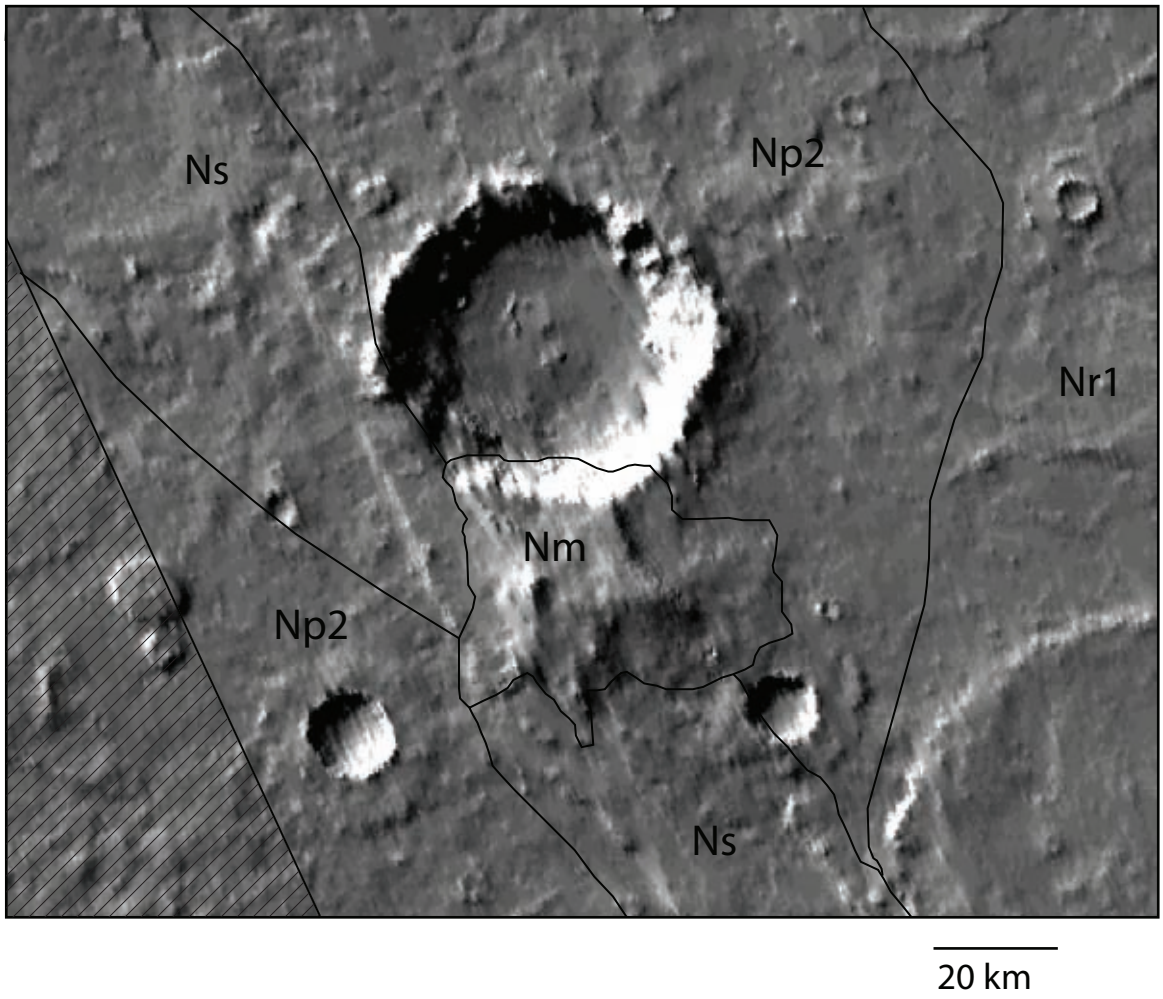

Figure 19. Topographic profiles for the four paterae constructed from MOLA elevation data. Profiles have been vertically exaggerated 50 times. Locations of cross section transects are shown on figure 2. Unit abbreviations (Nplr, Nda, and Hhi) correspond to units mapped in Figure 4. Inset shows generalized profiles of two types of coronae from Venus drawn to the similar scale. Twenty-five percent of coronae on Venus are depressions surrounded by a raised rim; seven percent are depressions without a significant rim (from Hoogenboom and Houseman, 2006).

Figure 19: Profiles

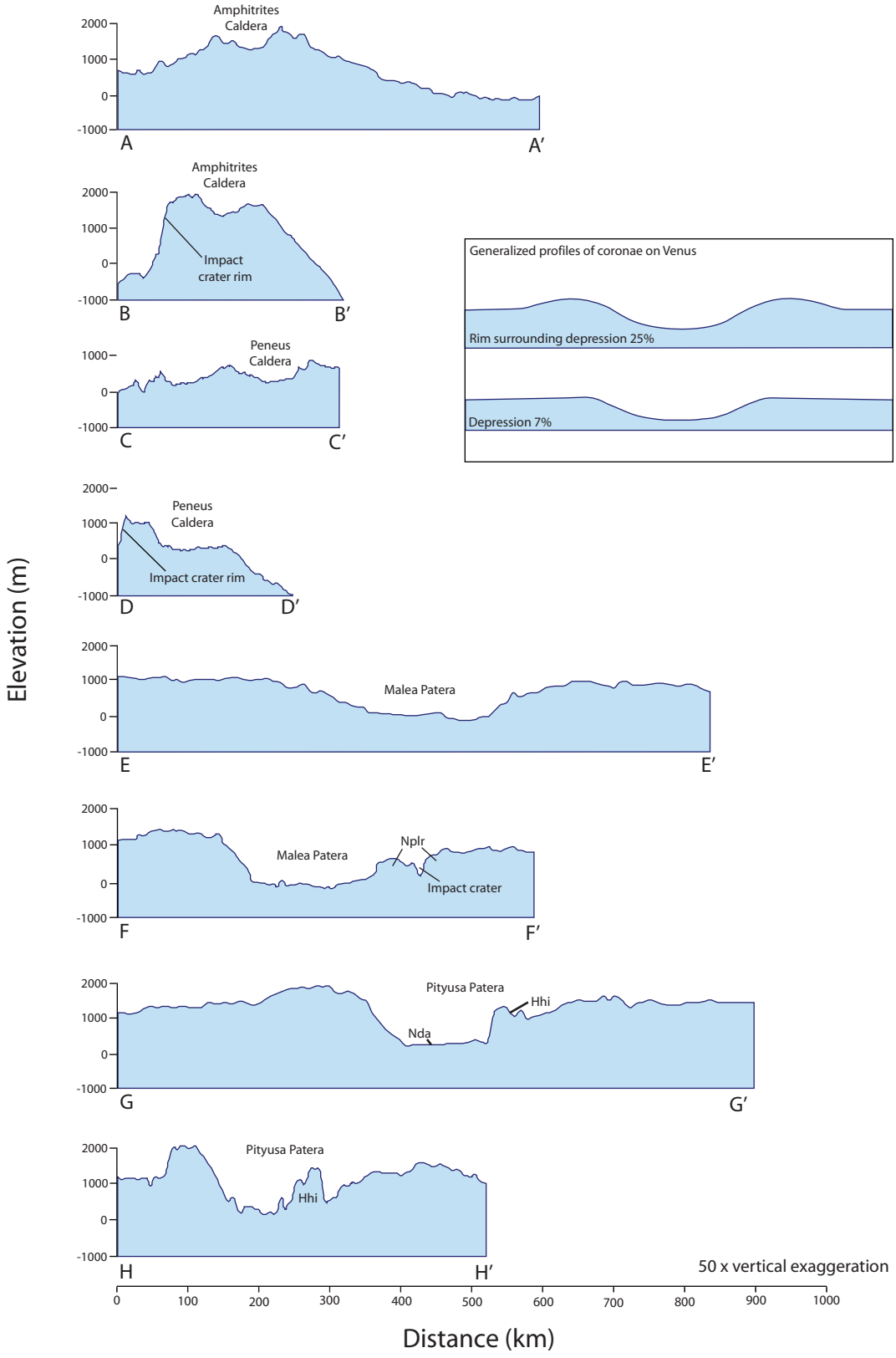

Figure 20. Theory proposed by Tanaka et al. (2002) for the formation of Malea Planum. 1. The rim of Hellas is intruded by sills of mafic lava. Interstitial H_2O and CO_2 melt or vaporize. 2. The surface rocks fluidize with the liquid/gaseous volatiles and flow into Hellas Basin. The rim massifs are removed. 3. Eruptions of flood lavas and the paterae cover the eroded surface.

FIGURE 20: Catastrophic Erosion of the Hellas Basin Rim

1. Sills intrude shallow, friable rocks of basin rim and melt/dissociate interstitial H_20, CO_2, and CO_2 clathrate.

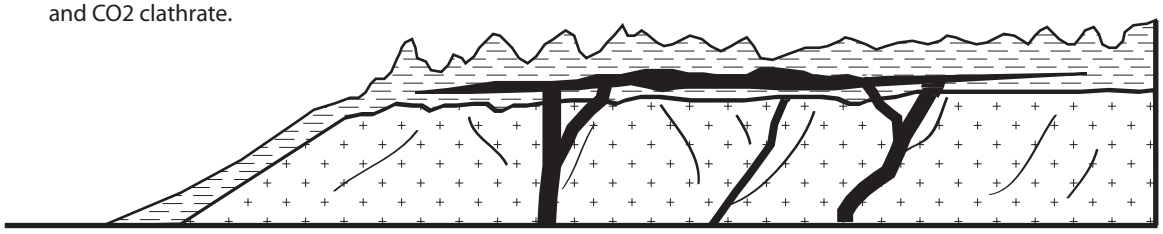

2. Surface rocks fluidize with liquid/gaseous H_2O/CO_2 and flow into adjacent basin, removing massifs.

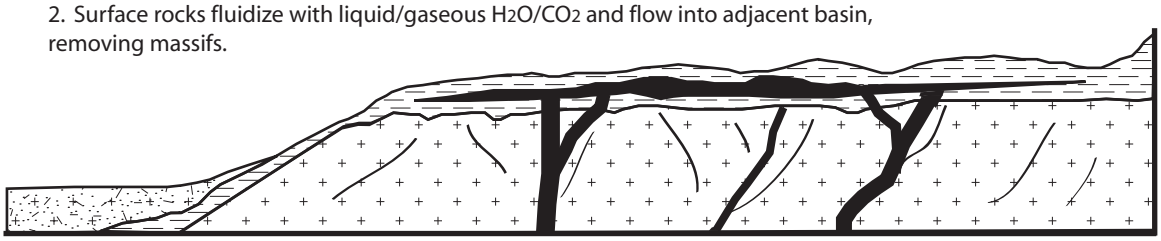

3. Subsequent eruptions cover eroded surface with lava plains; some erosion occurs on basin rim.

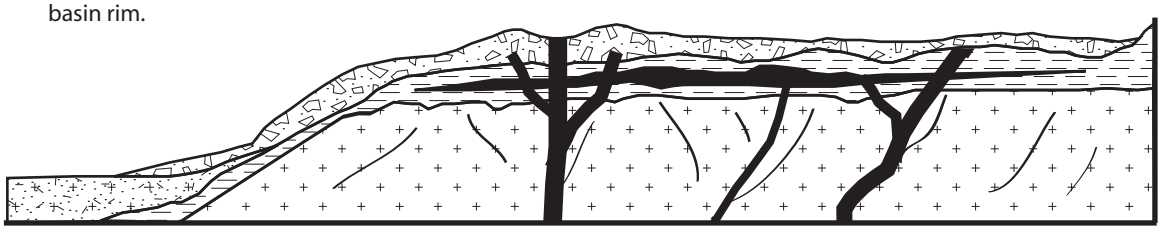

Figure 21. Model for the development of channeled highland paterae like Amphitrites. (A) Phreatomagmatic eruptions generate clouds of steam and volcanic ash. (B) Steam condenses and possibly freezes to fall as rain or snow. Snow collects on the flanks of the volcano. (C) Heat from the volcano causes basal melting of the snow pack. The water erodes narrow channels confined to the surface of the volcano. (D) Sagging of the caldera by intrusive load.

Figure 21: Development of Channeled Highland Paterae

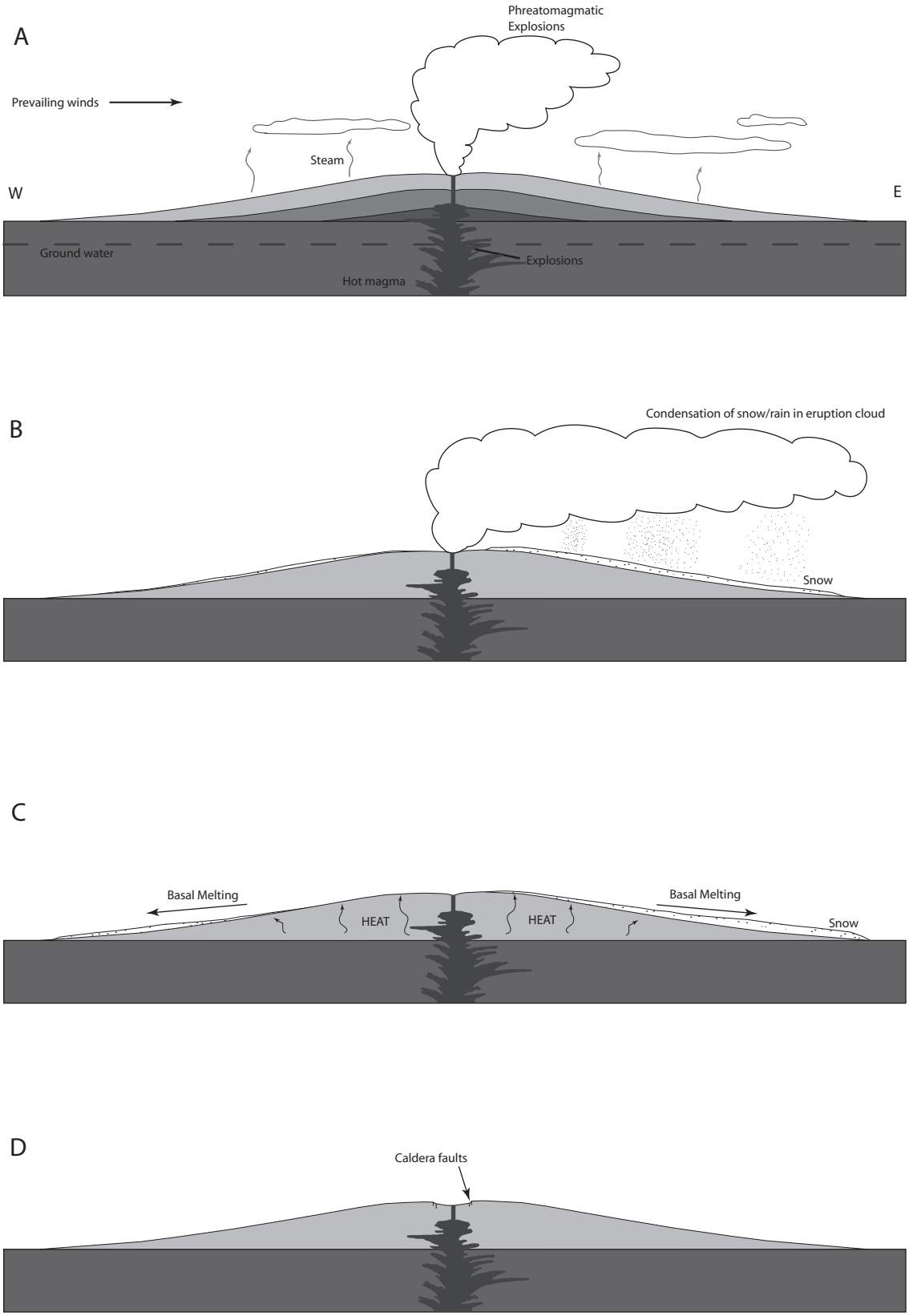

Figure 22. Mad Vallis is a flat bottomed valley partially filled with landslide, mantle, and eolian debris on the eastern edge of Malea Planum. (A) MOLA shaded relief map of Mad Vallis. Boxes show locations of 19 B and 19 C. The walls are scalloped where landslides have widened the valley. (B) MOC image E0101987 detailing the fill material in Mad Vallis. (C) MOC image R0802242 showing scallops in the walls of Mad Vallis. Lighting is from the top left for all images.

FIGURE 22: Mad Vallis

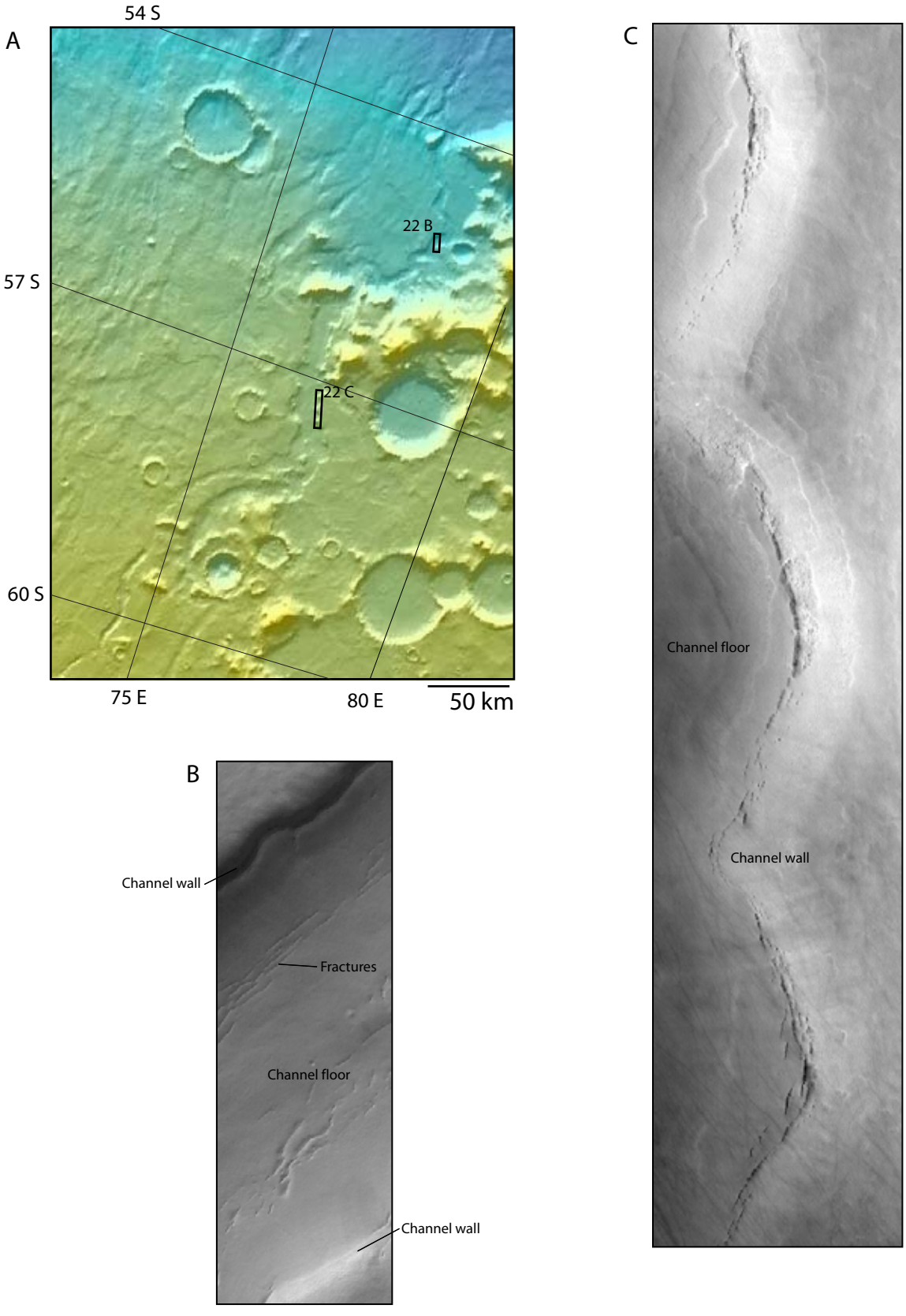

Figure 23. Collapse caldera models. (A) Cross-section of a stepped funnel caldera similar to Amphitrites (modified after Walker, 1988). A positive gravity anomaly centered on Amphitrites suggests a high density load beneath the volcano. The load can be attributed to a dense uncompensated network of solidified magma chambers and dikes. The caldera formed as the dense load sagged into the crust. (B) Peneus caldera resembles a simple piston collapse caldera with inward (B) or outward (C) dipping ring faults and a coherent floor. Noncoherent collapse occurs when the floor does not remain intact during subsidence (D) (modified after Roche et al., 2000).

FIGURE 23: Caldera Collapse

A. Stepped Funnel Caldera

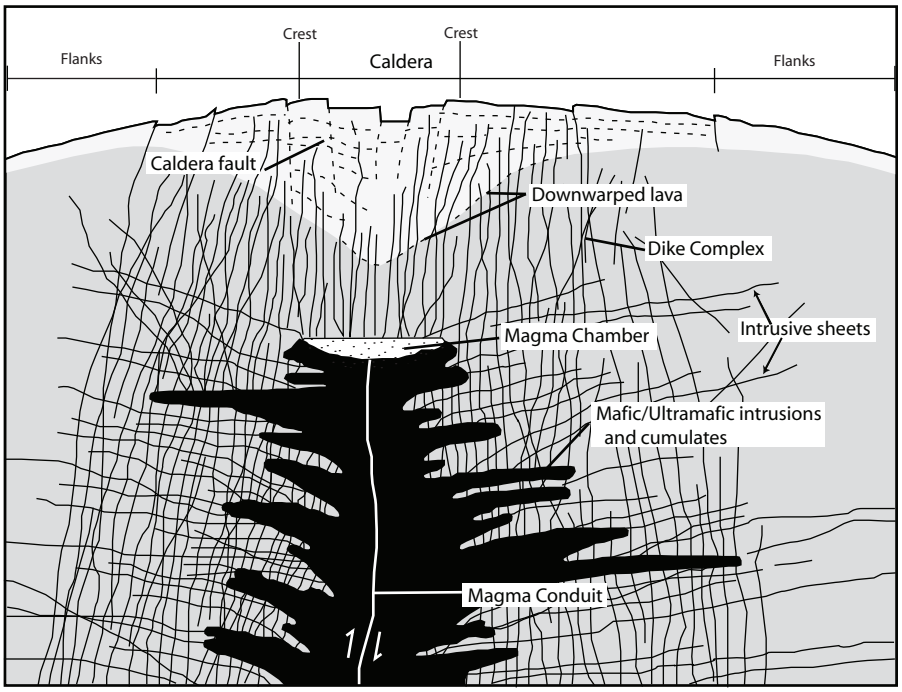

B. Piston Collapse: Inward dipping faults

C. Coherent Piston Collapse: Outward dipping faults

D. Noncoherent or Piecemeal Collapse

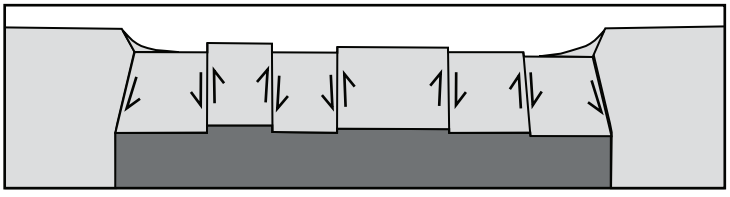

Figure 24. Possible methods of formation for Malea and Pityusa Paterae.
(A) Lunar mascons (large positive gravity anomalies over a basin), similar to the gravity anomaly centered over Malea Patera, may be due to high density material filling an impact basin. As mascon basins subside, the rims experience extension while the basin fill material contracts. (After Solomon and Head, 1980).

(B) Subsidence models indicate that a load applied to a basin should increase the topographic height of the fill material as the basin floor subsides (after Watts, 2001).

(C) Caldera collapse and sagging due to aggregates of solidified magma chambers and dikes may have contributed to the formation of Malea and Pityusa paterae (Walker, 1988). The diameters of the floors of Malea and Pityusa paterae are 200 km across at the maximum width; exceeding the largest recognized martian calderas by 100 km.

(D) Sagging at the surface may be caused by the emplacement of a dense, mafic/ultramafic mid-crustal sill, similar to a process proposed for the Snake River Plain in Idaho (adapted from McQuarrie and Rodgers, 1998, and Head and Wilson, 2002) or a sill complex (Shervais et al., 2006).

(E) Dense mafic lava flows can theoretically sink back through the less dense crust in a process called sagduction. This is a possible explanation for the depression and associated radial wrinkle ridges surrounding Pityusa and Malea Paterae (after Chardon et al., 1998).

(F) Mantle plumes are thought to cause the formation of coronae on Venus. As the plume reaches the lithosphere it flattens, causing doming, a fracture wreath, and perhaps volcanism. As it cools and contracts the elevation changes are greatest in the central part as support for the overlying topography is removed, forming a rim and interior depression. Loading forms a circumferential moat (after Squyres et al., 1992). Malea and Pityusa paterae display rims and central depressions, however, no moat is evident.

FIGURE 24: Possible Methods of Lithosphere Depression Formation

A. Loaded Impact Craters 1

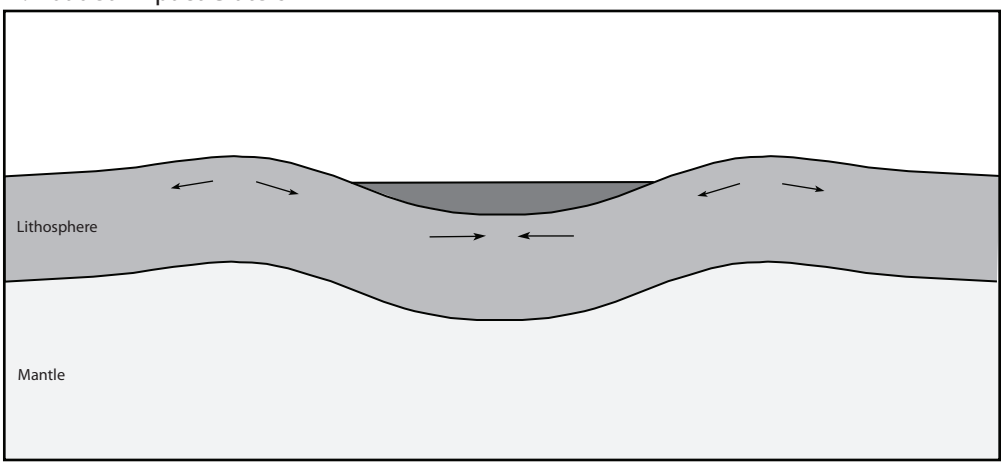

B. Loaded Impact Craters 2

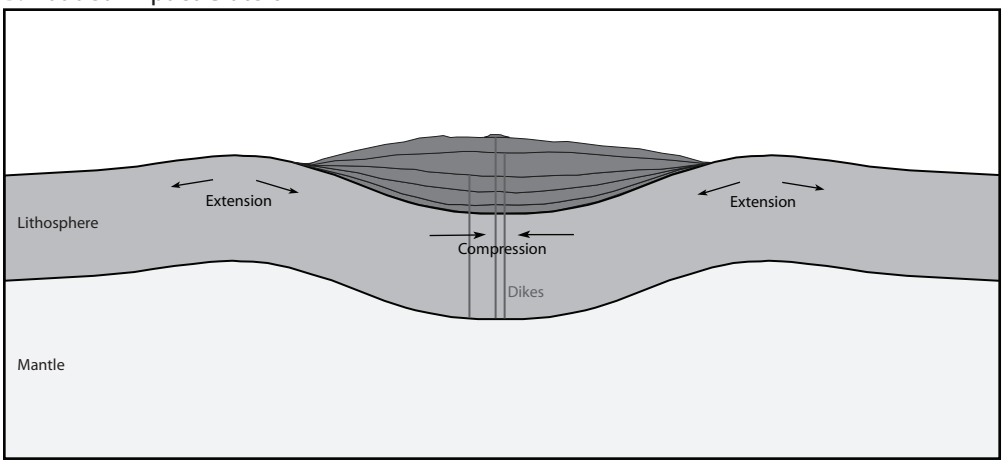

C. Sagduction

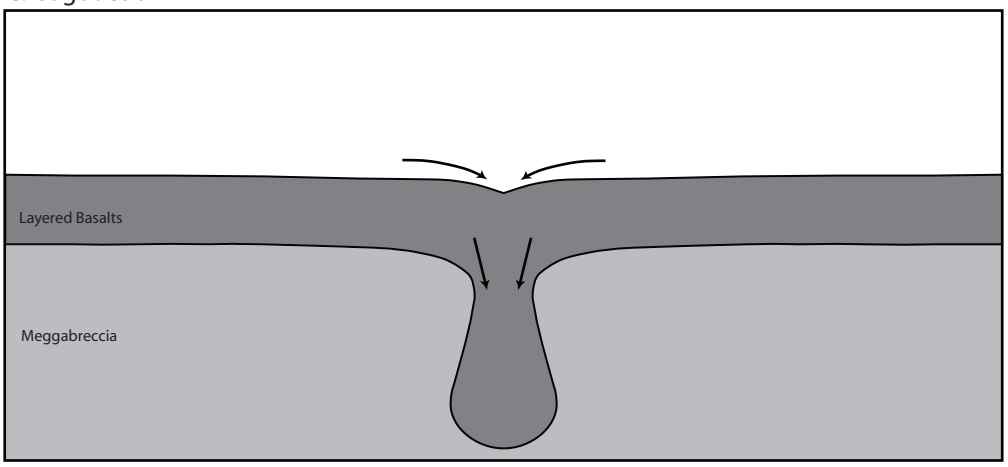

FIGURE 24 (continued)

D. Dense Mafic Sill

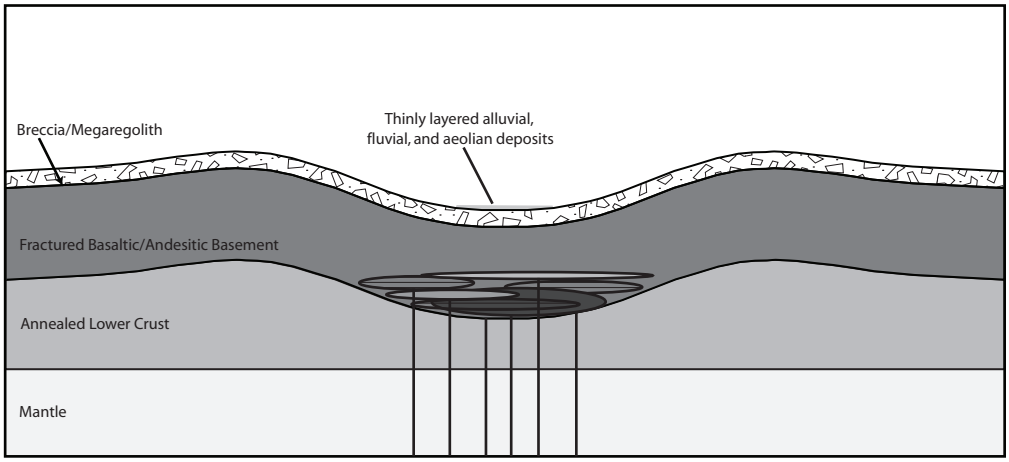

E. Caldera Collapse by Intrusive Loading

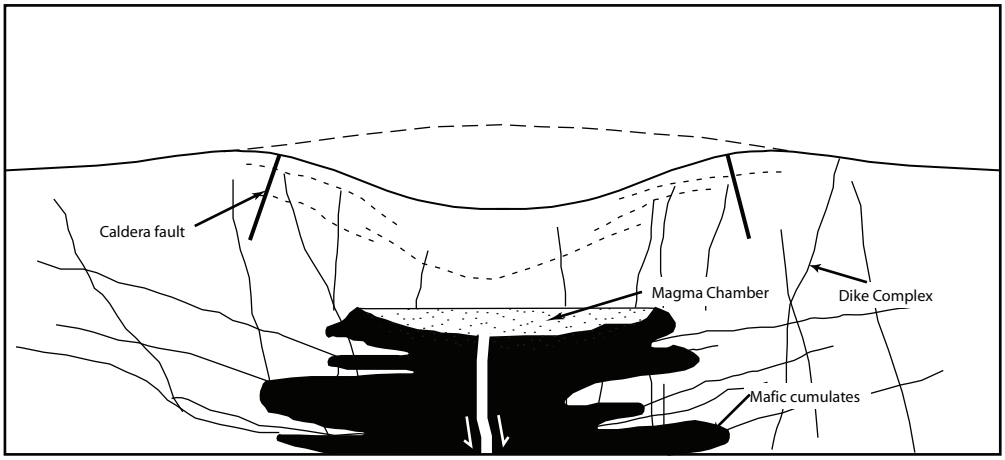

F. Mantle Plume

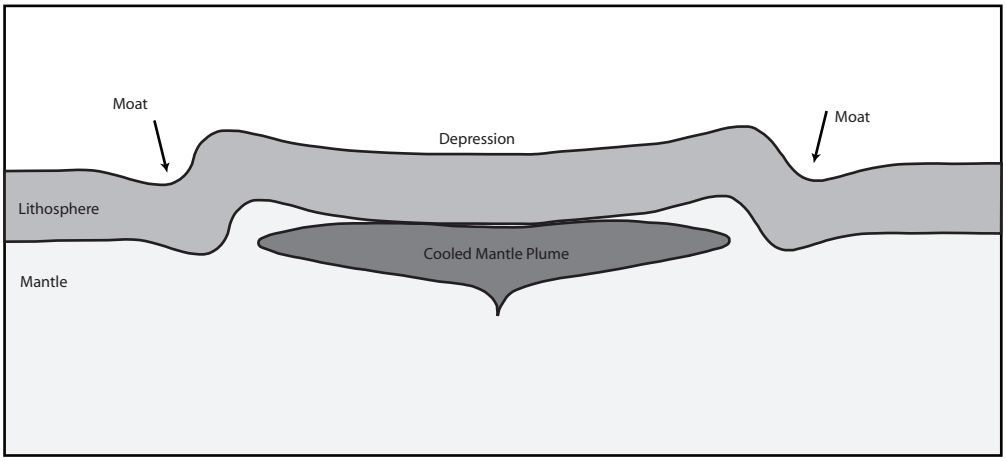

Appendix A: Geologic Map of the Malea Planum Region, Mars

GEOLOGIC MAP OF THE MALEA PLANUM REGION OF MARS

by

Susan K. Larson

Scale (km)

Appendix B

Geologic Map of the Malea Planum Region, Mars
Unit Descriptions

MALEA PLANUM ASSEMBLAGE

Dissected Units

AHv Vallis floor unit: Smooth, flat deposits forming the floors of Mad Vallis; a system of wide valleys along the eastern contact of Malea Planum and the Hellas rim unit (Nhr). The valleys are sinuous to linear with locally scalloped walls. In some places deposits completely fill the channels. The deposits are sparsely cratered and deflation pits are common. Lineations in the deposits run parallel to the valley walls.
Interpretation: Combination of mantle deposits, landslide material, and windblown sediment.
Type Area: 77 ° E, 57 ° 45' S

Nd_1 Dissected plains 1: Rough plains dissected by many linear to sinuous channels on the slope of Hellas Basin (Axius Valles). Channels become deeper and more numerous immediately north of Peneus and Amphitrites Paterae and in an area directly east of the paterae. The deepest channels are 200-300 meters deep and many are superposed by smaller channels a few meters deep. Few ridges are present. Channels often dissect the ridges.
Interpretation: Lava flows from Amphitrites, Peneus and fissures dissected by fluvial and sapping processes.
Type Area: 63 ° E, 56 ° S

Nd_2 Dissected plains 2: Channeled plains on the rim of Hellas Basin. Channels are sinuous and only a few meters deep, comparable to the smaller set of channels found in the dissected plains 1unit (Nd_1). Large linear and arcuate wrinkle ridges 200 m high trend northwest-southeast. Smaller ridges up to 50 m high are randomly oriented.
Interpretation: Lava flows originating from fissures or Peneus. Dissected by fluvial channels.
Type Area: 40 ° E, 54 ° S

Nd_3 Dissected plains 3: Smooth plains on the western margin of Malea Planum. Similar to dissected plains 2 (Nd_2) but with fewer channels and many small sinuous wrinkle ridges less than 100 m high. Many small pedestal craters are present.
Interpretation: Lava flows originating from fissures or Peneus. Dissected by fluvial channels.
Type Area: 36 ° E, 56 ° 30'S

Ridged Units

Nr_1 Ridged plains 1: Forms a smooth plain that slopes gently toward Hellas Impact Basin and is deformed by numerous linear to arcuate wrinkle ridges as much as 200 m high. Few smaller ridges are present but increase in number toward the edges of Malea Planum. Linear wrinkle ridges trend northwest to southeast in the eastern segment of the

unit and northeast to southwest in the western segment of the unit. Shallow channels also are more common toward the edge of Malea Planum.
Interpretation: Volcanic flows and thin mantle material deposited on cratered terrain.
Type Area: 47 ° E, 59 ° S

HNr_2 Ridged plains 2: Forms a flat plain deformed by small ridges reaching heights of 50 m. Similar to dissected plains 3 unit (Nd_3) but channels are present only along the eastern contact with Highland plains material. Small pedestal craters with diameters of a few kilometers are very common. Contact between this unit and the Scarped unit is marked by an abrupt change in slope. Unit terminates in a lobate front inside Mitchel crater.
Interpretation: Thin mantled lava flows deposited on cratered terrain.
Type Area: 60° E, 68 ° S

Amphitrites Patera Formation
Has Amphitrites shield: Forms the flanks of Amphitrites Patera. Terrain is corrugated by numerous radial channels extending approximately 100 km from the rim. A channel extends from an elongate pit 200 m deep on the western flank of the patera. Scarps concentric to the rim crosscut and are crosscut by the channels. Small wrinkle ridges radiate from the rim. Much of the unit is covered by pitted smooth plateau deposits a few meters thick.
Type Area: 61 ° E, 57 ° S

Har Amphitrites rim: Forms the smooth summit of Amphitrites Patera. It lacks the distinct channels found on the flanks. Radial wrinkle ridges and arcuate scarps extend into the rim unit from the shield. Terminates at the caldera floor with an abrupt change in slope. *Interpretation:* Downsagged and faulted rim formed by collapse and draining of a magma chamber beneath Amphitrites Patera.
Type Area: 59 ° 30’ E, 58 ° 20’ S

Haf Amphitrites caldera floor: Forms the smooth floor of Amphitrites caldera. Floor slopes upwards toward rim. Ringed by arcuate scarps. Small ridges trend N-S to NE-SW.
Type Area: 60 ° 30’ E, 59 ° S

Peneus Patera Formation
Nps Peneus shield: Forms the flanks of Peneus Patera.

Npr Peneus rim: A region of closely spaced arcuate scarps forming a horst and graben terrain on the summit of Peneus Patera. A section of the scarps on the southeast is offset toward the interior of the caldera. A section of scarps in the northwest contains a higher concentration of fractures, forming sharp ridges instead of flat-topped horsts.
Interpretation: Caldera ring faults formed during the collapse of the roof of a magma chamber beneath Peneus Patera.
Type Area 51 ° E, 58 ° 30’S

Npf Peneus caldera floor: Forms the smooth flat floor of Peneus caldera. Unit is flatter than Amphitrites caldera floor (Haf). A sinuous ridge trends NE. Other smaller ridges trend N-S. A few steep sided pits are located in the southeast.
Interpretation: Lava flows originating from fractures in the magma chamber roof, covered by thin mantle deposits.
Type Area: 53 ° E, 58 ° S

Malea and Pityusa Paterae Formation

Nmr Malea Patera rim: Includes the crest and central depression walls of Malea Paterae. Ridges with heights of 200 m extend radially away from the central depression. A smaller set of wrinkle ridges a few tens of meters high is concentric to the depression, particularly in the south and west. Arcuate flat-topped ridges ring the northwest corner of the patera.
Type Area: 50 ° E, 65° S

Nmf Malea Patera floor: Forms smooth, featureless plains with small (meters high) scarps and few craters. Appears similar to Dorsa Argentia formation (Nda) but not bounded by a high scarp. Terminates at depression walls. A sinuous ridge extends NE and smaller linear ridges extend E-W through the unit. Nda superposes the unit at the lowest topographic area in the depression.
Interpretation: Mostly mantle deposits, possibly interbedded with lava flows.
Type Area: 51 ° E, 64 ° S

HNpi Pityusa Patera rim: Includes the crest and central depression walls of Pityusa Paterae. Ridges with heights of 200 m extend radially away from the central depression. Smaller wrinkle ridges concentric to the depression are more numerous than around Malea patera and are most prominent in the west. A small valley on the eastern rim continues onto the depression floor. The southern unit boundary terminates in a 1 km high degraded scarp.
Type Area: 32 ° E, 68° 30’ S

Npif Pityusa Patera floor: Forms rough terrain filling the Pityusa depression. Dunes are present in the northwest corner and in isolated patches adjacent to the smooth plateaus and in some craters. A few ridges and channels extend through the unit.
Interpretation: Eroded mantle deposits and dunes of sediment removed from Nda.
Type Area: 36 ° E, 66 ° 15’S

<u>HELLAS BASIN ASSEMBLAGE</u>
Nhr Hellas rim: Smooth, moderately cratered plain on the rim of Hellas basin. Unit is missing in the region of Malea Planum. Numerous isolated massifs (Nhm) are surrounded by the unit. Unit is rougher in the north near the contact with Hellas basin floor materials and terminates in a steep scarp with the cratered unit (Np_1) in the south. Rare channels and ridges are found within the unit. Topographically lower than the

cratered unit (Np_1) but higher than Malea Planum materials. Local small deflation pits are found within craters and on the plains.
Type Area: 82 ° E, 55 ° S

Nhm Rim massifs: Forms rough conical to elliptical mountains within the Hellas rim unit (Nhr). Massifs are concentrated in the northern portion of the Nhr where the slope of the Hellas Basin rim is steepest. Lengths range from a few meters to 100 km in length with heights up to 4 km. Apron deposits surround some massifs.
Interpretation: Bedrock fractured by Hellas impact, subsequently eroded.
Type Area: 79 ° E, 54 ° S

HNhf Hellas Basin floor: Forms flat smooth plains on the floor of the Hellas Impact Basin with large north-south trending ridges (250 m high) and a set of smaller ridges (100 m high) trending east-west. Shallow channels (1 to 50 m deep) and a few deeper channels (100 m deep) run parallel to the ridges. Channels crosscut some ridges and the contact between the dissected plains 1 unit (Nd_1) and Hellas Basin floor material.
Interpretation: Mantle material and deposits of material eroded from Malea Planum units.
Type Area: 62 ° E, 51 ° 30" S

POLAR ASSEMBLAGE
Units associated with the southern polar ice cap.
Nda Dorsa Argentia Formation (Head and Pratt, 2001b): Forms very smooth plains and plateaus bounded by near-vertical scarps up to 500 m high. Found in depressions and low-lying areas south of 60°S latitude. Plateau surface is sparsely cratered, and sometimes etched and pitted. Plateau edges are smooth or scalloped and shallow channels can be present on the surface. No significant ridges are found within the unit.
Interpretation: Remnants of an ancient, thick, volatile-rich polar deposit.
Type Area: 36 ° E, 67 ° S

AHpc Pedestal material: Forms flat-topped smooth plateaus surrounding intermediate age impact craters. Pedestal material has little obvious texture and ends sharply in a scarp a few meters to 300m high. Rays and lobes of crater ejecta are eroded, truncated, or missing. Pedestals greater than 5 km in diameter are mapped.
Interpretation: Mantle material protected from erosion by less volatile crater ejecta material.
Type Area: 56 ° E, 72 ° S

Hhi Hilly unit: Forms a series of closely spaced, rounded hills a few kilometers across rising 1 km above the floor of the Pityusa Patera depression. Hills have steep sides and flat tops. Embayed by Dorsa Argentia Formation (Nda). *Interpretation:* Eroded remnant of an ancient, thick polar mantle deposit.
Type Area: 39 ° E, 67 ° 28'S

Nhu Hummocky material: Forms areas of rough low hills and knobs in the southern portion of the map area. Few cliffs, channels, and ridges are found within the unit. Sparsely cratered.
Interpretation: Erosional remnant of thick mantle materials.
Type Area: 31 ° E, 72 ° 15'S

Nplr Rough plateau material: High plateau material with an irregular, hummocky surface that covers the northern rim of Malea Patera and forms an isolated dome on the west slope of Amphitrites. The southern edge of the plateau in Malea terminates in a high, steep, scalloped scarp. The eastern and western edges are convex slopes. The smaller plateau is bounded by a rounded scarp in the east and grades into rougher knobby material in the west. *Interpretation*: Possibly the eroded remnant of an old, thick mantle deposit.
Type Area: 52 ° E, 62 ° S

Npi Pitted material: Forms an area of irregular smooth and rough plains surrounding many knobs and scarps.
Interpretation: Eroded mantle material.
Type Area: 40 ° E, 71 ° S

HIGHLAND PLATEAU ASSEMBLAGE

Np_1 Cratered unit: Forms heavily cratered plains topographically higher than Malea Planum materials. The craters mostly lack ejecta, have flat floors and are occasionally buried by smooth intercrater plains. Ghost craters and eroded or buried rims are common. Some ridges and channels are present.
Type Area: 30 ° E, 53 ° S

Np_2 Subdued cratered unit: Forms highland plains similar to the cratered unit (Np_1) but smoother and with fewer craters. Contact with Np_1 defined by an abrupt change in slope.
Type Area: 36 ° E, 51 ° 15' S

MISCELANEOUS MATERIALS

Nm Highland massif unit: Forms an isolated, roughly conical hill rising 900 m above the surrounding plains. Only one occurrence appears within the mapped area but additional examples are present in the plains to the west.
Interpretation: Possible old subglacial volcanic edifices.
Type Area: 29° E, 61° S

Ns Scarped unit: Forms fractured terrain on the south and west margins of Malea Planum. Individual scarp segments extend up to 200 kilometers in length. No horizontal displacement is apparent.

Interpretation: Normal faults possibly related to the formation of the Hellas Impact Basin.
Type Area: 57° E, 70 ° S

CRATER MATERIALS

AHc Younger crater material: Characterized by visible ejecta that has occasionally been mantled and exhumed. May form pedestals. The rims of these craters are intact to moderately degraded. Some contain central peaks. The crater floors are bowl shaped or filled with lineated apron material.
Interpretation: Young impact craters and surrounding ejecta blankets.
Type Area: 36 ° E, 54 ° S

Nc Older crater material: Little to no ejecta material remains. Rims are moderately to highly degraded. Craters are usually filled with smooth deposits. No central peaks are visible. Forms crater rims and ejecta of older craters. In some instances the craters have been buried and exhumed.

Valleys

Scarps

Wrinkle Ridges

Appendix C: Correlation of Map Units

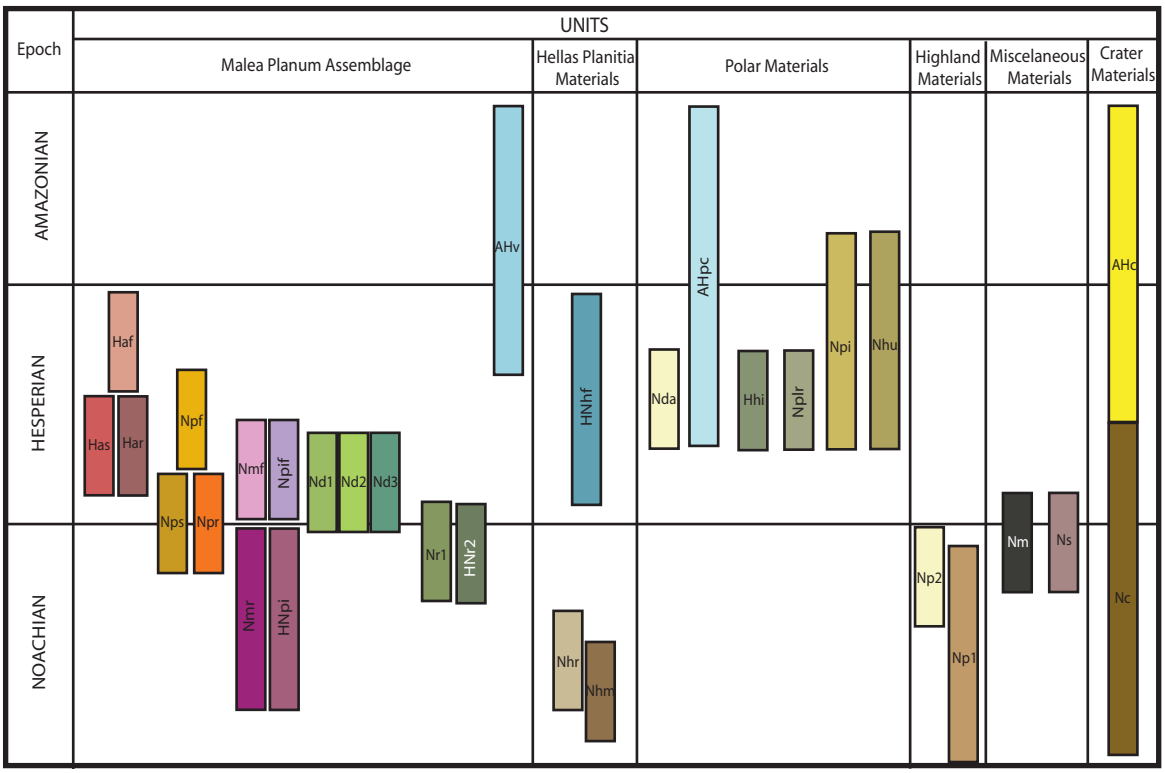

Appendix D

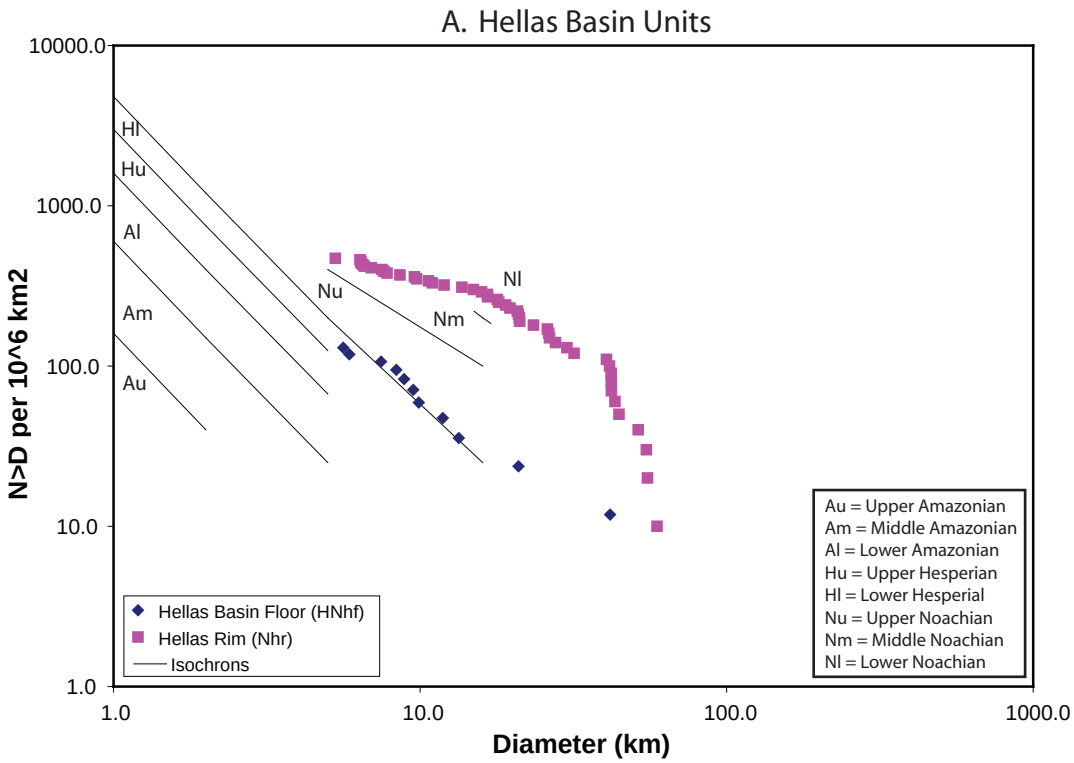

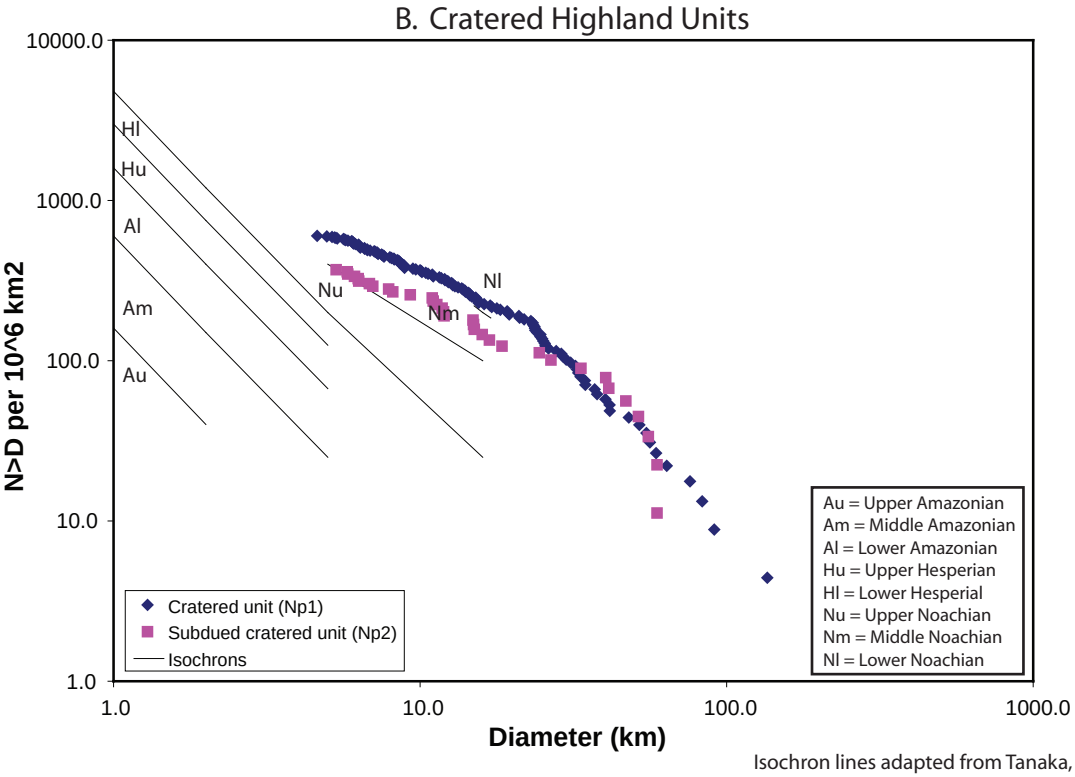

Isochron lines adapted from Tanaka, 1986

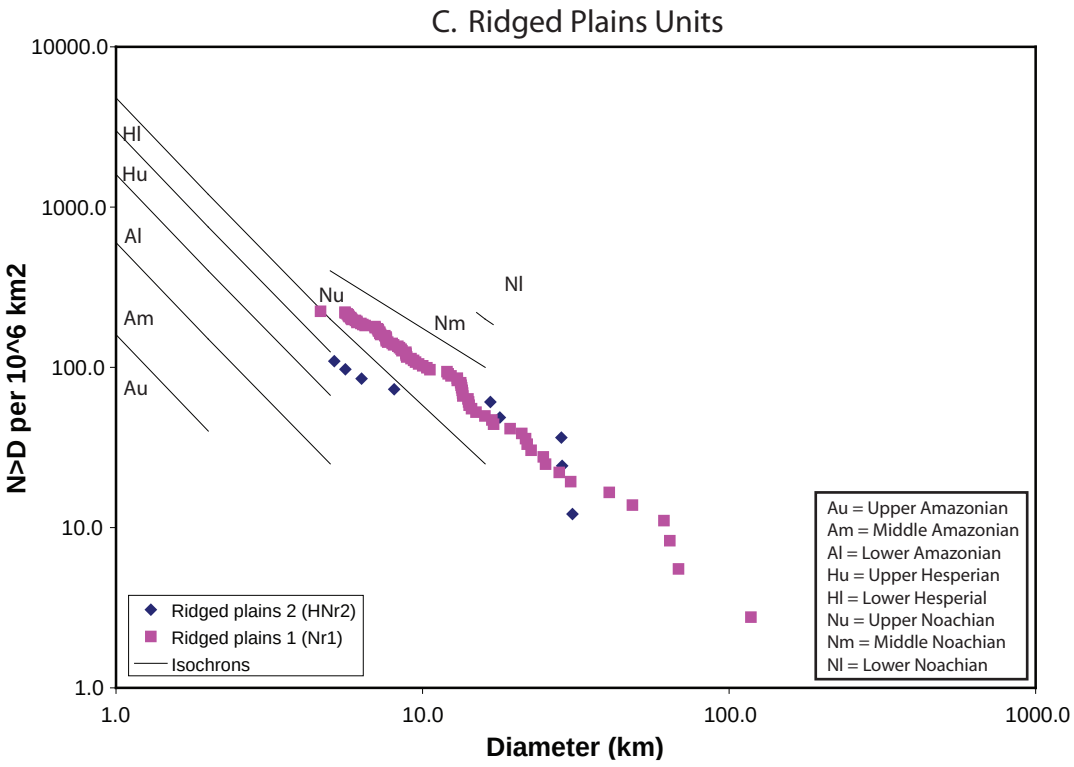

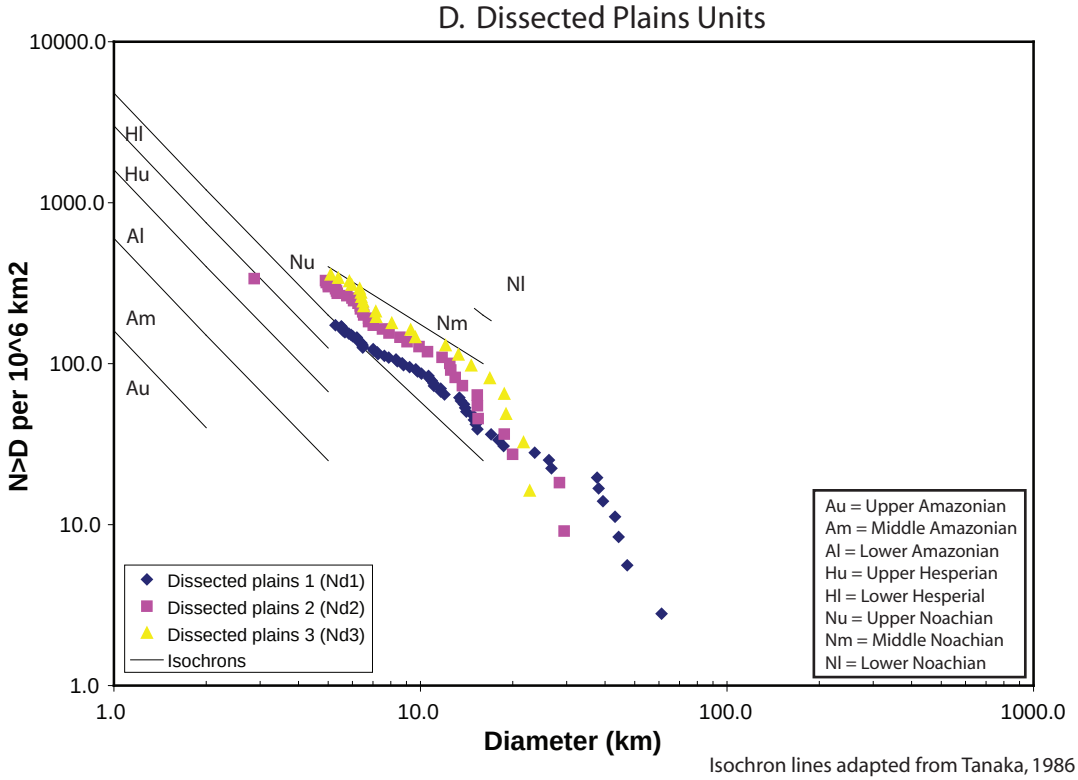

Isochron lines adapted from Tanaka, 1986

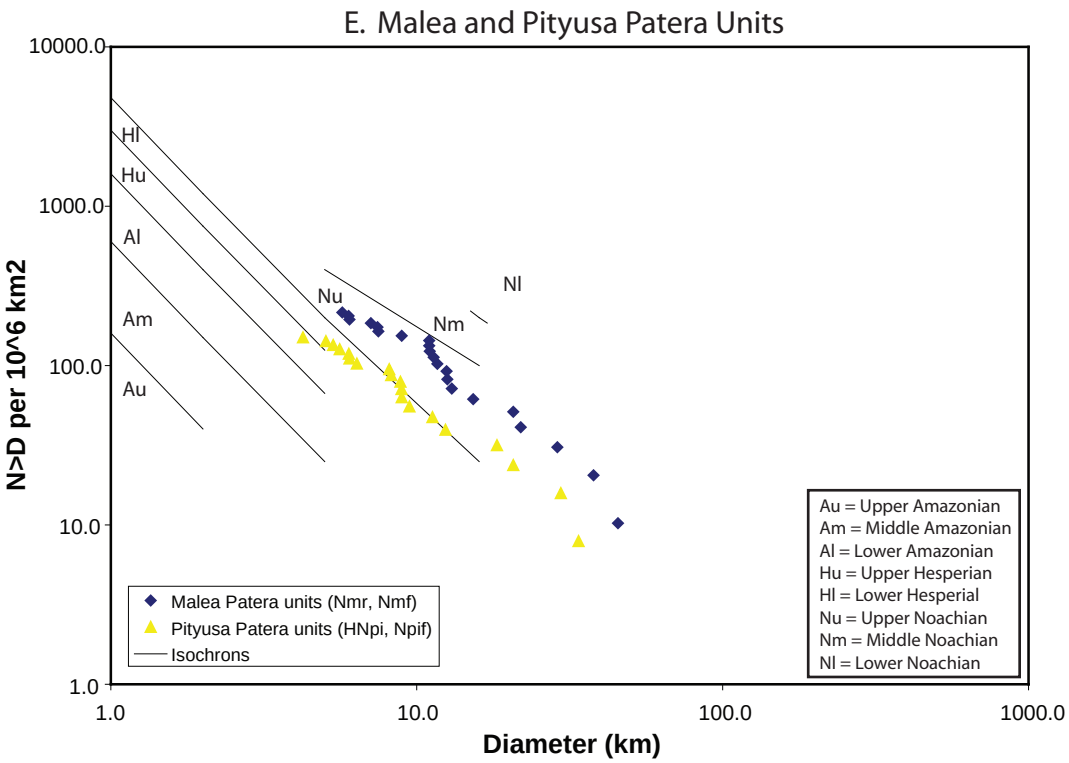

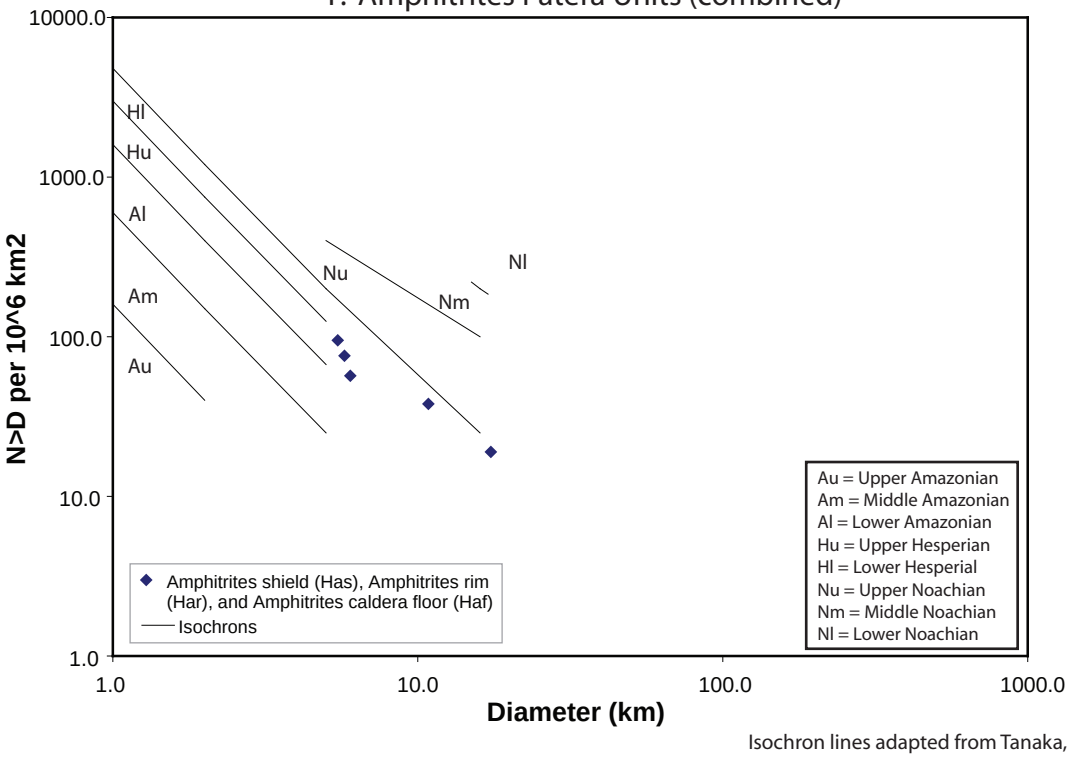

Isochron lines adapted from Tanaka, 1986

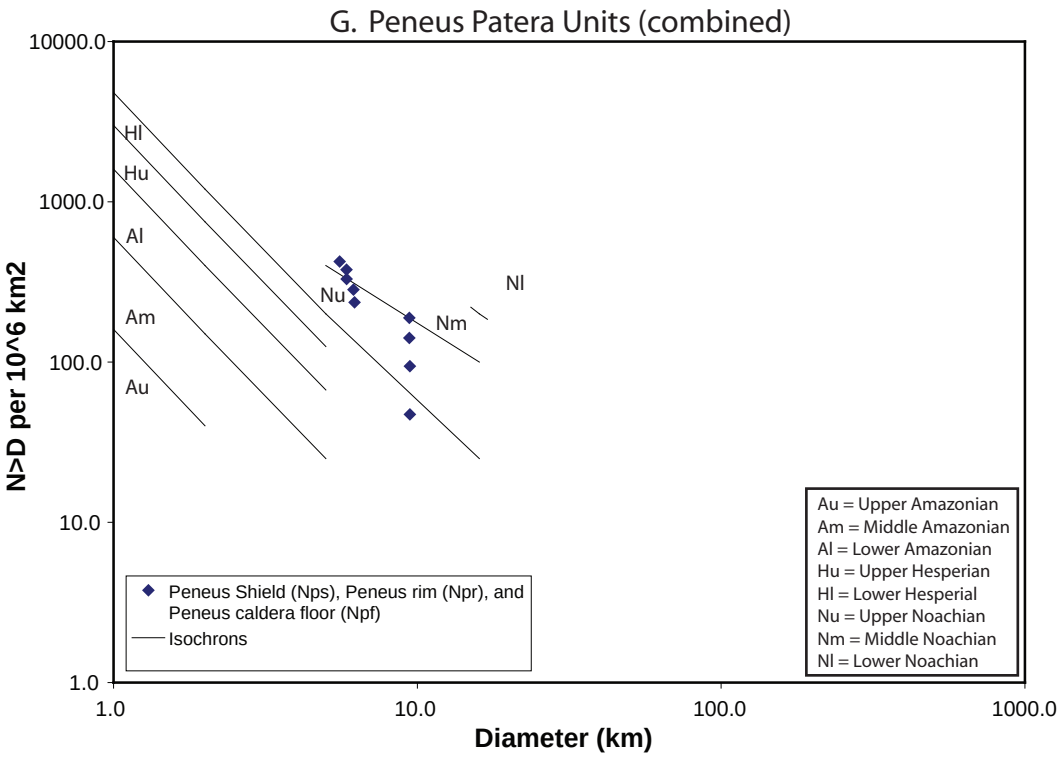

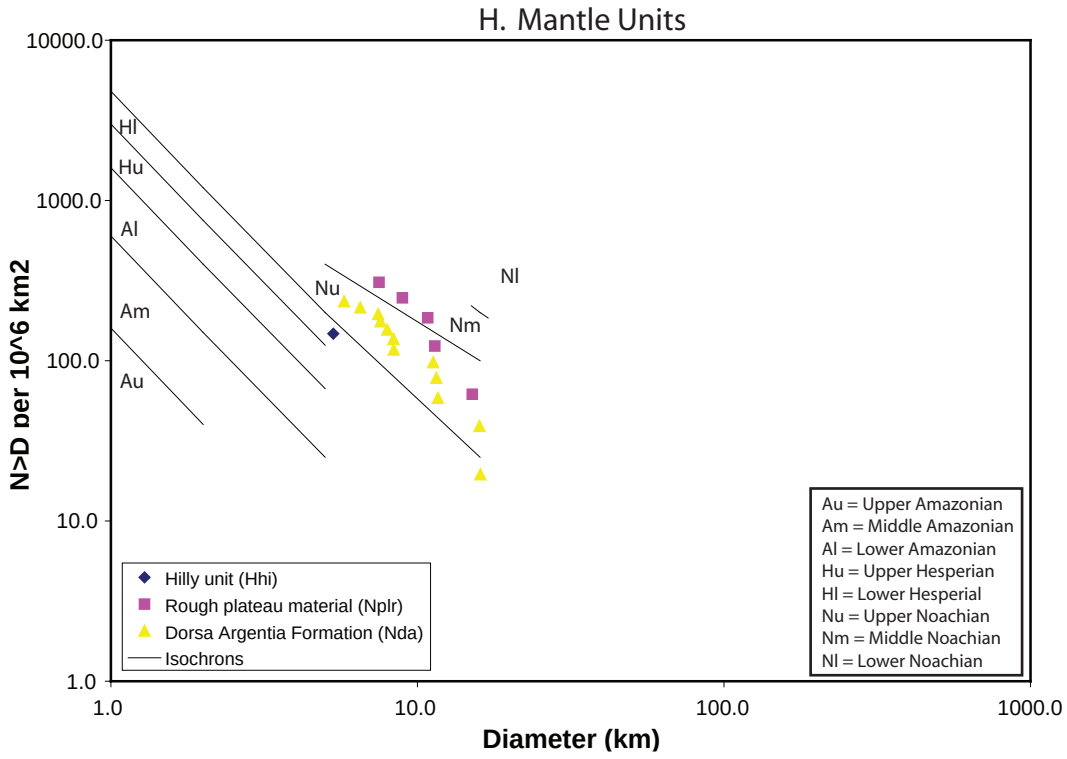

Isochron lines adapted from Tanaka, 1986

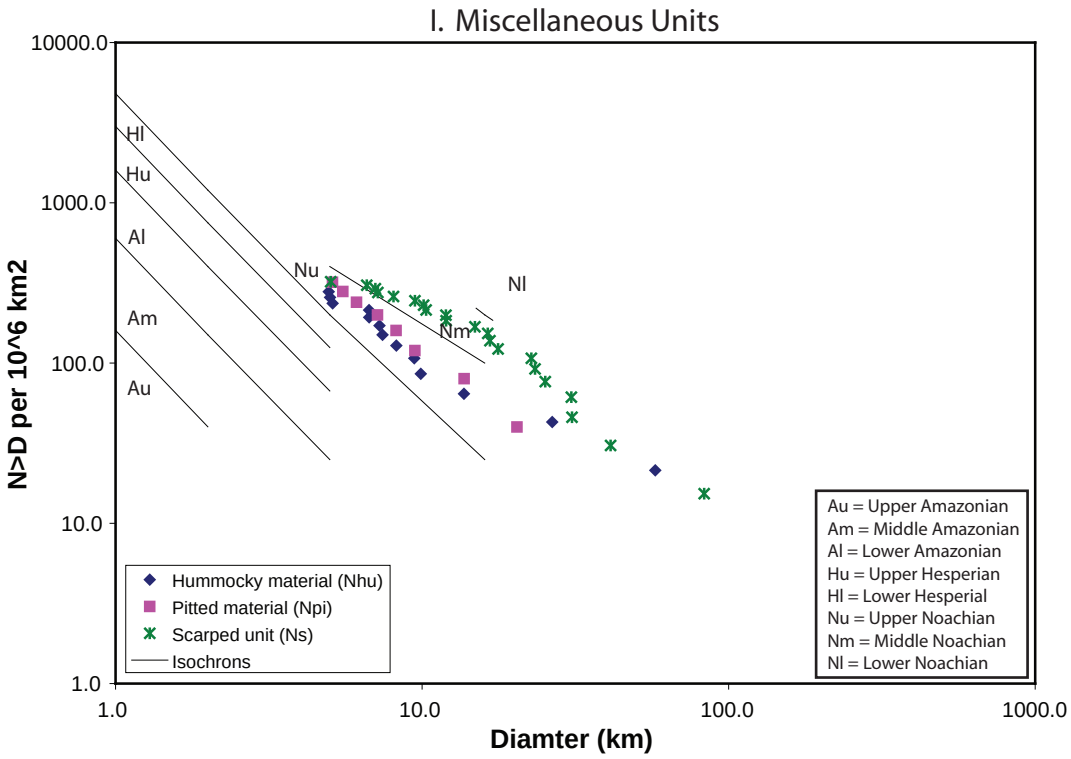

Isochron lines adapted from Tanaka, 1986